DEEP OCEAN CIRCULATION AND CONTINENTAL WEATHERING REGIMES DURING CLIMATE TRANSITIONS (LAST DEGLACIATION AND EOCENE-OLIGOCENE) USING Sr, Nd, AND Pb ISOTOPES IN SEDIMENTARY ARCHIVES

By

CHANDRANATH BASAK

A DISSERTATION PRESENTED TO THE GRADUATE SCHOOL
OF THE UNIVERSITY OF FLORIDA IN PARTIAL FULFILLMENT
OF THE REQUIREMENTS FOR THE DEGREE OF
DOCTOR OF PHILOSOPHY

UNIVERSITY OF FLORIDA

2011

To my mentors

ACKNOWLEDGMENTS

I would like to take this opportunity to thank a number of people whose direct and indirect support have helped me through years of graduate school. First, I thank my parents for their unconditional support towards my work and me. I am extremely thankful to my advisor Dr. Ellen E. Martin for her guidance and support throughout the Ph.D. program. Without Ellen's help and advisement this work would have never been successfully completed. I would also like to thank my entire committee (Dr. Paul A. Mueller, Dr. George Kamenov, Dr. Andrea Dutton, and Dr. John Krigbaum) for their valuable advice from time to time. Special thanks to Dr. George Kamenov for his patience while teaching the theory and instrumentation of mass spectrometer. I am grateful to my master's adviser Dr. Anthony E. Rathburn for introducing me to the field of paleoclimate research. I am also thankful to Dr. David Hodell, Dr. Thomas M. Marchitto, and Dr. Paul A. Mueller for scientific discussions, which helped shape some of the research ideas presented in this dissertation. I am very thankful for all the help and laughter that Derrick Newkirk has extended over the years. Long lab hours would have been quiet boring without Derrick's presence. I sincerely thank one of our alumni, Ms. Elodie Bourbon, and several undergraduate student researchers for their help with laboratory work from time to time. Continuous technical support from Mr. Ray G. Thomas and Mr. Dow Van Arnam had been very critical to continue day to day lab activity. Numerous discussion sessions with Dr. Keiji Horiwaka on myriad topics of paleoceanography often helped me evaluate old data with a newer perspective. I really appreciate all the help that I have received over the years from the entire faculty and the graduate students body within the department. Special thanks to

Nita, Pam, and Susan for all their help with paper work. I am thankful for the financial support extended by the National Science Foundation, the American Geochemical Society, the Geological Society of America, and the Department of Geological Sciences, University of Florida. Lastly, I would like to thank my wife and dear friend, Dr. Pinki Mondal, whose constant enthusiasm about my research often times, kept me going when I thought there were not much to accomplish.

TABLE OF CONTENTS

page

LIST OF TABLES

LIST OF FIGURES

Abstract of Dissertation Presented to the Graduate School
of the University of Florida in Partial Fulfillment of the
Requirements for the Degree of Doctor of Philosophy

DEEP OCEAN CIRCULATION AND CONTINENTAL WEATHERING REGIMES DURING CLIMATE TRANSITIONS (LAST DEGLACIATION AND EOCENE-OLIGOCENE) USING Sr, Nd, AND Pb ISOTOPES IN SEDIMENTARY ARCHIVES

By

Chandranath Basak

May 2011

Chair: Ellen E. Martin
Major: Geology

The global climate on earth is constantly changing and periodically the earth system crosses a climate threshold and enters a new climate state. The Eocene-Oligocene transition (EOT) ~33.4 Ma ago and the last deglaciation ~18 ka are two examples of major climate transitions. During the EOT the Antarctic cryosphere developed, there was global cooling of deep waters, and the carbonate compensation depth deepened. During the last deglaciation there was massive global ice meltback, a dramatic rise in atmospheric CO_2, and a decline in atmospheric $\Delta^{14}C$. These two events are climatologically important since the former represents the first Cenozoic transition from a greenhouse to an icehouse world, while the later represents the end of the last glacial period.

Major climate change is frequently associated with readjustment of carbon sources and sinks. The ocean is a relatively large carbon sink that can exchange carbon with the atmosphere over geologically short time scales. Chemical weathering of continental silicate rocks also plays a key role in sequestering atmospheric carbon over geologically long time scale. Therefore, the interplay between physical and chemical

continental weathering can have major implications for the long term carbon budget of the Earth.

In this dissertation I studied continental weathering regimes on Antarctica during the EOT and the role of carbon storage and circulation in the ocean during the last deglacial in order to improve our understanding of the relationship between climate, ocean circulation, and continental weathering. Radiogenic isotopes of Pb, and Nd were extracted from sedimentary archives such as Fe-Mn oxide coatings and fossil fish teeth to acquire meaningful information pertaining to weathering and ocean circulation readjustments. Pb isotopic data from this study confirm a change in the Antarctic weathering regime leading up to the EOT, which may have contributed to the drawdown of atmospheric CO_2 and ice buildup on Antarctica. I also documented a rearrangement of intermediate water circulation in the Pacific using Nd isotopic data recovered from fossil fish teeth. The old carbon that was trapped in the Southern Ocean abyss by sea ice or ocean stratification during the last glaciations was transported by intermediate waters and ventilated to the atmosphere following meltback of the ice at the end of the last glaciation.

CHAPTER 1
INTRODUCTION

Cenozoic Climatic Events

The Eocene-Oligocene (E/O) boundary and the last deglaciation are two important climate threshold events; the first was characterized by massive ice growth and the second by ice decay. While there are a lot of differences between these events, both are marked by dramatic changes in atmospheric CO_2 and temperature. Prior to the E/O boundary, the climate of the Paleocene and Eocene was dominated by warm global temperatures (Zachos et al., 2001) punctuated by episodes of short-lived, rapid global warming known as 'hyperthermals' (Sexton et al., 2011). Cenozoic cooling started following the mid-Eocene climatic optima with a major step of cooling and ice growth at the E/O boundary ~34 Ma ago (Miller et al., 1991; Zachos et al., 2001). This boundary is marked by development of an Antarctic cryosphere with a volume similar to today's volume (Pekar and DeConto, 2006; Pekar et al., 2006) and is often identified as the onset of the Cenozoic icehouse. The E/O boundary is also characterized by a general decreasing trend in atmospheric CO_2 (Pagani et al., 2005; Zachos et al., 2008; Pearson et al., 2009), a positive shift in benthic foraminifera $\delta^{18}O$ and $\delta^{13}C$ (Coxall et al., 2005), ~ 1 km deepening of the carbonate compensation depth (CCD) (Coxall et al., 2005), occurrences of ice rafted debris (IRD) in the Southern Oceans (Zachos et al., 1992a), and a shift in clay mineral assemblages from smectite to illite and chlorite in the Southern Ocean (Robert and Kennett, 1997; Robert et al. 2002). The development of icehouse conditions has been attributed to thermal isolation of Antarctica due to tectonic processes and opening of the Drake and Tasman gateways (Kennett, 1977; Exon, 2000), decreasing atmospheric greenhouse gas concentrations (mainly CO_2) below a

threshold value (DeConto and Pollard, 2003), and orbitally-paced climate cycles (Palike et al., 2006).

While all of these mechanisms may have contributed to Antarctic glaciation, the decreasing trend of atmospheric CO_2 has been identified as a critical factor in the observed continental ice growth (DeConto and Pollard, 2003). The large decrease in atmospheric CO_2 during the Eocene and Oligocene (Pagani et al., 2005) requires a major reorganization of the carbon cycle. Following the E/O boundary glaciation the earth has experienced periodic warming episodes, such as the late Oligocene warming and mid-Miocene climatic optimum (Zachos et al., 2001). Throughout these climate variations continental ice volume on Antarctic waxed and waned, but the continent never returned to an ice-free, pre E/O state (Pekar and Christie-Blick, 2008).

The late Pleistocene ice core data demonstrate a clear relationship between temperature and atmospheric CO_2 concentrations with atmospheric CO_2 fluctuations of approximately ~90 ppm between glacial and interglacial climatic intervals (Petit et al., 1999; EPICA community members, 2004). The Last Glacial Maximum (LGM) ~21 kry ago represents the peak of the last glacial event and was characterized by lower sea level (~120 m lower, Peltier and Fairbanks, 2006), extensive continental ice growth in the Northern hemisphere, changes in the deep ocean circulation (e.g., McManus et al., 2004; Lynch-Stieglitz et al., 2007) and extreme aridity. The last deglaciation, which began ~18 kyr ago marked another climate threshold event that was characterized by a major decline in continental ice sheet volume.

The tight coupling between atmospheric CO_2 and temperature observed during the E/O transition and the last deglaciation illustrates the importance of the global

carbon cycle on climate over millions of years and millennial time scales. The long-term global carbon cycle responds to variations in CO_2 sources, such as volcanism and weathering of organic carbon, and CO_2 sinks, such as silicate weathering, over millions of years (Berner, 1999). In contrast, the ocean participate in the short-term global carbon cycle through the biological pump, ventilation rates, and whole ocean alkalinity (Sigman et al., 2010), which is again controlled by the rate and pathways of deep-intermediate ocean circulation.

Data on continental weathering and deep-intermediate ocean circulation are critical for understanding the long and short term carbon cycles and climatic threshold events. In this dissertation, I study changes in weathering and ocean circulation for two climatologically important global events: the transition from a greenhouse to an icehouse world in at the E/O and the end of the last glaciation and the transition to modern climatic conditions. The key questions for the E/O study were whether we could develop an archive based on seawater Pb isotopes to identify changes in weathering conditions on Antarctica associated with climate change. The key question for the last deglacial study was whether we could identify the sources and pathways of old carbon that accumulated in the deep ocean during the glacial period and was transported to a region in the tropical Pacific during the deglaciation. This old carbon was ultimately vented to the atmosphere, thereby dramatically increasing the atmospheric CO_2 concentration and decreasing the atmospheric $\Delta^{14}C$.

Research Objectives

The initial glaciers on Antarctica at the E/O boundary were probably wet-based glaciers (Kennett and Barker, 1990; Zachos et al., 1999) that introduced massive pulses of continental material into the Southern Ocean. It is important to understand the extent

of chemical weathering and the composition of the source rocks exposed to weathering during this process because chemical weathering of silicate rocks sequesters atmospheric CO_2, while mechanical weathering and weathering of carbonate have minimal impact on the carbon cycle. Other important observations from the Eocene-Oligocene Transition (EOT) include deepening of the CCD and a positive shift in the $\delta^{13}C$ record from benthic foraminifera, which could also be affected by the type of material being weathered and the total cationic flux to the Southern Ocean. While the presence of ice rafted debris (IRD) is recognized as an indicator of mechanical weathering (Zachos et al., 1992a), IRD provides little information about chemical weathering rates. Thus, in order to better understand the composition of weathered material (silicate vs. chemical) and the mode of weathering (mechanical vs. chemical) at the EOT, I developed a weathering proxy (Chapter 2; Basak et al., *in press*) based on Pb isotopes that compares seawater values, which are recorded in oxide phases from bulk marine sediments, to values for terrigenous residues. This proxy is then used to reconstruct the weathering history on Antarctic during the EOT (Chapter 3).

One critical climatic tipping point occurred ~18 kyr at the end of the Last Glacial Maximum (LGM). This recent deglaciation is characterized by a fifty percent increase in atmospheric CO_2 and a dramatic decrease in the radiocarbon content of the atmosphere. Conceptual models indicate that extensive sea-ice cover (Stephen and Keeling, 2000) and upper ocean stratification in the glacial Southern Ocean (Francois et al., 1997; Sigman and Boyle, 2000) played a critical role in the storage of a dense, saline, CO_2-rich, and ^{14}C-depleted water. This water could have mixed back into the main body of the ocean during deglaciation as the sea-ice cover melted and ventilation

resumed in the Southern Ocean resulting in an increase in atmospheric CO_2. Evidence for saline, ^{14}C-depleted ("old") water during the LGM has been reported from the deep Southern Ocean (Adkins et al., 2002; Skinner et al., 2010). Recently, evidence of ^{14}C-depleted, old water was also reported from intermediate ocean depths (~700 m) in the tropical North Pacific and the Indian Ocean, suggesting an intermediate water pathway for transferring the CO_2 sequestered in the deep ocean during the glacial to the atmosphere (Marchitto et al., 2007; Stott et al., 2009; Bryan et al., 2010). Previous studies used $\Delta^{14}C$ from foraminifera to determine the age of the water mass involved, but this proxy does not provide any water mass information. In this study Nd isotopes preserved in fossil fish teeth/debris were used (Chapter 4; Basak et al., 2010) to identify the source and pathway of the water mass that delivered old carbon to the tropical Pacific during the last deglaciation.

CHAPTER 2
SEAWATER Pb ISOTOPES EXTRACTED FROM CENOZOIC MARINE SEDIMENTS

Overview

Variations in ocean circulation and continental weathering contribute to global climate change through the redistribution of heat and impacts on the carbon cycle. Seawater Nd, and Pb isotopes record information related to these processes; thus, it is critical to identify archives capable of recording and preserving these isotopic systems over geologic time scales. Owing to the short residence time of Nd (~200-1000 yrs; Tachikawa et al., 1999, 2003; Arsouze, 2009) compared to the ocean mixing time (~ 1500 yrs; Broecker and Peng, 1982) and distinct source inputs, Nd isotopic compositions can be used to track ocean circulation (Albareda and Goldstein, 1992; Albareda et al., 1997). In particular, different water masses have distinct Nd isotopic signatures that are acquired from continental inputs in the region of water mass formation. This signal, which is carried by water masses as they circulate through the oceans, can be altered by local weathering inputs, boundary exchange (Lacan and Jeandel, 2005) and reversible scavenging (Siddall et al., 2008; Jones et al., 2008) along the pathway. For this reason, Nd isotopes are often referred to as “quasi-conservative” tracers for water mass.

In contrast the residence time of Pb in the ocean (~50-200 yrs; Craig et al., 1973; Schaule and Patterson, 1981; Henderson and Maier-Reimer, 2002) is shorter than the Nd residence time. Therefore, seawater Pb isotopic compositions carry a combined signal of advection and weathering (Abouchami and Goldstein, 1995), which tends to be dominated by local weathering inputs. For this reason, Pb isotopic compositions are

often used to study changes in weathering provenance (Reynolds et al. 1999), as well as weathering regimes and rates (Foster and Vance, 2006).

Paleoceanographic studies of Nd isotopes have been conducted using a range of archives including Fe-Mn crusts, extracts of Fe-Mn oxides and hydroxides, fossil fish teeth/debris, and fossil foraminifera (for review see Martin et al., 2010). Early studies of Pb isotopic compositions in past seawater focused on Fe-Mn crusts (e.g. Abouchami et al., 1997; Burton et al., 1997; O'Nions et al., 1998; Reynolds et al., 1999; van de Flierdt et al., 2004; Foster and Vance, 2006); however, due to the slow accumulation rate this archive tends to integrate seawater signals over a period of 10^4-10^5 years (Frank, 2002). For higher resolution studies Gutjahr et al., (2007, 2009) recently used Pb isotopic compositions recorded in dispersed Fe-Mn oxides and hydroxides of bulk decarbonated marine sediments (henceforth referred to as 'Fe-Mn phases') on Holocene/ Pleistocene time scales. These Fe-Mn phases record bottom water Nd isotopic compositions (Rutberg et al., 2000; Palmer and Elderfield, 1985; Piotrowski et al., 2005; Martin et al., 2010), thus, they are believed to form at the sediment/water interface and to record bottom water Pb isotopic compositions as well.

Gutjahr et al. (2007) systematically studied sequentially leached fractions of several Pleistocene deep marine sediment samples and determined that Pb isotopic compositions obtained through reductive extraction of Fe-Mn phases are not perturbed by detrital contamination and the signal preserves seawater values. They then applied this technique to study continental weathering during the last deglaciation (Gutjahr et al., 2009; Kurzweil et al., 2010). Recently, Haley et al. (2008) extracted Pb isotopes from carbonate-free Arctic sediments (~ last 15Ma) to obtain reliable bottom water

values; however, these samples were unique compared to typical marine sediments because of the low carbonate contents. In this study we evaluate the seawater origin of Pb isotopic compositions obtained by reductive extraction of bulk samples on longer, Cenozoic time scales to test the integrity of this archive for paleoseawater studies. Although it is generally assumed that the Pb isotopes recovered by reductive extraction are derived from Fe-Mn phases in the form of oxides and hydoxides, the mineralogical sources of these isotopes have never been evaluated. Thus, we also evaluated the source of the extracted Pb using REEs and major element data. Finally, given that fossil fish teeth are well-established archives for bottom water Nd isotopic studies, we also test the suitability of this archive for Pb isotope work.

Methods

Sample Preparation

Ten deep sea sediment samples from ODP site 1090 in the Atlantic sector of the Southern Ocean were analyzed for this study. The samples range in age from mid Eocene to early Miocene (Channell et al., 2003) and their lithologies vary from mud-bearing diatom ooze and mud and diatom-bearing nannofossil ooze to chalk (Gersonde et al., 1999). In order to avoid contamination and minimize blank contributions during leaching, we used a slightly larger sample size than previous studies (Gutjahr et al., 2007, 2009). Approximately 1 gram of bulk sample was pulverized and homogenized with an agate mortar and pestle prior to chemical extraction.

Nd or Pb isotopes have been extracted from bulk marine sediments using several protocols (Chester and Hughes, 1967; Rutberg et al., 2000; Bayon et al., 2002; Tovar-Sanches et al., 2003; Piotrowski et al., 2004, 2005; Gutjahr et al., 2007; Martin et al., 2010). Although each protocol is slightly different all are guided by the principle of

exposing authigenically formed Fe-Mn phases to a reducing solution. The first step for all of the protocols is decarbonation of the bulk sediment. We used two decarbonation steps each with 20 mls of buffered 1M Na acetate in 2.7% optima glacial acetic acid (buffered to pH=5) followed by an additional decarbonation step in 10 mls of the buffered solution to insure complete carbonate removal. In order to minimize the blank in this reagent, which is largely contributed by the Na-acetate, we added 10-12 g of Chelex 100 cation exchange resin to a liter of buffered acetic acid and let the solution sit for at least 24 hours before filtering. The blank for this Chelex-cleaned buffered acetic acid is ~0.03 ppb and the reproducibility of Pb isotopic compositions extracted from samples decarbonated with this reagent improved remarkably.

Following decarbonation, the sample was centrifuged and two separate 5 ml aliquots of the supernatant were removed; one for isotopic analyses and one for elemental analyses. The remaining sample was triple rinsed in four times distilled water (4x H_2O) and then treated with 10 ml of 0.02 M Hydroxylamine hydrochloride (HH) in 25% acetic acid solution in order to reduce Fe-Mn phases. The sample and HH solution were mounted on a rotary shaker for 1.5 hrs and degassed. After centrifuging, the supernatant was divided into two 5 ml aliquots for isotopic and elemental analyses, and this fraction was designated the ‘first HH extraction.’ An additional 10 ml of fresh 0.02 M HH in 25% acetic acid solution were then added and allowed to react for 24 hours to insure complete reaction and removal of any remaining Fe-Mn phases. Again, the supernatant was divided into two 5 ml aliquots for isotopic and elemental analyses, and this fraction was designated as the ‘second HH extraction’. Unless specified, the general term ‘HH extraction’ refers to the first extraction. The aliquots set aside for

elemental analyses were analyzed for REE, U, Th, Pb, Mg, Al, Si, P, Ca, Mn, and Fe concentrations, while the isotopic fractions were analyzed for Sr, Nd, and Pb isotopic compositions.

The remaining detrital residues were triple rinsed with 4x H_2O and dried. Approximately 0.05 g of dried residue was powdered in a mortar and pestle and dissolved in a 1:2 mixture of concentrated HF: HNO_3 (Optima grade) in a clean teflon vial and allowed to react on a hot plate at >100°C for 24 to 48 hrs. Once the residues were completely dissolved, the solution was dried down in preparation for further analyses. As for the extracts, splits were collected for isotopic and elemental analyses.

Splits of each of the bulk sediment samples were also sieved using plastic sieves to avoid metal contamination. The coarse fractions (>125 μm) were dried and hand-picked for fossil fish teeth, which were then subjected to an oxidative/reductive cleaning to remove Fe-Mn oxide coatings (Boyle and Keigwin, 1985; Rosenthal et al., 1997). Two to three fossil fish teeth from each sample were combined and dissolved in a 1:1 solution of HNO_3 and HCl in preparation for Pb isotopic analyses.

Column Chemistry and Isotope Analyses

All sample preparation work for elemental and isotopic work was done in a class 1000 clean lab in the Department of Geological Sciences at the University of Florida (UF). Aliquots separated for isotopic work were dried down before being re-dissolved in 1N seastar HBr and passed through Dowex 1X-8 (100-200 mesh) resin (Manhes et al., 1978). Pb was collected in 20% Optima HNO_3 and the eluted 1N HBr waste contained the REEs and Sr. This waste fraction was collected in clean Teflon vials and dried down for subsequent Sr and Nd column chemistry. Sr and REEs were separated using a primary column with Mitsubishi resin and 1.6N HCl as an eluent. The Sr cuts were dried,

re-dissolved in 100 µl of 3.5 M HNO_3, and passed through cation exchange columns containing Sr-spec resin (Eichrom Technologies,Inc.) to further purify Sr from other ions (Pin and Bassin, 1992). Nd was isolated by passing the REE aliquot through Ln-spec resin with 0.25N HCl as an eluent. Collected Pb, Nd and Sr concentrates were dried and re-dissolved in 2% optima HNO_3 in preparation for analysis on the Nu Plasma Multi-Collector Inductively Coupled Plasma Mass Spectrometer (MC-ICPMS) at UF. Measured procedural blanks were 20 pg Pb, 14 pg Nd and 100 pg for Sr.

A Tl normalization technique was used for Pb isotope analyses (Kamenov et al., 2004). Tl spiked Pb concentrates dissolved in 2% HNO_3 were adjusted for appropriate dilution to obtain a 2-5 V beam on ^{208}Pb. Samples were aspirated through a Nu-Instruments desolvating nebulizer (DSN-100) into the plasma source. Long term NBS 981 values analyzed over several years at UF are $^{206}Pb/^{204}Pb$=16.937 (2σ =0.004), $^{207}Pb/^{204}Pb$=15.489 (2σ =0.003), and $^{208}Pb/^{204}Pb$=36.695 (2σ =0.008). In order to better constrain the overall external reproducibility (including the chemical extraction, column chemistry, and MC-ICPMS analyses), an UF in-house standard was prepared by mixing multiple deep sea sediments. Four runs of this UF in-house standard processed through the HH extraction protocol yielded values of 39.041(+/-0.006), 15.667(+/- 0.003), 18.862 (+/- 0.006), for $^{208}Pb/^{204}Pb$, $^{207}Pb/^{204}Pb$, and $^{206}Pb/^{204}Pb$ respectively.

Similar to Pb isotope work, Nd samples were diluted with unspiked 2% HNO_3 and aspirated into the source of the MC-ICPMS using the DSN-100 nebulizer. Preamplifier gain calibrations were run before the beginning of each analytical session. All Nd isotope data reported in this study were analyzed using a time-resolved analysis (TRA) method (Kamenov et al., 2008). Prior to sample introduction baseline was measured for

30 seconds. Data were then acquired in a series of 0.2 seconds integrations over 1-3 minutes. All reported $^{143}Nd/^{144}Nd$ ratios were corrected for mass fractionation using $^{146}Nd/^{144}Nd$ =0.7219. International standard JNdi-1 was analyzed between every 5-6 unknown samples and the average of these standard runs was compared to the long term TIMS JNdi-1 value of 0.512103 to determine a correction factor for each of the samples analyzed on that day. Long term external reproducibility of JNdi-1 is 0.000014 (0.3 ε_{Nd} units).

Sr isotopes were analyzed on the Nu-Plasma MC-ICPMS in wet plasma mode using the same TRA method. Each sample was normalized to $^{86}Sr/^{88}Sr$ =0.1194. All analyses used on-peak measured zeros determined on clean 2% HNO_3 to correct for isobaric interferences due to Kr impurities in the Ar gas. The long-term average value of the TRA-measured $^{87}Sr/^{86}Sr$ of NBS 987 is 0.710246 (+/- 0.000030, 2σ).

Major Elements and REE Analyses

Aliquots saved for REE, U, Th, Pb, and major element concentration measurements were dried down and re-dissolved in 5% HNO_3 (spiked with 8 ppb Re-Rh) prior to analysis on an Element II ICP-MS at UF. All analyses were done at medium resolution with Re and Rh as an internal standard to correct for instrumental drift. All concentration measurements were based on calibration curves generated using a set of gravimetrically prepared dilutions of commercial ICP-MS standard (SPEX CertiPrep, Inc.). USGS whole rock standards (AGV-1, BCR-2) and USGS Fe-Mn nodule standards (NOD-A1, NOD-P1) were frequently analyzed to test the quality of concentration measurements. Reported elemental concentrations were corrected for the analyzed acid blank measured at the beginning. Long term error based on multiple AGV-1 and BCR-2 analyses was +/- 5%.

Results

Pb Isotopes in Sequentially Extracted Fractions

All three Pb isotope systems produce ratios that are within error for the first and second HH extractions for Eocene to Miocene samples, with values ranging between 18.69-18.81 ($^{206}Pb/^{204}Pb$), 15.65-15.67 ($^{207}Pb/^{204}Pb$), and 38.76-38.86 ($^{208}Pb/^{204}Pb$) (Figure 2-1; Table 2-1). The Pb isotopic compositions from the acetic acid decarbonation fraction also agree within error with the HH extractions for all of the Miocene and many of the Eocene - Oligocene samples; however, one Oligocene and one Eocene acetic acid fraction plot well above the HH data, particularly for $^{207}Pb/^{204}Pb$ and $^{208}Pb/^{204}Pb$, while one Eocene acetic acid fraction plots well below the HH data for $^{208}Pb/^{204}Pb$ (Figure 2-1).

Residue $^{206}Pb/^{204}Pb$, $^{207}Pb/^{204}Pb$, and $^{208}Pb/^{204}Pb$ values range from 18.65-18.79, 15.64-15.66, and 38.76-38.88 respectively. $^{206}Pb/^{204}Pb$ values of the Eocene residues tend to be less radiogenic than the HH and acetic acid fractions, while the Oligocene residues are more radiogenic, and the Miocene residues agree with other fractions within error. In contrast, the residues tend to have $^{207}Pb/^{204}Pb$ values that are slightly lower, but generally within error of the other fractions, and $^{208}Pb/^{204}Pb$ values that are within error or slightly higher than the other fractions.

Pb Isotopes Compositions in Fossil Fish Teeth

$^{206}Pb/^{204}Pb$, $^{207}Pb/^{204}Pb$, and $^{208}Pb/^{204}Pb$ isotopic ratios were analyzed for fossil fish teeth hand-picked from the same samples as the extractions (Figure 2-2; Table 2-2). $^{206}Pb/^{204}Pb$, and $^{208}Pb/^{204}Pb$ isotopic compositions measured in fossil fish teeth were corrected for ingrowth of radiogenic Pb using measured U/Pb and Th/Pb concentration ratios. Because of the low abundance of ^{235}U in the samples, corrections

for ingrowth of ^{207}Pb on $^{207}Pb/^{204}Pb$ ratios are negligible. Similar corrections were not made for the HH extractions because accurate U/Pb and Th/Pb ratios were not obtained in the extracts and data from Fe-Mn oxide nodules (Axelsson et al., 2002) indicated that expected ratios were too small to require correction for Eocene to Miocene material. Measured Pb isotopic compositions for corrected fossil fish teeth, and HH extractions do not agree within error or exhibit any systematic relationship (Figure 2-2A, B). There is a general correlation between the magnitude of the correction and the age of the fossil fish teeth with older teeth requiring a greater correction (Figure 2-2D, E), but in detail the correction factor depends on U/Pb and Th/Pb ratios as well as age of the fossil fish teeth.

Major Elements in Fe-Mn Extracted Fraction

A suite of major elements (Mg, Al, Ca, Mn, Fe, P; Table 2-3) was analyzed for all fractions (Table 2-3). Major elements measured in HH extractions were compared to Pb concentrations in order to identify the source of the Pb in the extracted fractions, although this analysis might be complicated by multiple sources. A plot of Ca vs. Pb shows no distinct relationship, and three of the samples record anomalously high Ca and Pb concentrations (Figure 2-3A). These three outliers have been excluded in subsequent elemental plots. Mn and Pb exhibit a strong correlation (R^2 =0.94); however, much of this correlation is guided by a single high point for both elements (Figure2- 3B). A wide range of Fe, Mg, and P concentrations are found to correspond with very narrow range of Pb concentrations, suggesting no clear relationship between these elements and Pb.

REE in HH Extractions

Rare earth element patterns obtained from the HH extraction of NOD-A1 and NOD-P1 (representing Atlantic and Pacific oceans respectively) exhibit pronounced negative Ce anomalies and a slight middle REE bulge (Figure 2-4A). The middle REE bulge is similar to patterns reported for most site 1090 samples in this study (Figure 2-4B), as well as patterns reported in other studies that employed an extraction technique (Haley et al., 2004, Gutjahr et al., 2007; Martin et al., 2010). In comparison, REE values derived from the total digestion of nodule standard NOD-A1 and NOD-P1 exhibit a slight to prominent positive Ce anomaly and a slightly reduced middle REE bulge (Axelsson et al., 2002; Figure 2-4A). Three samples in this study had middle rare earth patterns that did not match the characteristic MREE bulge for HH extractions (Figure 2-4B). These same samples had anomalously high Ca, Mn, and Pb concentrations and low P concentrations in the HH extractions (Table 2-4) suggesting there is something fundamentally different about these samples.

The acetic acid, HH extractions (first and second), and residue fractions form individual clusters on a plot of HREE/LREE ((Tm+Yb+Lu)/(La+Pr+Nd)) vs. MREE/MREE* ((Gd+Ty+Db)/[(Tm+Yb+Lu+La+Pr+Nd)/2]) (Figure 2-4C), indicating a common source for each fraction. The first HH extractions for the three samples with anomalous REE patterns plot outside of the HH cluster (Figure 2-4C); however, the second HH extractions for these samples plot within the cluster.

Discussion

Integrity of Pb Isotopes from HH Extractions

To qualify as an effective archive for deepwater Pb, the Pb isotopic compositions chemically extracted from decarbonated bulk sediments must be: a) reproducible, b)

unaffected by detrital components present during the extraction, and c) record bottom seawater values. Two sets of seven Paleogene deep sea samples were analyzed a year apart using the same protocol and the measured Pb isotope values for each sample are within reported external error (Figure 2-5A; Table 2-5). Three Holocene samples from the North Atlantic reported in Gutjahr et al. (2009) were also analyzed at UF and these replicate Pb isotopic compositions are also within error of reported values (Figure 2-5A). Thus, both intra- and inter-lab comparisons illustrate that our extraction protocol produces reproducible results.

One of the concerns of any chemical extraction technique is whether the procedure specifically targets the desired phases and does not introduce contamination from other phases, such as the detrital fraction. Although we specifically selected weak reagents and short leaching times, it is still important to verify that there is no contamination. One test for detrital contamination is to evaluate Al concentrations in the extracts based on the assumption that all Al is sourced from detrital material. This technique assumes there is no Al in the leachable fraction, therefore it tends to overestimate the detrital contribution to extraction solutions. Pb isotope values from the HH extractions were adjusted for the percent contribution from the detrital fraction based on the mass balance equations below, following a technique used by Gutjahr et al., (2007) for Sr isotopes.

$$[Pb]_{\%\ contrib.\ of\ detrital\ Pb} = [Al]_{HH\ extraction}/[Al]_{residue}$$

$$[Pb]_{detrital\ contrib.\ in\ HH\ extraction} = [Pb]_{\%\ contrib.\ of\ detrital\ Pb} * [Pb]_{residue}$$

$$[Pb]_{sw\ contrib.\ in\ HH\ extraction} = [Pb]_{HH\ extraction} - [Pb]_{detrital\ contr.\ in\ HH\ extraction}$$

$$^{206}Pb/^{204}Pb_{\text{sw corrected}} = \frac{([Pb]_{\text{HH extraction}} * {}^{206}Pb/^{204}Pb_{\text{HH extraction}}) - ([Pb]_{\text{detrital contr. in HH extraction}} * {}^{206}Pb/^{204}Pb_{\text{residue}})}{[Pb]_{\text{sw contrib. in HH extraction}}}$$

A comparison of $^{206}Pb/^{204}Pb$ values measured in the HH extractions and values corrected assuming all Al is derived from the detrital fraction illustrates that measured and corrected values plot within error (Figure 2-5B). Therefore, even using the worst case scenario that all Al is derived from the detrital fraction, detrital contamination did not impact the Pb isotopic compositions of our samples. We recommend testing for detrital contamination on a case by case or site by site basis, especially for samples from regions with very low carbonate contents and high clay fractions, since different lithologies may produce different results.

Given that detrital contamination did not affect the measured seawater Pb isotopic values, the similarity between seawater and residue Pb values in some of our samples requires an alternative explanation. One possibility is that for the relevant time intervals continental weathering input dominated the seawater Pb isotopic values. Therefore, these isotopic comparisons may be useful for understanding past weathering regimes.

Another important aspect of this study was to demonstrate that Pb isotope values obtained through chemical extraction represents bottom water Pb. This verification is complicated by the fact that bottom water Pb isotopic compositions are not known for older samples and even modern samples are likely to be compromised by anthropogenic Pb. $^{87}Sr/^{86}Sr$ ratios have been used in several Nd extraction studies to

demonstrate the seawater origin of Nd isotopic compositions (Rutberg et al., 2000; Piotrowski et al., 2005; Gutjahr et al., 2007; Martin et al., 2010). However, these studies point out that this is a highly conservative test. Many samples have unaltered Nd isotopic compositions despite the fact that Sr isotopic compositions have been altered, because Sr tends to be more mobile in the sediment than Nd. Similarly, any disagreement between the Sr isotopic values of HH extractions (Table 2-6) and the seawater curve does not necessarily imply that the Pb isotopic compositions are altered. In contrast, agreement between Sr isotopic compositions in HH extractions and the seawater curve tends to confirm the seawater origin of the extractions, assuming there is no residual carbonate with seawater Sr isotope values remaining after the de-carbonation step. Fifty percent of the $^{87}Sr/^{86}Sr$ ratios in our HH extractions do agree with seawater values (Figure 2-5C), which suggest, but does not insure, a seawater origin for the Pb isotopic compositions in those samples.

Additional support for the seawater origin of the Pb isotopic compositions in the HH extractions can be obtained by comparing the HH extraction values to another archive from the same environment. This has been done successfully for Nd isotopes by comparing HH extractions and fossil fish teeth (Martin et al., 2010), because fish teeth have been shown to record bottom water values (Martin and Scher, 2004). However, based on this study, fish teeth do not appear to be robust archives for Pb isotopic compositions. Instead, we again compare Nd isotopes in the site 1090 HH extractions (Table 2-6) and fish teeth and illustrate that both record the same bottom water value (Figure 2-5D). Pb is very particle reactive and, thus, should be even less

mobile than Nd; therefore, a seawater origin for Nd in the HH extraction argues for a seawater origin for Pb as well.

Further evidence for a seawater origin of Pb in HH extractions comes from studies of modern sediments. It is well-known that anthropogenic Pb has a very distinct isotopic signal that dominates modern seawater Pb (e.g., Wu and Boyle, 1997; Alleman et al. 1999). Therefore, analyses of core top Fe-Mn oxyhydroxides should record an anthropogenic Pb signal. Hamelin et al. (1989) analyzed leachates of modern surface sediments in the Atlantic and did recover anthropogenic Pb isotopic compositions indicating that the Pb dissolved in the ambient seawater is faithfully recorded in the leachable fractions. Furthermore, a recent study of low-temperature Fe-Mn oxyhydroxide sediments precipitating in the Mediterranean Sea also recovered a strong signal of anthropogenic Pb (Kamenov et al., 2009). Overall, these studies of modern sediments indicate that Fe-Mn phases efficiently scavenge Pb derived from ambient seawater.

Finally, Pb isotopic compositions from Fe-Mn crusts and nodules are considered to be accurate proxies for ambient seawater. These crusts/nodules have a similar mineralogy to the Fe-Mn phases (Martin et al., 2010) that are believed to contribute Pb during the HH extraction. In addition, Pb isotope values for HH extracts from Fe-Mn nodule standards NOD-A1 and NOD-P1 (Table 2-1) are similar to published values derived from total digestion of these standards (Baker et al., 2004), suggesting the extraction procedure does not introduce analytical artifacts perturbing the isotopic ratios. In the absence of direct measurements of Pb in deep water samples or another Pb isotope archive known to record bottom water, these lines of indirect evidence provide

the strongest argument that Pb isotopic compositions in the chemical extractions record bottom water values.

The Pb isotopes measured in the acetic acid fractions are broadly in agreement with the Pb isotopic compositions measured in the HH extractions, which could indicate that the de-carbonation step is dissolving Fe-Mn phases on the carbonate (Gourlan et al., 2008). Alternatively, carbonates are the major contributor to the acetic acid fraction, thus Pb introduced from this fraction is likely to record a surface water signal while HH extractions are believed to record a deep water signal. Agreement between these two fractions suggests little stratification of the Pb isotopes with depth in the water column for these samples.

Fossil Fish Teeth as a Pb Isotope Archive

Fossil fish teeth are one of the most robust archives for bottom water Nd studies (Martin and Scher, 2004) and they have been applied in numerous studies of deep ocean circulation (e.g., Scher and Martin, 2004, 2006, 2008; Via and Thomas, 2006; Thomas and Via, 2007; Newkirk and Martin, 2009; Roberts et al., 2010). However, fossil fish teeth have never been tested as a suitable archive for Pb. In order to qualify as an archive for deepwater Pb isotopes we need to understand the source of Pb, U, and Th to the fossil fish teeth and also understand whether the hydroxyflouroapatite behaves as a closed system.

Concentrations of Pb reported for fossil fish teeth in this study range from 30-366 ppm (Table 2-7), while modern fish teeth analyzed during the course of this study contained 0.5-2.6 ppm. Based on these modern and fossil fish teeth Pb concentrations, the initial Pb incorporated during the life of the fish represents a maximum of 8.6% of the total Pb in fossilized fish teeth samples. The higher concentrations of Pb in fossil

teeth presumably represent post-mortem or early diagenetic enrichment by several orders of magnitude, similar to that observed for Nd (Martin and Haley, 2000; Martin and Scher, 2004). In that case, the post-mortem or early diagenetic Pb is likely to record deep water isotopic values that dominate the Pb isotopic signal of the fossil fish teeth. Substitution and adsorption are the two most commonly discussed enrichment mechanisms for REE, Pb, Th and U in biogenic apatite (Reynard et al., 1999; Trueman and Tuross, 2002; Grun et al., 2010). For the Pb system, both daughter and parent isotopes are incorporated during early diagenesis. As a result, Pb isotopic compositions in fossil fish teeth are comprised of a complex mixture of unknown proportions of initial Pb presumably reflecting shallow seawater incorporated *in vivo*, early diagenetic Pb with a deep water isotopic composition and radiogenic Pb produced *in situ.*

Given that the initial Pb concentration constitutes a small percentage of the total Pb pool in the fossil fish teeth, seawater Pb isotopes incorporated during early diagenesis are likely to dominate the system, indicating that suitable corrections for radiogenic Pb ingrowth should yield pristine bottom water Pb isotopic compositions if the teeth behave as a closed system. Unfortunately, the magnitude of correction vs. age (Figure 2-2D, E; Table 2-2) for Pb isotopes suggests that they exhibit open system behavior with respect to U, Th, and/or Pb. As figure 2-2 illustrates, the relationships between teeth and HH fractions are complex. In some cases, the corrected fish teeth plot below the HH fractions indicating either recent addition of U or Pb loss, which leads to overcorrection. In other cases the corrected ratios are higher than the HH fraction, suggesting either recent U loss or Pb addition, which leads to undercorrection. However, in one sample both the measured and corrected ratios plot below the HH

fraction suggesting that a high initial Pb or intial Pb with very different isotopic signature compared to the bottom water may have played a role in the Pb isotope systematics. In summary, these data demonstrate that the teeth do not behave as a suitable archive for bottom water Pb isotopes.

Previous studies attempting U-series dating of bones have also concluded that bones remain an open system with respect to U (Pike et al., 2002). Similar claims of open system behavior in fossil fish teeth has also been made with respect to REE mobilization; although the open system behavior was not pervasive enough to alter the geochemically useful Nd isotopic signal acquired during early diagenesis (Kocsis et al., 2010).

Our study suggests that fossil fish teeth are not a suitable archive for seawater Pb isotopic studies due to presence of initial Pb, variable U, Th, Pb uptake and loss leading to unconstrained proportion of radiogenic growth, and open system behavior. However, there are limited data for Pb isotopic compositions of fossil fish teeth in the marine environment and this archive should be carefully evaluated with a larger data set spanning both older and younger samples before rejecting it as a suitable archive for paleoceanographic work.

Phases Contributing Pb to the HH Extraction: Major Elements

Although the correlation between Mn and Pb is dominated by one high point, these two elements generate the most robust correlation measured between Pb and any major element, which supports the idea that Mn oxides are a major phase contributing Pb. Published Mn/Fe ratios for complete digestion of the nodule standards range between ~1.6-5.0 (Axelsson et al., 2002). Mn/Fe ratios measured on HH extracts of NOD-A1 and NOD-P1 during the course of this study ranged from 3.6-4.6. The seven

HH extracts from site 1090 with normal REE patterns exhibit Mn/Fe ratios that varied between 0.74 and 3.70. Thus, measured Mn/Fe ratios in HH extracts from site 1090 are similar to the total range (i.e. 1.6-5.0) obtained from HH extracts and complete digestion of NOD-A1 and NOD-P1, again supporting the idea that Fe-Mn oxides are one of the major contributing phases to the total major element pool in the HH extracts.

The three HH extraction samples with anomalously high Ca and Mn concentrations and uncharacteristic REE patterns have Ca concentrations that are even higher than concentrations measured in the acetic acid fractions (Table 2-3). These three samples were also the only samples that degased during the first HH extraction step. These anomalous samples also have high Mn/Fe ratios of 9.9 to 49.5, which are well beyond measured Mn/Fe ratios for Fe-Mn oxides, suggesting the presence of a Mn-rich phase that survived the buffered acetic acid dissolution step. Pure manganoan carbonate is one possible Mn-rich, dissolution-resilient phase (best represented by a mixed manganese-calcium-magnesium carbonate) (Mucci, 2004).

Boyle (1983) documented the presence of manganoan carbonate, specifically 'kutnahorite,' in marine sediments. Kutnahorite has a general formula of $Ca(Mn,Mg(CO3)_2)$ and commonly occurs as overgrowths on foraminiferal calcite surfaces. X-ray diffraction, geochemistry, and laser ablation studies of foraminiferal calcite tests later revealed the presence of kutnahorite or a kutnahorite-like phase (known as 'pseudokutnahorite' due to its disordered structure, but similar chemical composition) in marine sediments (Pena et al., 2005, 2008a). Authigenic manganoan carbonates could be common in the carbonate-rich environment (Boyle, 1983) of site 1090 (35-80% carbonate) and precipitation in the sediment would suggest a deep water

geochemistry. The relative stability of this phase demonstrated by preferential dissolution in the HH extraction rather than the buffered acetic acid step, suggests it might have a chemical composition closer to the structurally ordered kutnahorite, which is more resistant to dissolution than disordered or pseudokutnahorite (Mucci, 1991).

Thus, data on Fe/Mn ratios and anomalously high Ca and Mn concentrations in some HH extracts suggest contributions from Fe-Mn oxides and manganoan carbonates respectively, indicating that the Pb measured in the HH extracts is sourced from multiple phases. However, both of these phases are authigenic minerals that form in bottom waters close to the sediment water interface. Thus, both should record the same bottom water isotopic values.

Phases contributing Pb to the HH extraction : REEs

The middle REEs (MREE) bulge pattern observed in reductive extracts has typically been attributed to Fe-Mn oxides (Bayon et al., 2002; Gutjahr et al., 2007), with an emphasis on Fe-oxides (Haley et al., 2004). With the exception of multi-valant Ce (III and IV) and Eu (II and III), the REEs are a group of trivalent elements that decrease in ionic radii with increasing atomic number. Seawater REE patterns, which have a prominent negative Ce anomaly and relatively heavy REEs enrichment, can be explained by conversion of Ce(III) to insoluble Ce(IV) and preferential scavenging of light REEs (LREE) compared to HREE from the surface ocean by organics, and detrital particles (Elderfield and Grieves, 1982; Elderfield, 1988). Authigenically precipitated Fe-Mn phases in the ocean do not incorporate this seawater pattern, instead preferential scavenging of MREE produces a characteristic MREE bulge in the oxide phase that is apparent in the HH fractions as well (Axelsson et al., 2002; Haley et al., 2004; Gutjahr et al., 2007; Martin et al., 2010). A similar MREE bulge pattern is also produced by

phosphates (Byrne et al., 1996; Martin et al., 2010). Thus, MREE patterns observed in HH extracts could indicate extraction from Fe-Mn oxides or from phosphates.

To evaluate the contribution of Pb from phosphates we compared P and Pb concentrations in the acetic acid fractions and HH extractions. Concentrations of P in the buffered acetic acid fraction (buffered at pH=5) range from 0.02 - 282.0 ppm (Table 2-3), while concentrations in the HH extractions (pH<5) range from 8 - 407 ppm. Both of these fractions tend to have higher concentrations than HH extractions of NOD-A1 and NOD-P1, which contained 12.7 – 27.2 ppm P. Higher concentrations in the site 1090 samples suggest a source of P other than Fe-Mn oxides; however, there is no positive correlation between [P] and [Pb] in the HH extracts, which argues against phosphate as a major source of Pb, as does the fact that the teeth record different Pb isotopic compositions than the HH extracts. Charette et al. (2005) extracted oxides from bulk sediments and found high P association with Fe (hydr)oxides, which he attributed to P adsorbed on Fe-(hydr)oxides. Well-defined changes in phosphate sorption by iron oxyhydroxides defined by P/Fe ratios have also been reported for the last 3 Gyr of earth's ocean chemistry evolution, indicating a close relationship between adsorbed phosphate and Fe oxyhydroxides (Planavsky et al., 2010). Thus, an alternative source of high P concentration in the extracts could be absorbed phosphates.

Trivalent REE patterns are remarkably similar for both HH extractions and total digestions of NOD-A1 and NOD- P1 (Figure 2-4A); however, multivalent Ce patterns yield a positive Ce anomaly in the HH extractions and a negative Ce anomaly in the complete digestions of standards (Figure 2-4A). This fractionation of Ce during the HH extraction procedure suggests that the reducing solution, which re-mineralizes other

REEs effectively, must not have a strong enough reduction potential to reduce Ce(IV) oxides. These results are distinct from Gutjahr et al (2010), who report a positive Ce anomaly for their HH extracts of NOD-A1 and NOD-P1. While this study and Gutjahr et al. (2010) used broadly comparable extraction methods, Gutjahr et al. (2010) employed an additional $MgCl_2$ step and used a slightly stronger reducing solution. They also exposed smaller amounts of sediments to similar volumes of HH solution. These small differences in technique appear to produce very different results, implying that the extraction of Ce may be sensitive to subtle differences in technique and studies of Ce anomalies based on HH extractions should be viewed with caution.

In order to distinguish between different potential REE sources in different fractions we have made a HREE/LREE vs. MREE/MREE* plot using the same ratios employed by Martin et al. (2010) (Figure 2-4C). The first and second HH extractions and standard nodule HH extracts generally fall within a narrowly defined same field. Detrital residues and acetic acid fractions also plot in distinct fields, although the acetic acid field covers a relatively large range. Clustering of HH and standard nodule extracts indicates a common source for the REE in these fractions supporting the idea that a primary Pb archive in our extraction procedure is Fe-Mn oxyhydroxides and that the extraction protocol does not attack the detrital fractions, which plot in a different field. Martin et al., (2010) also showed that published fossil fish teeth and pore waters occupy the same space as the HH extracts. The three anomalous first HH extraction samples that have flatter REE patterns (open circles in Figure 2-4B) also plot separately in HREE/LREE vs. MREE/MREE* space. Coupled with their distinct major element concentrations these data imply a unique REE source, possibly manganoan carbonate

as suggested by major element data. The second HH extractions from these three samples plot in the main HH field, suggesting the Mn-carbonate is largely removed during the first HH extraction step. Overall, figure 2-4C illustrates that HREE/LREE and MREE/MREE* data may be a useful tool to test for cross contamination between the major fractions that constitute a typical deep sea sample before making paleoceanographic interpretations.

Summary

Pb isotopes were analyzed for the acetic acid fractions, first and second HH fractions, and detrital fractions for ten samples ranging in age from mid Eocene to early Miocene from ODP site 1090 on the Agulhus Ridge. The acetic acid and HH extraction fractions all tend to produce $^{206}Pb/^{204}Pb$, $^{207}Pb/^{204}Pb$, and $^{208}Pb/^{204}Pb$ values that are within error. Agreement between Pb isotopic compositions for these fractions either indicates a common deep water source or no water column stratification with respect to Pb isotopic compositions for these samples. Excellent inter- and intra-lab reproducibility of Pb isotope in the HH extracts illustrates that the extraction protocol used in this study is an effective method for recovering seawater Pb isotopic compositions.

Additional evidence for a seawater origin of the Pb isotopic compositions obtained from HH extraction includes a number of indirect tests, such as an Al mass balance approach to evaluate the impact of detrital contaminants, comparison of Sr isotopic compositions from the HH extraction and the seawater Sr isotope curve, and comparison of Nd isotopic compositions from the HH extraction and co-existing fossil fish teeth. We recommend applying the Al mass balance test to confirm low inputs from detrital material, particularly in low carbonate settings. Nodule standard NOD-A1 and NOD-P1 are recognized to record ambient bottom water isotopic signatures and close

agreement between total digestion and HH extracted Pb isotopic compositions from these nodules also indicates that the HH extracted Pb isotopes represent bottom water values. Thus, all tests suggest that the measured Pb isotopic compositions in HH extractions are not only seawater, but presumably record bottom water values.

Fish teeth are one of the most widely accepted archives for deep ocean Nd isotopic compositions, but this study demonstrated that the total Pb pool in fossil fish teeth is composed of an unconstrained combination of initial Pb incorporated in the biophosphate, Pb incorporated during diagenetic enrichment, and radiogenic Pb produced from *in situ* decay of U and Th. A comparison of Pb isotopes measured on fossil fish teeth, and corrected for radiogenic growth in the teeth shows little correlation with isotopes from HH extractions, suggesting that fish teeth have a tendency to behave as an open system with exchange of U, Pb, and Th between the teeth and surrounding waters. It is impossible to correct for this exchange, thus fish teeth may not be effective archives for paleo Pb isotope studies. This evaluation is based on samples from one site and a limited age range, thus a more systematic evaluation of fossil fish teeth archive is warranted.

Elemental data do not show any strong correlation between most major elements and Pb; however, there is a positive correlation between [Mn] and [Pb] based largely on one high data point suggesting a predominance of Mn oxides. Anomalously high Ca and Mn concentrations in HH extracts of three samples that also have anomalous REE patterns suggest the presence of a Mn-bearing, refractory carbonate phase, such as manganoan carbonate. Therefore, Fe-Mn oxides, and Mn-carbonate appear to be

potential sources of the Pb isotope signals. Both of these phases form at the sediment water interface and record the bottom water signal.

A characteristic MREE bulge which is very often attributed to the presence of oxides, is observed in most of the HH extracts. In addition, clustering of most HH extracts with nodule standards in HREE/LREE vs. MREE/MREE* space indicates that Fe-Mn oxides may be the dominant source of Pb. The three samples with anomalous REE patterns and elemental concentrations that plot outside the acetic acid, HH, and residue clusters presumably reflect the manganoan carbonate source. These results illustrate that the REE crossplot is an effective tool for identifying cross contamination or unique sources.

A comparison between chemical analyses of completely dissolved Fe-Mn nodule standards and HH extractions from these same standards reveals a typical MREE bulge pattern for trivalent REEs for both fractions, however, there is apparent fractionation with respect to multivalent Ce (using the extraction procedure reported in this study). Changes in the strength of the HH solution and sediment-to-solution ratio may yield more quantitative extraction of Ce. Thus caution is advised when interpreting Ce anomalies from HH extractions, but these extractions from bulk deep sea sediments appear to be excellent recorders of bottom water Pb isotopes.

Table 2-1. Pb isotopes in different bulk sediment fractions from ODP site 1090

	Age(Ma)	mcd	$^{206}Pb/^{204}Pb$	$^{207}Pb/^{204}Pb$	$^{208}Pb/^{204}Pb$
Acetic decarbonation					
1090D,11-4A,38-41	20.31	104.91	18.777	15.658	38.843
1090E,11-5A,72-75	20.79	110.73	18.755	15.655	38.836
1090E,12-3A,71-74	21.61	116.62	18.775	15.656	38.846
1090D,17-3A,18-21	25.06	162.96	18.749	15.696	38.905
1090D,19-3A,90-93	26.98	185.45	18.729	15.655	38.800
1090B,31-1W,16-19	35.58	293.85	18.705	15.646	38.758
1090B,37-1W,124-126	37.68	342.99	18.727	15.651	38.754
1090B,38-2W,123-126	38.71	352.32	18.686	15.652	38.754
1090B,38-7W,42-46	39.51	361.01	18.733	15.656	38.776
1090B,40-3W,124-126	41.26	375.03	19.018	15.694	38.941
First HH Extraction					
1090D,11-4A,38-41	20.31	104.91	18.782	15.651	38.838
1090E,11-5A,72-75	20.79	110.73	18.768	15.656	38.856
1090E,12-3A,71-74	21.61	116.62	18.774	15.657	38.852
1090D,17-3A,18-21	25.06	162.96	18.723	15.656	38.827
1090D,19-3A,90-93	26.98	185.45	18.739	15.660	38.830
1090B,31-1W,16-19	35.58	293.85	18.714	15.655	38.808
1090B,37-1W,124-126	37.68	342.99	18.730	15.650	38.759
1090B,38-2W,123-126	38.71	352.32	18.690	15.652	38.765
1090B,38-7W,42-46	39.51	361.01	18.735	15.658	38.782
1090B,40-3W,124-126	41.26	375.03	18.808	15.671	38.846
NOD-A1			18.958	15.674	38.917
NOD-P1			18.696	15.630	38.662
Second HH Extraction					
1090D,11-4A,38-41	20.31	104.91	18.776	15.654	38.846
1090E,11-5A,72-75	20.79	110.73	18.766	15.655	38.853
1090E,12-3A,71-74	21.61	116.62	18.772	15.655	38.847
1090D,17-3A,18-21	25.06	162.96	18.725	15.659	38.828
1090D,19-3A,90-93	26.98	185.45	18.733	15.656	38.811
1090B,31-1W,16-19	35.58	293.85	18.700	15.650	38.804
1090B,37-1W,124-126	37.68	342.99	18.730	15.650	38.762
1090B,38-2W,123-126	38.71	352.32	18.693	15.654	38.775
1090B,38-7W,42-46	39.51	361.01	18.738	15.658	38.789
1090B,40-3W,124-126	41.26	375.03	18.819	15.670	38.852
Residues					
1090D,11-4A,38-41	20.31	104.91	18.763	15.651	38.849
1090E,11-5A,72-75	20.79	110.73	18.757	15.652	38.861
1090E,12-3A,71-74	21.61	116.62	18.763	15.656	38.865
1090D,17-3A,18-21	25.06	162.96	18.768	15.659	38.878
1090D,19-3A,90-93	26.98	185.45	18.763	15.655	38.852
1090B,31-1W,16-19	35.58	293.85	18.676	15.646	38.821
1090B,37-1W,124-126	37.68	342.99	18.706	15.644	38.764
1090B,38-2W,123-126	38.71	352.32	18.650	15.646	38.757
1090B,38-7W,42-46	39.51	361.01	18.706	15.652	38.769
1090B,40-3W,124-126	41.26	375.03	18.791	15.664	38.837

Long term NBS 981 values analyzed over several years on the MC-ICPMS at UF are $^{206}Pb/^{204}Pb$ =16.937 (2σ=0.004), $^{207}Pb/^{204}Pb$=15.489 (2σ=0.003), and $^{208}Pb/^{204}Pb$=36.695 (2σ=0.008).

Table 2-2. Pb isotopes measured in fossil fish teeth

Fossil fish teeth	Age(Ma)*	$^{208}Pb/^{204}Pb$	$^{207}Pb/^{204}Pb$	$^{206}Pb/^{204}Pb$	Corrected $^{206}Pb/^{204}Pb$	Corrected $^{208}Pb/^{204}Pb$
1090D,11-4A,38-41	20.31	38.805	15.643	18.776	18.742	38.793
1090E,11-5A,72-75	20.79	38.822	15.654	18.781	18.741	38.810
1090E,12-3A,71-74	21.61	38.845	15.658	18.869	18.802	38.837
1090D,17-3A,18-21	25.06	38.671	15.646	18.687	18.634	38.651
1090D,19-3A,90-93	26.98	38.785	15.653	18.748	18.717	38.775
1090B,31-1W,16-19	35.58	38.776	15.633	18.744	18.640	38.717
1090B,37-1W,124-126	37.68	38.749	15.649	18.790	18.701	38.697
1090B,38-2W,123-126	38.71	38.920	15.697	18.812	18.750	38.829

* Age model after Channell et al. (2003)

Long term NBS 981 values analyzed over several years on the MC-ICPMS at UF are $^{206}Pb/^{204}Pb$ =16.937 (2σ=0.004), $^{207}Pb/^{204}Pb$=15.489 (2σ=0.003), and $^{208}Pb/^{204}Pb$=36.695 (2σ=0.008).

Table 2-3. Major elements in different bulk sediment fractions from ODP Site 1090.

	Mg	Al	Si	P	Ca	Mn	Fe	Pb	Al/Pb	Mn/Fe
Acetic decarbonation										
1090D,11-4A,38-41	647	-*	141	-*	6162	614	13.54	0.51	-*	45.37
1090E,11-5A,72-75	1181	-*	290	24	3378	448	-*	0.90	-*	-*
1090E,12-3A,71-74	1618	17	338	192	1017	200	-*	1.15	15	-*
1090D,17-3A,18-21	1601	11	327	282	58	396	5.00	0.57	19	79.28
1090D,19-3A,90-93	1618	34	450	216	557	732	2.62	1.13	30	279.39
1090B,31-1W,16-19	1432	-*	235	44	2470	1530	0.27	2.73	-*	-*
1090B,37-1W,124-126	868	9	295	17	2762	1364	-*	2.91	3	-*
1090B,38-2W,123-126	1020	-*	270	118	743	410	-*	1.29	-*	-*
1090B,38-7W,42-46	-*	-*	-*	-*	-*	-*	-*	1.47	-*	-*
1090B,40-3W,124-126	397	-*	24	-*	6116	403	-*	0.47	-*	-*
First HH Extraction	Mg	Al	Si	P	Ca	Mn	Fe	Pb	Al/Pb	Mn/Fe
1090D,11-4A,38-41	51	47	45	12	18448	236	4.75	0.31	151	49.55
1090E,11-5A,72-75	128	224	119	281	135	21	12.19	0.14	1555	1.68
1090E,12-3A,71-74	159	268	158	273	63	96	25.85	0.47	571	3.71
1090D,17-3A,18-21	112	154	154	166	31	19	12.75	0.14	1127	1.53
1090D,19-3A,90-93	96	153	134	319	58	24	9.61	0.19	811	2.53
1090B,31-1W,16-19	68	157	116	347	77	24	32.67	0.09	1669	0.74
1090B,37-1W,124-126	41	94	161	407	70	21	16.28	0.17	543	1.27
1090B,38-2W,123-126	12	38	93	395	39	5	3.65	0.09	407	1.50
1090B,38-7W,42-46	70	29	76	21	12154	103	10.39	1.14	25	9.92
1090B,40-3W,124-126	131	14	30	8	38704	268	10.02	3.87	4	26.75
NOD-A1	1918	808	400	27	349	6037	1673.09	0.12	6538	3.61
NOD-P1	1291	332	683	13	133	5226	1135.63	0.07	4795	4.60
Second HH Extraction	Mg	Al	Si	P	Ca	Mn	Fe	Pb	Al/Pb	Mn/Fe
1090D,11-4A,38-41	65	155	97	44	718	11	23.31	0.11	1354	0.46
1090E,11-5A,72-75	350	549	261	19	777	33	42.62	0.47	1167	0.76
1090E,12-3A,71-74	491	903	403	27	739	184	140.54	1.14	792	1.31
1090D,17-3A,18-21	484	677	364	9	376	64	59.97	0.65	1036	1.07
1090D,19-3A,90-93	472	510	379	7	575	56	47.17	0.80	635	1.19
1090B,31-1W,16-19	255	243	273	10	491	19	84.76	0.38	636	0.22
1090B,37-1W,124-126	403	161	400	11	1003	46	34.50	0.52	309	1.34
1090B,38-2W,123-126	142	56	296	103	439	16	22.45	0.10	545	0.71
1090B,38-7W,42-46	92	158	244	945	2790	50	20.75	0.24	672	2.42
1090B,40-3W,124-126	45	70	116	226	1272	25	14.06	0.16	448	1.79

Table 2-3. Continued

Residue	Mg	Al	Si	P	Ca	Mn	Fe	Pb	Al/Pb	Mn/Fe
1090D,11-4A,38-41	11165	71510	479	189	8715	899	38606	13.93	5133	0.02
1090E,11-5A,72-75	11656	67094	494	183	7498	1050	38966	13.91	4822	0.03
1090E,12-3A,71-74	11003	66095	1508	211	8992	1907	38617	14.84	4454	0.05
1090D,17-3A,18-21	12183	75618	1556	169	7461	1376	38969	14.84	5094	0.04
1090D,19-3A,90-93	8081	44635	1627	101	4320	773	23011	9.49	4702	0.03
1090B,31-1W,16-19	9436	40557	786	68	7049	235	27498	4.18	9700	0.01
1090B,37-1W,124-126	19728	74079	4127	99	12792	676	54202	10.27	7216	0.01
1090B,38-2W,123-126	14436	86119	546	150	17479	1056	44024	17.32	4972	0.02
1090B,38-7W,42-46	13340	73907	887	1023	21502	1409	40025	18.98	3895	0.04
1090B,40-3W,124-126	15460	71878	1020	212	13725	1687	45079	8.76	8207	0.04

-* no data

Table 2-4. REE data in different bulk sediment fractions from ODP site 1090.

Acetic decarbonation	La	Ce	Pr	Nd	Sm	Eu	Gd	Tb	Dy	Ho	Er	Tm	Yb	Lu
1090D,11-4A,38-41	1.00	1.13	0.15	0.63	0.12	0.03	0.13	0.02	0.14	0.03	0.10	0.02	0.12	0.02
1090E,11-5A,72-75	1.08	1.85	0.20	0.94	0.22	0.06	0.26	0.04	0.29	0.07	0.24	0.04	0.33	0.06
1090E,12-3A,71-74	3.03	5.15	0.72	3.73	0.91	0.24	1.09	0.15	1.00	0.22	0.65	0.08	0.59	0.10
1090D,17-3A,18-21	4.52	9.86	1.19	6.08	1.47	0.38	1.75	0.25	1.54	0.33	0.97	0.13	0.89	0.15
1090D,19-3A,90-93	3.11	6.84	0.72	3.73	0.89	0.24	1.11	0.16	1.04	0.23	0.69	0.10	0.68	0.11
1090B,31-1W,16-19	1.69	1.68	0.22	0.90	0.18	0.06	0.20	0.03	0.25	0.06	0.21	0.04	0.29	0.05
1090B,37-1W,124-126	1.34	2.57	0.22	0.99	0.22	0.06	0.25	0.04	0.27	0.06	0.19	0.03	0.21	0.03
1090B,38-2W,123-126	1.07	2.25	0.22	1.20	0.31	0.09	0.43	0.06	0.39	0.09	0.27	0.04	0.25	0.04
1090B,38-7W,42-46	0.91	0.91	0.12	0.48	0.10	0.03	0.11	0.02	0.13	0.03	0.11	0.02	0.16	0.03
1090B,40-3W,124-126	0.96	0.92	0.12	0.47	0.09	0.03	0.09	0.02	0.11	0.03	0.09	0.01	0.12	0.02
First HH extraction	La	Ce	Pr	Nd	Sm	Eu	Gd	Tb	Dy	Ho	Er	Tm	Yb	Lu
1090D,11-4A,38-41	1.37	1.93	0.25	0.76	0.13	0.04	0.10	0.02	0.11	0.02	0.07	0.01	0.08	0.01
1090E,11-5A,72-75	1.89	4.32	0.83	3.85	1.05	0.27	0.93	0.13	0.67	0.12	0.33	0.04	0.30	0.04
1090E,12-3A,71-74	2.34	4.93	1.00	4.62	1.22	0.30	1.03	0.15	0.80	0.14	0.38	0.05	0.36	0.05
1090D,17-3A,18-21	0.72	2.18	0.32	1.49	0.42	0.10	0.35	0.05	0.26	0.04	0.12	0.02	0.11	0.02
1090D,19-3A,90-93	1.01	2.98	0.43	2.04	0.56	0.14	0.48	0.07	0.37	0.07	0.18	0.02	0.16	0.02
1090B,31-1W,16-19	1.26	3.37	0.48	2.20	0.56	0.13	0.48	0.07	0.35	0.06	0.17	0.02	0.15	0.02
1090B,37-1W,124-126	0.51	1.80	0.24	1.14	0.33	0.08	0.27	0.04	0.20	0.03	0.09	0.01	0.08	0.01
1090B,38-2W,123-126	0.56	2.01	0.26	1.29	0.38	0.09	0.32	0.05	0.24	0.04	0.11	0.01	0.10	0.01
1090B,38-7W,42-46	1.17	2.08	0.21	0.78	0.15	0.05	0.14	0.02	0.18	0.04	0.12	0.02	0.13	0.02
1090B,40-3W,124-126	3.10	3.60	0.42	1.34	0.20	0.06	0.15	0.03	0.21	0.04	0.14	0.02	0.18	0.02
NOD-A1	6.63	7.25	1.46	7.39	1.81	0.48	2.19	0.29	1.52	0.31	0.86	0.11	0.72	0.12
NOD-P1	5.19	2.54	1.77	9.12	2.51	0.64	2.51	0.35	1.71	0.31	0.84	0.11	0.78	0.13
Second HH extraction	La	Ce	Pr	Nd	Sm	Eu	Gd	Tb	Dy	Ho	Er	Tm	Yb	Lu
1090D,11-4A,38-41	0.60	1.14	0.23	1.04	0.25	0.06	0.23	0.03	0.16	0.03	0.08	0.01	0.06	0.01
1090E,11-5A,72-75	2.70	5.60	1.01	4.46	1.04	0.25	0.96	0.13	0.73	0.14	0.37	0.05	0.30	0.04
1090E,12-3A,71-74	4.00	7.64	1.47	6.36	1.48	0.35	1.32	0.19	1.04	0.19	0.53	0.07	0.46	0.06
1090D,17-3A,18-21	1.94	5.33	0.74	3.15	0.76	0.18	0.65	0.09	0.51	0.09	0.25	0.03	0.22	0.03
1090D,19-3A,90-93	2.23	6.10	0.86	3.81	0.94	0.23	0.85	0.12	0.66	0.12	0.33	0.04	0.28	0.04
1090B,31-1W,16-19	1.56	3.65	0.52	2.32	0.54	0.13	0.50	0.07	0.37	0.07	0.18	0.02	0.15	0.02
1090B,37-1W,124-126	0.86	2.64	0.35	1.65	0.44	0.10	0.37	0.05	0.26	0.05	0.12	0.02	0.10	0.01
1090B,38-2W,123-126	0.33	1.09	0.14	0.67	0.18	0.04	0.15	0.02	0.10	0.02	0.05	0.01	0.04	0.01
1090B,38-7W,42-46	3.90	8.72	1.36	6.19	1.45	0.38	1.40	0.19	1.08	0.21	0.57	0.07	0.46	0.06
1090B,40-3W,124-126	0.44	1.35	0.19	0.91	0.24	0.06	0.21	0.03	0.15	0.03	0.07	0.01	0.06	0.01

Table 2-4. Continued

Residues	La	Ce	Pr	Nd	Sm	Eu	Gd	Tb	Dy	Ho	Er	Tm	Yb	Lu
1090D,11-4A,38-41	28.86	55.35	7.26	26.74	4.94	1.37	4.63	0.67	3.76	0.73	2.11	0.28	1.80	0.25
1090E,11-5A,72-75	33.93	64.72	8.34	30.54	5.71	1.51	5.42	0.79	4.60	0.91	2.63	0.36	2.28	0.31
1090E,12-3A,71-74	30.58	58.27	7.74	28.14	5.30	1.46	4.97	0.74	4.34	0.84	2.49	0.35	2.28	0.31
1090D,17-3A,18-21	23.37	53.52	5.78	20.55	3.76	1.08	3.32	0.48	2.77	0.54	1.64	0.24	1.59	0.22
1090D,19-3A,90-93	17.42	39.70	4.41	16.37	3.07	0.85	2.92	0.43	2.50	0.50	1.46	0.20	1.31	0.19
1090B,31-1W,16-19	19.52	40.04	4.49	16.65	3.04	0.90	2.96	0.43	2.48	0.49	1.38	0.18	1.15	0.16
1090B,37-1W,124-126	26.97	69.12	7.15	27.15	5.33	1.60	4.93	0.72	4.00	0.76	2.13	0.28	1.78	0.24
1090B,38-2W,123-126	40.69	107.58	10.78	40.85	8.12	2.70	7.27	1.04	5.87	1.12	3.19	0.44	2.85	0.39
1090B,38-7W,42-46	98.08	200.44	25.80	97.72	19.44	5.24	18.75	2.75	16.16	3.10	8.89	1.16	7.26	0.96
1090B,40-3W,124-126	38.35	96.60	10.67	41.25	8.18	2.26	7.66	1.10	6.35	1.23	3.50	0.46	2.81	0.37

All data are normalized to initial sample bulk weight and concentrations are expressed in µg/g

Table 2-5. Inter and intra laboratory Pb isotope duplicates of authigenic Fe-Mn phases.

	mbsf	$^{208}Pb/^{204}Pb$	$^{207}Pb/^{204}Pb$	$^{206}Pb/^{204}Pb$
1139A-27R,1W,15-20	252.5	38.940	15.633	18.659
Duplicate		38.961	15.634	18.662
1139A-27R,02W,20-25	255	38.904	15.612	18.543
Duplicate		38.913	15.613	18.556
1139A,30R,01W,26-31	282	38.886	15.613	18.542
Duplicate		38.900	15.621	18.548
1139A,35R,2W,34-38	332.5	38.827	15.645	18.669
Duplicate		38.834	15.649	18.665
1139A,38R,4W,9-13	356	38.841	15.633	18.566
Duplicate		38.847	15.636	18.570
1139A,40R,3W,0-4	375	38.780	15.618	18.552
Duplicate		38.769	15.614	18.547
1139A,40R,1W,12-16	385	38.889	15.665	18.768
Duplicate		38.876	15.661	18.758
12JCP, 4250m*				
50cm		39.532	15.690	19.330
77cm		39.217	15.667	19.137
251cm		38.882	15.632	18.939

All data are normalized to NIST SRM 981 values as reported in Galer and Abouchami (1998).
Duplicate samples were chemically processed and analyzed one year after the initial samples.
* Replicate of samples from Gutjhar er al.(2009) analyzed at UF.

Table 2-6. Sr and Nd isotopes measured in authigenic Fe-Mn phases.

First HH extraction	Age(Ma)[1]	$^{87}Sr/^{86}Sr$[2]	$^{143}Nd/^{144}Nd$[3]	$\varepsilon_{Nd(t)}$
1090D,11-4A,38-41	20.31	0.708093	0.512234	-7.38
1090E,11-5A,72-75	20.79	0.708403	0.512199	-8.05
1090D,12-3A,71-74	21.61	0.708304	0.512211	-7.80
1090D,17-3A,18-21	25.06	0.708125	0.512245	-6.71
1090D,19-3A,90-93	26.98	0.708052	0.512247	-6.96
1090B,31-1W,16-19	35.58	0.707759	0.512275	-6.20
1090B,37-1W,124-126	37.68	0.70854	0.512231	-7.00
1090B,38-2W,123-126	38.71	0.707594	0.512248	-6.65
1090B,38-7W,42-46	39.51	0.707576	0.512239	-6.80
1090B,40-3W,124-126	41.26	0.707664	0.512164	-8.22

[1] Age model after Channell et al.(2003)

[2]Sr ratios were measured in a static mode and using time resolved analysis (TRA) on a Nu MC-ICPMS and $^{87}Sr/^{86}Sr$ ratios were corrected for mass-bias using an exponential law and $^{87}Sr/^{88}Sr$=0.1194. The long-term average value of the TRA-measured $^{87}Sr/^{86}Sr$ of NBS 987 is 0.710246 (+/- 0.000030, 2σ).

[3]All reported $^{143}Nd/^{144}Nd$ ratios were corrected for mass fractionation using $^{146}Nd/^{144}Nd$ =0.7219. International standard JNdi-1 was analyzed between every 5-6 unknown samples and the average of these standard runs were compared to a long term TIMS JNdi-1 value of 0.512103 to determine a correction factor for each of the samples analyzed on that day. Long term external reproducibility of JNdi-1 analyses on the Nu is 0.000014 (0.3 ε_{Nd} units).

Table 2-7. Measured Pb, U, and Th concentrations in fossil and modern fish teeth.

Fossil fish teeth	Age (Ma)	[Pb]	[U]	[Th]
1090D,11-4A,38-41	20.31	191.62	28.53	31.25
1090E,11-5A,72-75	20.79	161.34	28.10	25.72
1090E,12-3A,71-74	21.61	50.95	13.86	4.81
1090D,17-3A,18-21	25.06	102.74	19.33	23.06
0190D,19-3A,90-93	26.98	366.61	37.23	36.58
1090B,31-1W,16-19	35.58	17.30	4.51	7.91
0190B,37-1W,124-126	37.68	29.96	6.24	11.38
1090B,38-2W,123-126	38.71	38.14	5.38	24.62
Modern fish teeth		[Pb]	[U]	[Th]
13_14_Mackerel		0.71	0.24	0.15
13_14_Mackerel_Replicate		0.49	0.24	0.13
15_16_Mackerel		1.25	0.30	0.16
15_16_Mackerel_Replicate		2.03	0.27	0.14
7_8_unknown		2.61	0.25	0.13
7_8_unknown_Replicate		1.62	0.23	0.12
23_24_Halibut		1.48	0.26	0.13
23_24_Halibut_Replicate		0.55	0.24	0.12

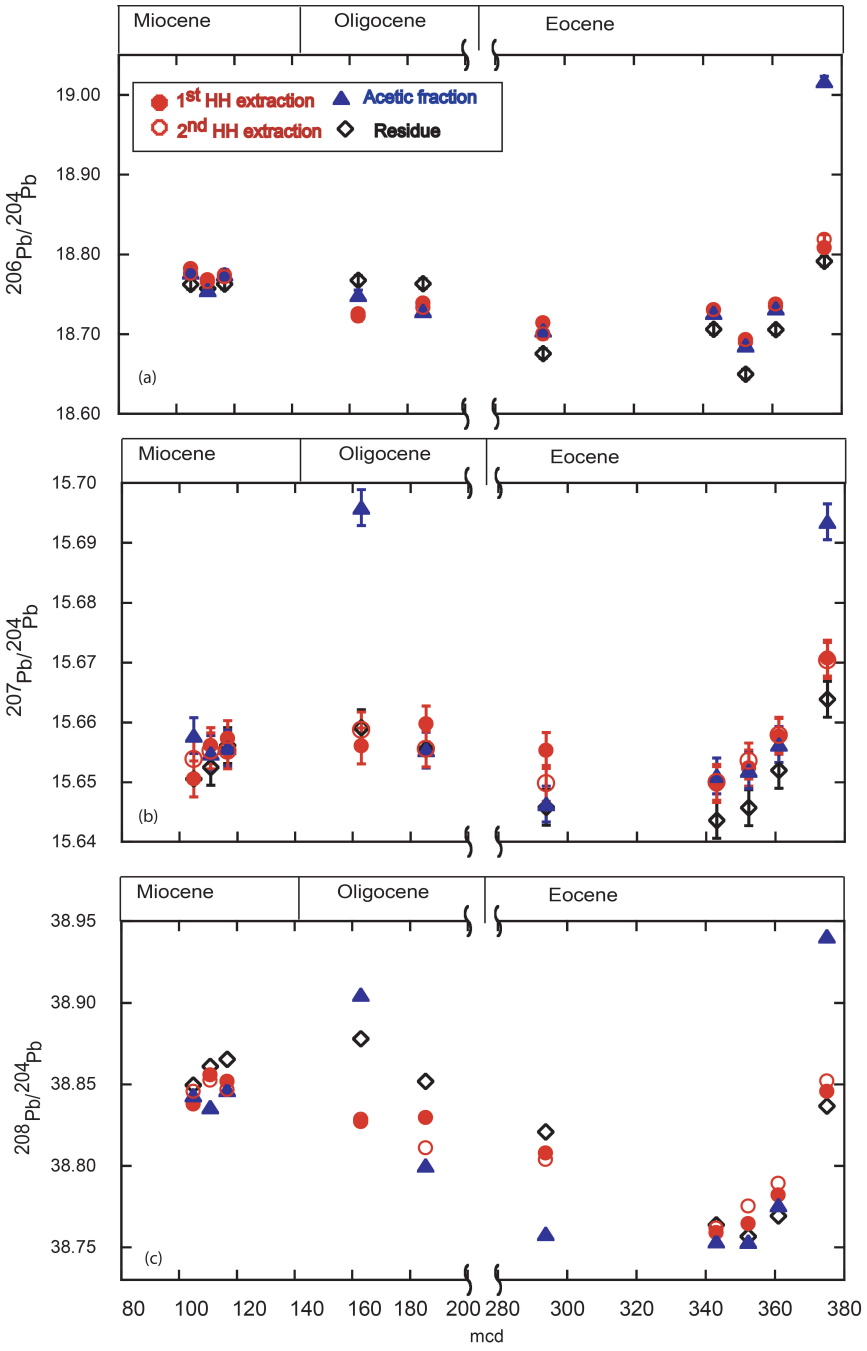

Figure 2-1. Pb isotopes measured in the initial acetic acid decarbonation fraction, the first and second HH extraction, and residues from deep sea sediments at ODP site 1090 ranging in age from mid Eocene to early-Miocene. (a) $^{206}Pb/^{204}Pb$, (b) $^{207}Pb/^{204}Pb$, and (c) $^{208}Pb/^{204}Pb$.

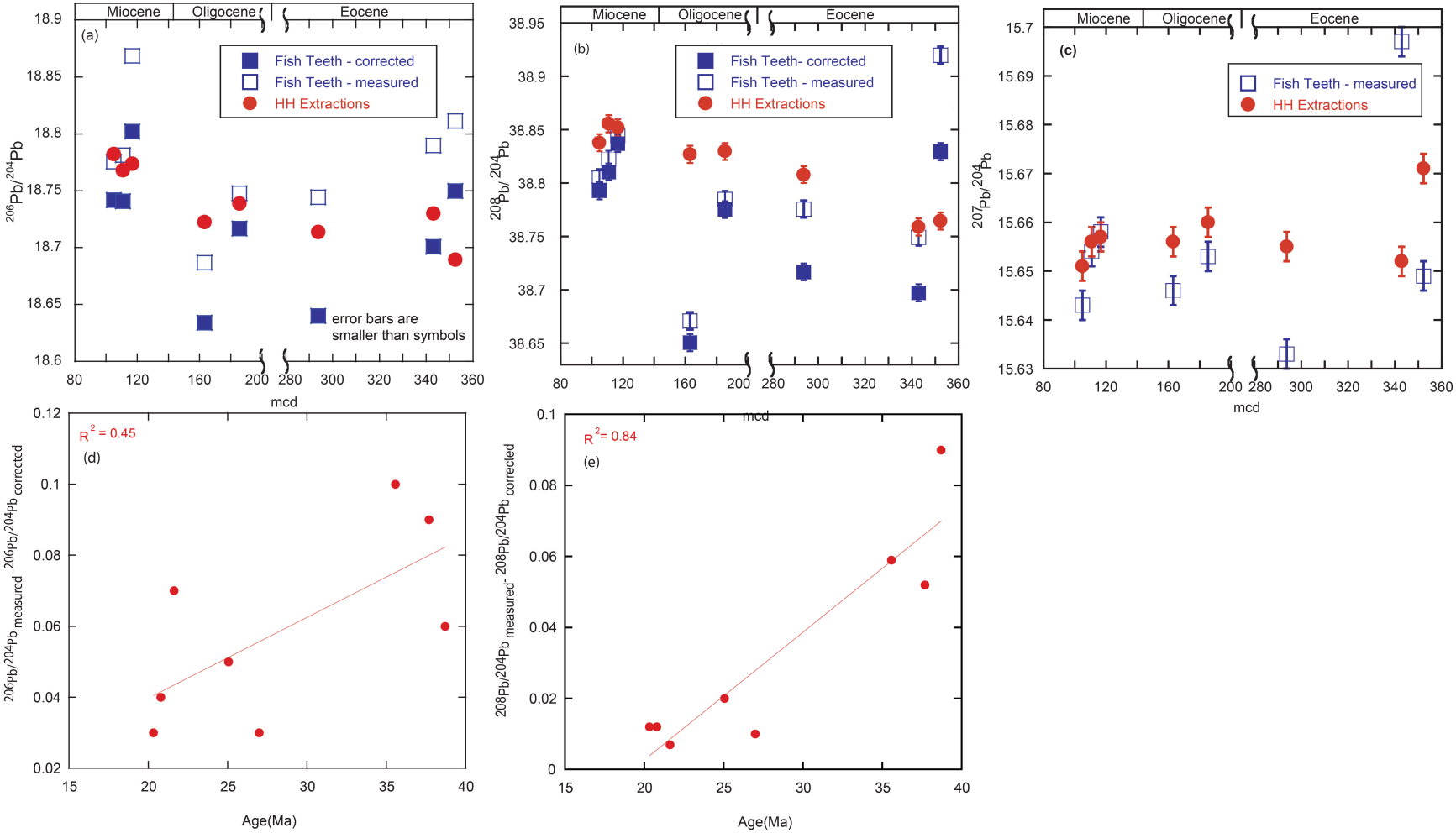

Figure 2-2. Measured Pb isotopic values for fossil fish teeth, fossil fish teeth corrected for radiogenic growth, and for HH extractions plotted against depth (meters composite depth) (a) $^{206}Pb/^{204}Pb$ and (b) $^{208}Pb/^{204}Pb$, (c) $^{207}Pb/^{204}Pb$ (fossil fish teeth were not corrected for this system). (d) The magnitude of the correction for radiogenic Pb ingrowth for $^{206}Pb/^{204}Pb$ and (e) $^{208}Pb/^{204}Pb$ in fossil fish teeth plotted against age illustrates a poorly defined relationship with age.

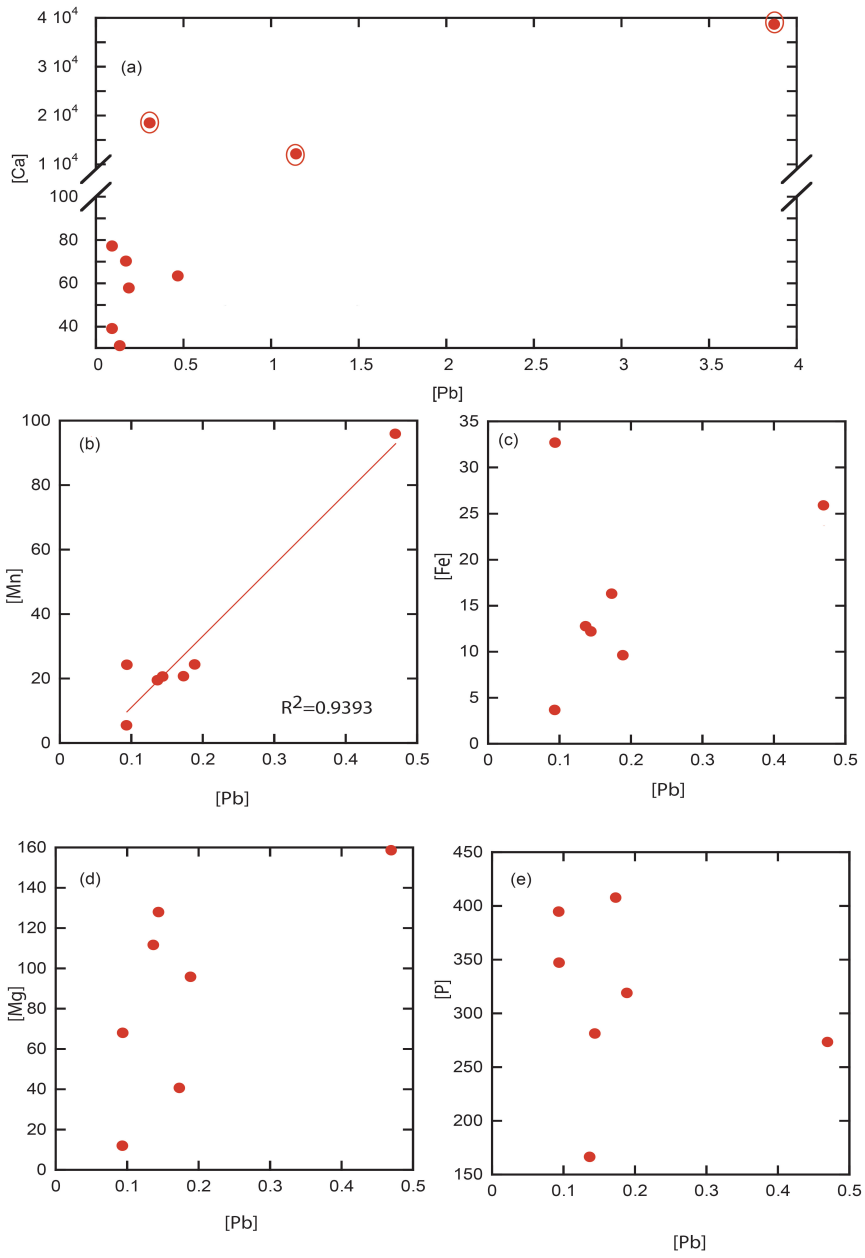

Figure 2-3. Plots showing relationship of measured major elemental concentrations with respect to Pb concentrations. (a) Pb vs. Ca concentrations for all ten site 1090 HH extractions. The three circled data points are with anomalously high [Ca]. Pb concentrations vs. (b) Mn, (c) Fe, (d) Mg, and (e) P major element concentrations for the seven first HH extractions with typical REE patterns. [Pb] vs. [Mn] is the only plot with a positive linear correlation, indicating that most of the Pb in the HH extraction is coming from Mn-bearing phases. In contrast, the other [Pb] vs. [major element] plots do not illustrate a coherent increase in Pb that correlates with an increase in the major element.

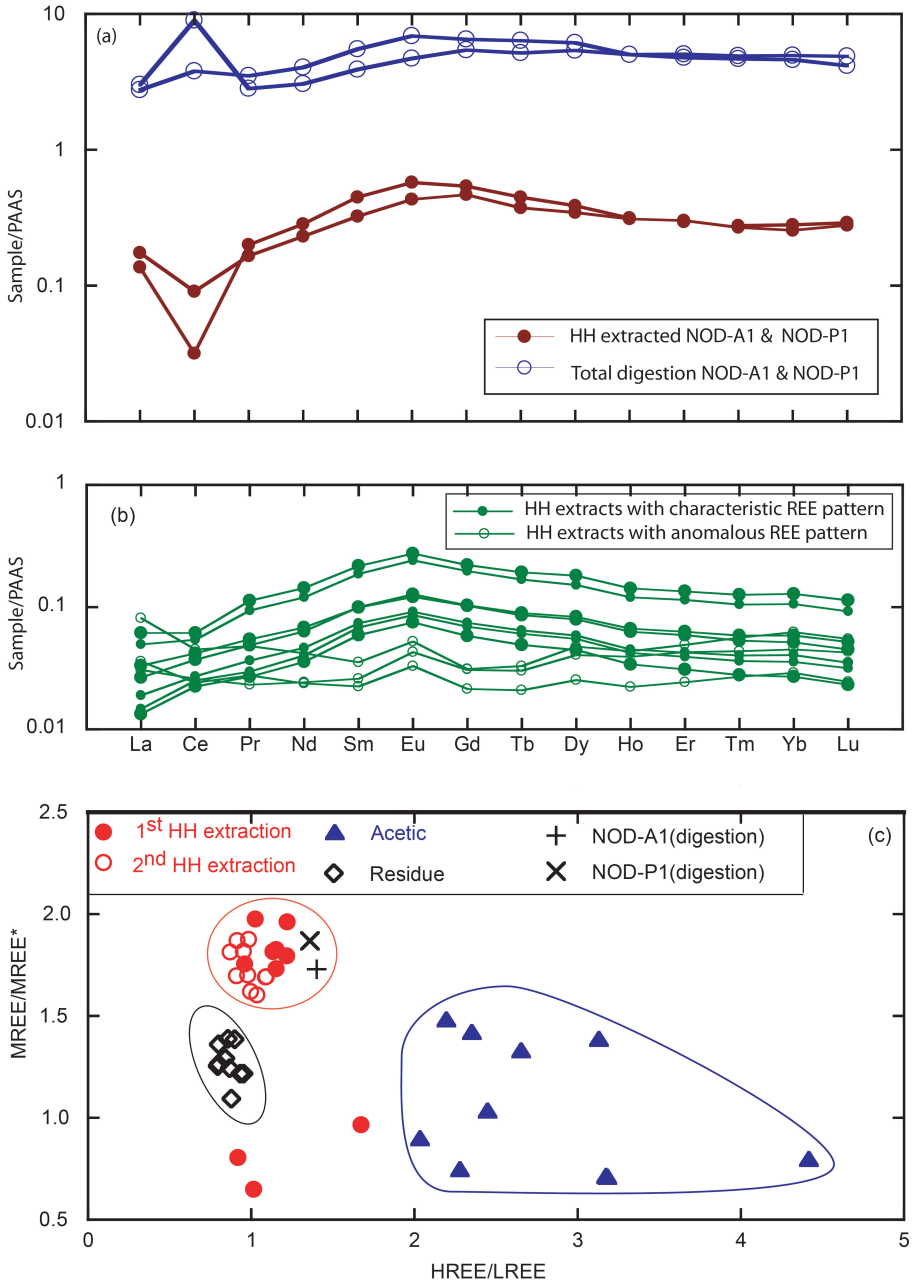

Figure 2-4. Plots showing REE behavior of the extracted fractions. (a) REE patterns normalized to Post-Archean Australian Shale (PAAS, Taylor and McLennan, 1985) for nodule standards NOD-A1 and NOD-P1. Blue open circles are published data for a total digestion of the standards (Axelsson et al., 2002). Brown filled circles represent measured values for HH extractions. (b) REE/PAAS patterns for HH extractions from all samples from ODP site 1090. Green filled circles represent samples that exhibit a typical MREE bulge. Green open circles represent samples with unusual REE patterns that also have unusual major element concentrations. (c) A comparison of PAAS normalized HREE/LREE ((Tm+Yb+Lu)/(La+Pr+Nd)) vs. MREE/MREE* ((Gd+Ty+Db)/average of HREE and LREE) for all fractions.

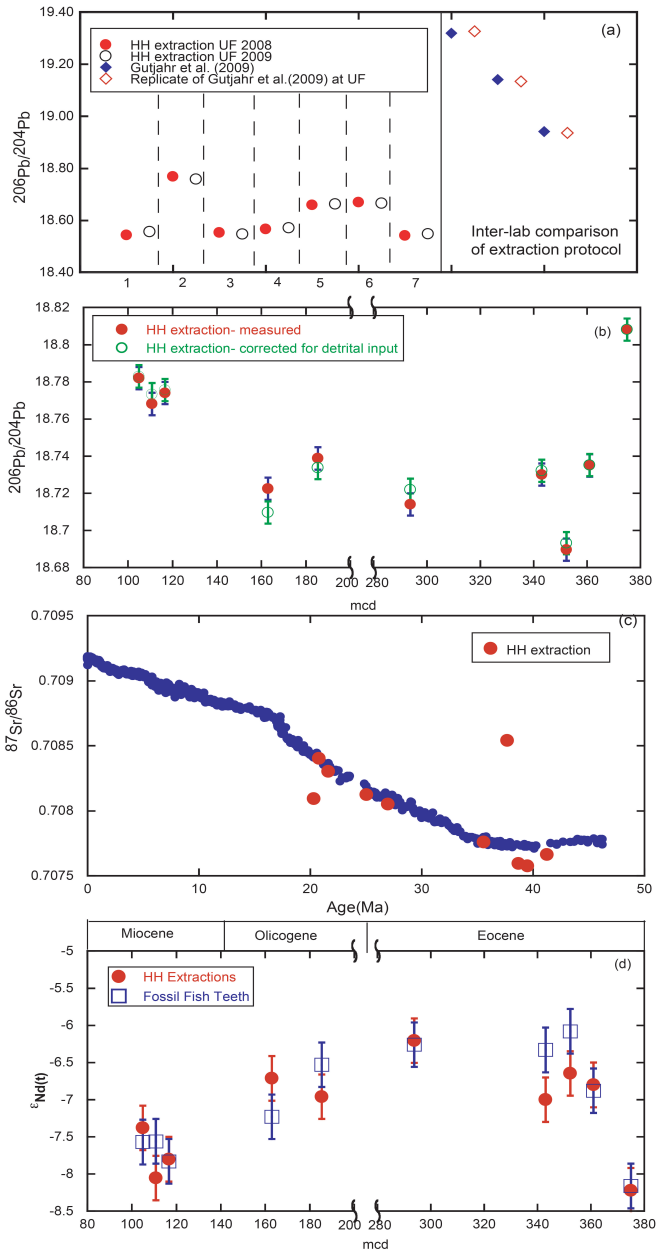

Figure 2-5. Compilation of plots showing the reproducibility and integrity of the extraction procedure. (a) A plot of seven replicate $^{206}Pb/^{204}Pb$ ratios for HH extractions from ODP site 1139 measured one year apart at UF and three samples from Blake Nose (Gutjahr et al., 2009) that were also analyzed at UF. Error bars are smaller than symbols (b) A plot of $^{206}Pb/^{204}Pb$ vs. depth comparing measured HH extraction values to values that have been corrected for detrital contamination based on [Al]. (c) $^{87}Sr/^{86}Sr$ vs. age for the seawater curve (blue circles; Hodell and Woodruff (1994), Farrell et al. (1995), Mead and Hodell (1995), and Martin et al. (1999)) and HH extractions from this study (red circle for HH extractions and fossil fish teeth (Scher and Martin, 2006) illustrates excellent agreement between the two archives.

CHAPTER 3
WEATHERING HISTORY OF ANTARCTICA DURING THE EOCENE-OLIGOCENE TRANSITION

The initiation of Antarctic continental glaciation at the end of the Eocene is one of the most dramatic climate events in the Cenozoic. Although ephemeral glaciers have been documented during the late Eocene (Browning et al., 1996; Tripati et al., 2005), continental-scale glaciers that reached the sea did not develop until the Eocene-Oligocene boundary ~ 34Ma ago. This interval has been intently studied due to both the rate and magnitude of this climatic phenomenon. Several mechanisms have been proposed to explain the onset of the Antarctic cryosphere. These include thermal isolation of Antarctica due to tectonic gateway processes (Kennett, 1977), and decreasing greenhouse gas concentrations (primarily CO_2) below a threshold value (DeConto and Pollard, 2003) combined with orbitally-paced climate cycles (Palike et al., 2006).

In addition to massive continental ice growth, the Eocene-Oligocene (E/O) greenhouse to icehouse transition is characterized by a rapid two step increase in benthic foraminifera $\delta^{18}O$ (~1.5‰), worldwide deepening of the calcite compensation depth (CCD) by ~1 km, a positive shift in seawater $\delta^{13}C$ (Coxall et al., 2005), occurrences of ice rafted debris (IRD) in the Southern Ocean (Zachos et al., 1992), and a shift in clay mineral assemblages from smectite to illite and chlorite in the Southern Ocean (Robert and Kennett, 1997; Robert et al. 2002). While ice growth and deep water cooling can explain the shifts in oxygen isotopes, they do not account for the carbon isotope shift or deepening of the CCD. Instead these changes have been attributed to increased carbon burial (Zachos et al., 1996; Salamy and Zachos, 1999), increased silicate weathering (Ravizza and Peucker-Ehrenbrink, 2003; Zachos and Kump, 2005),

increased export production of global siliceous plankton (Coxall et al., 2005), and a shift in $CaCO_3$ sedimentation from the shallow shelf to deep ocean basins (Opdyke and Wilkinson, 1988; Kump and Arthur, 1997; Merico et al., 2008).

Continental weathering of silicate rocks is a key component of the long term carbon cycle. Congruent chemical weathering produces a weathering solution with the same chemical signature as the parent rock. In contrast, incongruent chemical weathering produces a weathering solution with a distinct chemical signature compared to the parent material. Previous studies illustrated that incongruent weathering of silicate rocks preferentially releases a labile, radiogenic Pb fraction (Erel et al., 1994; Harlavan et al., 1998). Expanding on this concept, one of the goals of this study is to test the idea that combined mechanical and incongruent weathering will yield seawater Pb isotopes that record this more radiogenic fraction, while the corresponding detrital fraction of the marine sediment will maintain its original composition or a slightly less radiogenic composition. In contrast, during times of more intense chemical weathering both seawater and the detrital fractions should record values closer to the whole source rock Pb isotopic value.

Seawater Pb isotopic signatures may also distinguish between carbonate and silicate weathering. Carbonates contain high initial U/Pb and low initial Th/Pb ratios, therefore chemical weathering of carbonates should produce high $^{206}Pb/^{204}Pb$ values in the weathering solutions that are not accompanied by high $^{208}Pb/^{204}Pb$. It is also likely that the seawater $^{207}Pb/^{204}Pb$ produced by weathering Phanerozoic carbonates would not change, because the flux of ^{207}Pb has been low for last several hundred million years due to the short half life of ^{235}U. In comparison, weathering of silicates is likely to

produce solutions with variable $^{206}Pb/^{204}Pb$, $^{207}Pb/^{204}Pb$, and $^{208}Pb/^{204}Pb$ ratios that depend on the composition of the parent rock and the intensity of weathering. Unlike Pb isotopes, seawater Nd isotopes primarily track water mass mixing; however, during times of intense weathering Nd isotopes in seawater have also been shown to record a pulse of continental inputs (Scher et al., 2011).

We analyze Pb isotopes from Fe-Mn oxide coatings and Nd isotopes from fossil fish teeth to monitor seawater values (Martin and Scher, 2004; Martin et al., 2010; Scher et al., 2011; Basak et al., *in press*), which we then compare to isotopic ratios from detrital residues that represent the bulk composition of weathered continental material. The data are derived from two intermediate depth cores; one in the Atlantic sector and one in the Indian Ocean sector of the Southern Ocean. Our ultimate goal is to use these data to evaluate the intensity of physical and chemical weathering and to determine the source rock composition (silicate vs. carbonate) of material being weathered from continental Antarctica during the Eocene-Oligocene transition (EOT) in order to better understand the forcing mechanisms associated with this climatic perturbation.

Background

Radiogenic isotopes in seawater are often used to study continental weathering and ocean circulation. High temperature and low temperature processes that fractionate Sm-Nd and U-Th-Pb parent and daughter isotopes lead to unique geochemical signatures in rocks and sediments that can be used to track provenance and evaluate low temperature processes.

Sm-Nd Systematics

Sm and Nd are light rare earth elements (LREE). They are also incompatible elements, meaning they preferentially fractionate into melt phases in the mantle. Nd is

slightly more incompatible than Sm. As a consequence, the concentrations of both Sm and Nd increase in the melt with increasing differentiation, but the corresponding Sm/Nd ratio typically decreases with more extensive fractionation. Once a rock forms with a particular Sm/Nd ratio, the abundance of ^{143}Nd will increase with time due to decay of ^{147}Sm. Because Sm and Nd have comparable ionic radii and valance states, these elements do not show appreciable fractionation during weathering processes. As a consequence, the Sm/Nd ratio and Nd isotopic composition (expressed as ε_{Nd}) of weathering products largely preserve the parent rock composition. Thus, Nd isotopic compositions of detrital silicates have direct implications for provenance studies.

Dissolved Nd in seawater is primarily derived from the continents via weathering and riverine inputs. Nd has a short oceanic residence time of ~600-1200 yrs (Jeandel, 1993; Tachikawa et al., 1997) compared to the ocean mixing time of ~1500 yrs (Broecker and Peng, 1982). Thus, ε_{Nd} is heterogeneously distributed in the world's oceans and individual ocean basins record characteristic ε_{Nd} signatures derived from surrounding terranes. This acquired signal can be altered along the flowpath by weathering inputs and boundary exchange (Lacan and Jeandel, 2005). While Nd isotopes in seawater predominantly record water mass mixing and advection, transient pulses of intense weathering, such as at the E/O boundary, can temporarily dominate the water mass signal (Scher et al., 2011).

U-Th-Pb Systematics

Pb has three radiogenic isotopes ^{206}Pb, ^{207}Pb, ^{208}Pb, which are the products of ^{238}U, ^{235}U, ^{232}Th decay respectively. There is also a non radiogenic isotope, ^{204}Pb. Of the parent isotopes, ^{235}U has the shortest half-life (0.7038×10^{9}), ^{238}U has an intermediate half-life (1.551×10^{-10}), and ^{232}Th has the longest half-life (14.010×10^{9}).

Owing to its relatively short half-life, ^{235}U has largely decayed away and currently has a low natural abundance of 0.72%. As a result, the flux of ^{207}Pb has been negligible for the last ~ billion years. Therefore, increases in ^{207}Pb imply a contribution from ancient (e.g., Archean) source rocks. Because of the long ^{232}Th half-life, ^{208}Pb has a slower growth rate than ^{206}Pb. U, Th and Pb are all incompatible elements during mantle melting and U is slightly more incompatible than Pb. As a result, U, Th, and Pb concentrate in early melts and are ultimately enriched in the continental crust compared to bulk earth. Since ^{238}U has the highest natural abundance of U isotopes (99.3%), uranogenic Pb is enriched in the crust over time.

Eolian, hydrothermal, and riverine inputs are the major sources of dissolved Pb in the modern oceans (Boyle et al., 1986; Abouchami and Goldstein, 1995; Frank, 2002; Ling et al., 2005; Klemm et al., 2007). Seawater Pb has a very short residence time (~50-200 years; Craig et al., 1973; Schaule and Patterson, 1981: Henderson and Maier-Reimer, 2002) compared to the oceanic mixing time (~1500 years; Broecker and Peng, 1982), indicating that local weathering inputs probably play a greater role in its distribution than inter-basin advection (van de Fleirdt et al., 2006). Thus, variations in seawater Pb isotopes, especially from sites in close proximity to continental inputs, can be interpreted in terms of continental weathering.

Methods

Pb isotopes for seawater were derived from Pb extracted from Fe-Mn oxides or similar authigenic phases in marine sediments using a multi step, selective, extraction technique applied to the bulk sediment (Basak et al., *in press*; also see Chapter 2). Selective extraction steps include de-carbonation using Na-acetate buffered glacial acetic acid (pH=5) followed by 1.5 hrs treatment with 0.02M Hydroxylamine

Hydrochloride (HH) in 25% glacial acetic acid. HH treatment reduces the Fe-Mn oxides, which preserve the bottom water Pb isotopic signature (Basak et al., *in press*). This short HH step was followed by a longer 24 hr step with a fresh aliquot of HH solution to ensure complete removal of the seawater signal. Material remaining after these dissolution and extraction steps is referred to as "residues," and primarily represents the carbonate-free terrigenous silicate fraction of the sediment. About 0.05 g of residue was completely dissolved in a 1:2 mixture of HF and HNO_3 prior to further chemical analyses.

Aliquots from the short HH step and digested residues were passed through cation exchange columns (for details see Chapter 2) to separate Pb and Nd from other ions. Following column chemistry Pb and Nd isotopes were analyzed on a Nu Instruments multi-collector inductively coupled mass spectrometer (MC-ICPMS) at the University of Florida (UF). Pb concentration measurements were made using an Element II ICP-MS at UF. Concentration measurements were performed under medium resolution using Re and Rh as internal standards to correct for instrumental drift. All concentration measurements were based on calibration curves generated using a set of gravimetrically prepared solutions of commercial ICP-MS standard (APEX CertiPrep, Inc.).

Site 689 (64^{o} 31′S) is currently located on the Maud Rise (Figure 3-1) within the Atlantic sector of the Southern Ocean at a water depth of 2080 m (Barker et al., 1988a). The paleodepth estimate for this site puts it at an intermediate water depth of ~1638 m (Mead and Hodell, 1995). The age model used in this study is taken from Mead and Hodell (1995) and modified to the timescale of Cande and Kent (1995). Site 738 (62^{o}

42′S) is currently located on the southern tip of the Kerguelen Plateau (Figure 3-1) within the Indian Ocean sector of the Southern Ocean at a water depth of 2253 m (Barron et al., 1989). An 1853 m paleodepth has been estimated for this site (Coffin, 1989). Site 738 has a well-preserved Eocene-Oligocene boundary; however, this site is marked by an unconformity spanning from early Oligocene to late Miocene (~33-10 Ma), thereby limiting the possibility of sampling sediments younger than 33 Ma. In the absence of an appropriate magnetostratigraphic record, Bohaty (2006) developed an age model for site 738 using biostratigraphic datums (Huber, 1991; Wei and Thierstein, 1991; Huber and Quillevere, 2005) and refined the model using several unique features of the $\delta^{18}O$ and $\delta^{13}C$ records of bulk sediments, which were correlated to other Southern Ocean sites, especially site 689, site 690, and site 748. This site 738 age model from Bohaty (2006) was applied to this study.

Results

The primary goal of this study is to understand the relationship between climate and weathering on Antarctica during the development of the Antarctic cryosphere. Specifically, this study evaluates the weathering regime and the types of rock being weathered during a one million year interval across the EOT. This interval is divided into three time slices: 1) pre EOT (34-34.5 Ma) at the end of the late Eocene warmth, 2) EOT (33.7-34 Ma) during the dramatic climate reorganization and ice sheet growth, and 3) post EOT (33.3-33.7 Ma) following full establishment of the ice sheet.

Pre EOT (34 – 34.5 Ma)

The pre EOT time-slice is characterized by similar $^{206}Pb/^{204}Pb$, $^{207}Pb/^{204}Pb$ and $^{208}Pb/^{204}Pb$ values for seawater and residue samples at site 689 with values of 18.80, 15.69, and 38.85 respectively (Figure 3-2; Table 3-1). Site 738 also shows similar

seawater and residue $^{206}Pb/^{204}Pb$ ratios of 18.80; however, seawater $^{207}Pb/^{204}Pb$ and $^{208}Pb/^{204}Pb$ values of 15.67 and 38.85 at this site are slightly less radiogenic than residue values of 15.68 and 39. Both records show similar variations through time (Figure3-2). The ε_{Nd} values for sites 689 and 738 also show agreement between seawater, as recorded by fish teeth, and residues, with both samples from both sites recording values around -7.5 (Figure 3-3).

EOT (33.7 – 34 Ma)

The EOT time-slice covers the two-step glacial transition defined by oxygen isotopes (Coxall et al., 2005). During this interval $^{206}Pb/^{204}Pb$ values for seawater show a gradual transition towards more radiogenic values at both sites, while the residues become progressively less radiogenic (Figure 3-2). In contrast, both sites record more radiogenic seawater and residue values for $^{207}Pb/^{204}Pb$ and $^{208}Pb/^{204}Pb$, and much of the increase at site 738 occurs during the second $\delta^{18}O$ step (33.7 Ma) (fig 2-3e, f, h, i). The sample distribution in site 689 is too sparse during this interval to determine a pattern, but like site 738, the residue $^{207}Pb/^{204}Pb$ value is slightly more radiogenic than the seawater value; however, the residue $^{208}Pb/^{204}Pb$ at site 689 appears to be slightly less radiogenic than contemporaneous seawater. Seawater and residue ε_{Nd} values become less radiogenic and start to separate during the EOT at site 738 with a greater decrease observed in the residues. Seawater ε_{Nd} values are ~ - 10 at the end of the time-slice, while residue values are ~ - 15. Again, most of the changes occur during the second step of the glaciation.

Post EOT (33.3 - 33.7 Ma)

Towards the end of the post EOT time-slice, seawater $^{206}Pb/^{204}Pb$ values maintain the radiogenic value of 19 for both sites. There is a bit more structure in earliest portion

of the post EOT in the site 738 record. Residue $^{206}Pb/^{204}Pb$ values at site 689 also maintain their less radiogenic value of 18.8, while site 738 residue $^{206}Pb/^{204}Pb$ values document a generally decreasing trend, ranging from 18.7 to 18.3 (Figure 3-2G). As during the EOT, residue $^{207}Pb/^{204}Pb$ values remain more radiogenic than contemporaneous seawater with an average offset of ~0.03 between the two sample types at site 689 compared to ~0.01 at site 738 (Figure. 3-2E, H). Residue $^{208}Pb/^{204}Pb$ values are slightly more radiogenic than seawater values at site 689 and much of site 738, but there is more variability in the site 738 record and the final residue $^{208}Pb/^{204}Pb$ value suggests a decreasing trend ending with a value less radiogenic than seawater (Figure. 3-2I). Early post EOT residue ε_{Nd} values continue to be less radiogenic than seawater values, and both seawater and residue samples return to values similar to the early EOT by 33.3 Ma (~-10 for residues and -8 for seawater).

Discussion

Source of Radiogenic Pb During Weathering

Several studies of weathering in glacial and paleosol environments demonstrate that the radiogenic Pb fraction of a parent rock is preferentially released during early weathering of fresh material, indicating incongruent weathering (Erel et al., 1994; Harlavan et al., 1998; von Blanckenburg and Nagler, 2001; Blum and Erel, 2003). Whole rock Pb isotopic values are dominated by Pb residing within feldspar (characterized by low μ [i.e.$^{235}U/^{204}Pb$]),), while the most radiogenic Pb is concentrated in accessory phases (characterized by high μ), such as allanite, monazite, and zircon, as well as other minerals forming from late stage fluids. Several studies suggest the radiogenic Pb in weathering solutions is derived from the accessory phases during incongruent weathering (Harlavan et al., 1998; Blum and Erel, 2003; von Blankenburg

and Nagler, 2001; Frank, 2002; Foster and Vance, 2006); however, common accessory phases are relatively insoluble in weak acids and rarely constitute more than a minor (~1%) fraction of the whole rock. An alternative source of labile radiogenic Pb during incongruent weathering could be interstitial oxides and cryptocrystalline aggregates that form from late-stage magmatic fluids (Brown and Silver, 1955) and are enriched in U and Th relative to Pb (Rollinson, 1998). As in the case of accessory minerals, these late-stage interstitial oxides and cryptocrystalline aggregates are likely to constitute a very small fraction of the Pb in the whole rock. To re-evaluate the source of this radiogenic Pb during incongruent weathering, we conducted a leaching experiment on well-characterized silicate rocks.

Three granitic rock samples from a single pluton with well-constrained whole rock Pb concentrations and isotopic values were pulverized to simulate mechanically generated rock flour. These granitic rocks contain no carbonate fraction and the leaching experiment was designed to purely evaluate the behavior of the silicate fraction. Three 1-gram sub-samples were taken from each rock and treated with 10% acetic acid to leach out any labile fraction. Following this step, the samples were treated with 2% HNO_3. One sample from each subset was exposed to the acid for 1 day, another for 3 days and the last one for 5 days. The 10% acetic acid fraction and the 1, 3, and 5 days HNO_3 leachates for each sample were then analyzed for Pb isotopic values and concentrations. Irrespective of the reagent used and the duration of reaction, the leached fractions yielded $^{206}Pb/^{204}Pb$, $^{207}Pb/^{204}Pb$, and $^{208}Pb/^{204}Pb$ values that far exceeded the whole rock ratios (Figure 3-4). This observation is consistent with other leaching experiments on granitic glacial moraine soil chronosequences (Harlavan et al.,

1998). In general, high U-bearing accessory phases have very low initial Pb concentrations, thus typical accessory minerals with radiogenic Pb tend to have very high initial U/Pb ratios. If the radiogenic leachates in this experiment were produced by dissolution of such phases, the isochron defined by the leachates should pass through a value very close to the origin, indicating initial $^{206}Pb/^{204}Pb$ and $^{207}Pb/^{204}Pb$ of approximately 0. Instead, the secondary isochron in figure 3-4 passes through $^{206}Pb/^{204}Pb$ and $^{207}Pb/^{204}Pb$ values of ~15. These data indicate the acids are not attacking typical accessory phases. Although interstitial oxides and cryptocrystalline aggregates formed from late-stage magmatic fluids can contain labile radiogenic Pb, these phases are more abundant in volcanic rocks and are practically absent in the plutonic rocks used for this experiment.

The total Pb concentration in the leachates represents 0.05-2% of the whole rock Pb, illustrating that the labile radiogenic Pb in the silicate fraction constitutes a very small proportion of the total Pb in the whole rock. The results also indicate that the radiogenic Pb in the leachates comes from a phase with slightly higher U/Pb ratio compared to the mean whole rock value, but still within the range of the whole rock U/Pb. Thus, a major rock forming mineral phase with a slightly elevated U/Pb ratio would be an appropriate source for the radiogenic Pb observed in the leaching experiment. In general, major rock forming minerals are not easily leached with weaker acids; however, the metamict portions of the major minerals represent one possible readily leachable source that can contain radiogenic Pb. Metamictization is a process whereby alpha emissions and spontaneous fission products from radioactive decay of U & Th gradually damage the mineral's crystal structure, making that portion of the

mineral more susceptible to leaching by weak acids. Pb leached from these domains would be more radiogenic than the whole rock, reflecting the radioactive source, and would plot on a secondary isochron along with the whole rocks. While our leaching experiment with plutonic rocks suggests the metamict portions of minerals may be an import source of radiogenic Pb in the leached solution, it would be difficult to isolate this source from radiogenic Pb leached from interstitial oxides and cryptocrystalline aggregates from volcanic rocks in the natural environment.

Even with the increased surface area produced by mechanical glacial activity, mass balance calculations suggest the radiogenic contribution from metamict portions of minerals (or interstitial oxides and cryptocrystalline aggregates) would be volumetrically too small to produce the variations in seawater $^{206}Pb/^{204}Pb$ isotopes observed during the EOT. The U concentration in seawater today is ~3.2 ppb, which is two to three orders higher than seawater concentrations of Pb or Th (Chen et al., 1986). Even though Pb is easily complexed with CO_3^{2-} and Cl^-, its concentration diminishes rapidly due to scavenging processes that transport it to the sediment. Thorium is known to be highly insoluble and is easily removed from seawater through adsorption on suspended particles. Because of these distinct geochemical behaviors, seawater is highly enriched in uranium compared to thorium (U/Pb>> Th/Pb) (Jahn and Cuvellier, 1994). Carbonates formed from seawater reflect these U/Pb and Th/Pb ratios. Over time these carbonates become a source of easily weatherable uranogenic Pb that is largely decoupled from thorogenic Pb. Therefore, weathering of early Paleozoic or older marine carbonate provides an alternative explanation for radiogenic $^{206}Pb/^{204}Pb$ observed during early stages of glacial weathering that is not accompanied by

radiogenic $^{208}Pb/^{204}Pb$ or $^{207}Pb/^{204}Pb$, which is limited by the low abundance of ^{235}U in Phanerozoic seawater.

Weathering at the EOT

The type of weathering (mechanical vs. chemical) and the substrate that is being weathered (silicate vs. carbonate) controls the long-term drawdown of CO_2. It is widely accepted that atmospheric CO_2 dropped below a critical threshold as a precondition for Antarctic glaciation during the EOT (DeConto and Pollard, 2003; Pagani et al., 2005). Here, we use Pb isotopes in seawater and residues to evaluate the intensity of chemical weathering and source rock composition (silicate vs. carbonate) across the EOT.

Mechanical vs. chemical weathering

The similarity between seawater and residue Pb isotopic values at the end of the Eocene, particularly for $^{206}Pb/^{204}Pb$, is interpreted to indicate extensive transfer of the whole rock isotopic signature to seawater, suggesting extensive chemical weathering on Antarctica during this warm interval. A strong chemical weathering regime is also supported by studies of clay minerals from circum Antarctic sediments during the late Eocene (Roberts and Kennett, 1997).

Immediately following the EOT increases in both seawater and residue $^{207}Pb/^{204}Pb$ and $^{208}Pb/^{204}Pb$ (Figure 3-2) track the two step glaciation observed in the benthic $\delta^{18}O$ record (Coxall et al., 2005). Synchronous changes in ice growth and residue values suggest increased mechanical weathering during the EOT, which introduced fresh rock and grains with large surface areas. Although the change in residue isotopic values can be explained by introduction of this fresh terrigenous material from various sources via mechanical weathering, associated changes in seawater isotopes require active chemical weathering as well. In this scenario, glacial mechanical weathering increased

the surface area/mass ratio of weathered material, which would have facilitated subsequent chemical reactions. Since the initial EOT glaciers on continental Antarctica were mostly wet-based (Zachos et al., 1999), it is possible that a sufficient volume of water was available to maintain the chemical reactions needed to weather the radiogenic Pb fraction from these freshly exposed surfaces. Global cooling associated with glacial conditions would also have increased the CO_2 solubility, producing stronger carbonic acid and further facilitating chemical reactions.

The pattern of a gradual shift in Southern Ocean seawater towards more radiogenic $^{206}Pb/^{204}Pb$ values and the separation between seawater and residue values at the EOT (Figure 3-2) is distinct from observed $^{207}Pb/^{204}Pb$ and $^{208}Pb/^{204}Pb$ patterns in which the isotopes for both seawater and residues rise gradually. Although, the more radiogenic $^{206}Pb/^{204}Pb$ in seawater also suggests active chemical weathering, the source rock being weathered must have been fundamentally different leading to the observed decoupling between seawater and residue Pb isotopes. Thus, the weathering regime following the development of ice on Antarctica included both mechanical and chemical weathering. Foster and Vance (2006) also argued for active chemical weathering for glaciated domain based on a Pleistocene study using Pb isotopes.

Silicate vs. carbonate weathering

The radiogenic Pb contribution from metamict minerals or cryptocrystalline aggregates during silicate weathering is probably volumetrically insufficient to generate the increase in seawater Pb observed in the Southern Ocean during the EOT. While it is difficult to estimate the total flux of radiogenic Pb from metamicts during E/O weathering, observations from the leaching experiment indicate that radiogenic Pb contributed from metamict minerals is less than 2% of the whole rock Pb. Therefore it is

reasonable to assume that metamict minerals do not play a major role in the composition of E/O weathering solutions. Thus, chemical and mechanical weathering of silicates will define the Pb isotopes of seawater and residues during this transition. In contrast, seawater $^{206}Pb/^{204}Pb$ values become more radiogenic while contemporaneous residue $^{206}Pb/^{204}Pb$ values become less radiogenic during the EOT and post EOT. So, in addition to the contributions from silicate weathering apparent in the $^{207}Pb/^{204}Pb$ and $^{208}Pb/^{204}Pb$ records, the $^{206}Pb/^{204}Pb$ data require an additional source that can account for the greater magnitude of increase in seawater $^{206}Pb/^{204}Pb$, but had little impact on $^{207}Pb/^{204}Pb$ and $^{208}Pb/^{204}Pb$. One possible candidate is a change of source to weathering of old carbonate rocks. Due to high initial U/Pb these old carbonates would contribute radiogenic $^{206}Pb/^{204}Pb$ to seawater, but are unlikely to affect the $^{207}Pb/^{204}Pb$ ratios, because they are too young relative to the time period of active ^{235}U decay, or the $^{208}Pb/^{204}Pb$ ratios, because of low initial Th/Pb in carbonates. The carbonates are also likely to be more susceptible to glacial mechanical and chemical weathering than silicate basement rocks.

Carbonate rocks represent 5-10% of the total exposed basement rock volume of the east Antarctic (Elliot, 1975). During the early Cambrian, epicontinental seas formed along the western boundary of the East Antarctic shield, leading to extensive shallow marine carbonate deposition under warmer conditions. Isolated outcrops of Shackleton Limestone, an ~500 Ma old carbonate sequence along the southwestern Antarctic shoreline near the Ross Sea, represent important evidence for the Cambrian platform (Elliot, 1975; Rowell and Rees, 1987; Goodge et al., 2002). Model data support extensive glacial development in the Ross Sea sector during the EOT (DeConto and

Pollard, 2003), providing a possible mechanism to initiate weathering of this old carbonate.

Residue Pb Isotopes

Pb isotopes from the residues can be used for provenance studies. Residue $^{206}Pb/^{204}Pb$ values in the Southern Ocean decrease while $^{207}Pb/^{204}Pb$ and $^{208}Pb/^{204}Pb$ values increase after the E/O boundary at both sites 689 and 738 (Figure 3-3). The increase in $^{207}Pb/^{204}Pb$ typically indicates an ancient source rock. Detailed observations from the higher resolution records at site 738 show small positive excursions in $^{207}Pb/^{204}Pb$ and $^{208}Pb/^{204}Pb$ at ~33.9 Ma and larger positive excursions at ~33.7 Ma during the second step of the E/O glaciation. Smaller negative excursions are also detected in residue $^{206}Pb/^{204}Pb$. The timing of these variations implies a relationship between the two step Antarctic glaciation (Coxall.et al., 2005; Lear et al., 2008) and the weathering response (Scher et al., 2011). In particular, the rapid Pb excursions observed during the second step of the E/O glaciation are consistent with the idea that intensified weathering of crustal rocks accompanied the intense interval of glacial growth.

Pre EOT seawater and residue ε_{Nd} values in sites 689 and 738 show (Figure 3-3) similar values suggesting a well mixed seawater signal and efficient mixing of detrital inputs following onset of the proto ACC in the Eocene (Scher and Martin, 2006, 2008). At the beginning of the EOT, both seawater and residue Nd isotopes at site 738 start to become less radiogenic reaching minimum values during the second step of the E/O glaciation. Rapid recovery to values similar to pre EOT values is also observed during the post EOT time window (Figure 3-3). These observations support the interpretation deduced from Pb isotopic compositions of residues that intense glaciation increased the

weathering inputs. Introduction of this weathered material into seawater overwhelmed the advective signal for both the short residence time Pb and intermediate residence time Nd, producing rapid excursions in seawater isotopes for both systems.

Pre EOT residue $^{207}Pb/^{204}Pb$ and ε_{Nd} values plot within a limited range. The composition of the EOT and Post EOT continental input is defined by variable $^{207}Pb/^{204}Pb$ and ε_{Nd} values in $^{207}Pb/^{204}Pb$ vs. ε_{Nd} space. (Figure 3-5). This overall shift suggests a source change, possibly indicating introduction of multiple new sources as the glaciers grew and weathered older silicate basement rocks from new locations.

Weathering and Paleoceanogrpahic Significance

Pb isotopes in seawater and residues provide important information about the mechanisms of weathering and the types of rock being weathered during the EOT. Seawater Pb isotopes highlight the impact of glacial mechanical weathering combined with active chemical weathering associated with wet-based glaciers on continental Antarctica. Observed seawater and residue Pb isotopes are best explained by the combination of carbonate and silicate weathering, with silicate weathering dominating both seawater and residue $^{207}Pb/^{204}Pb$ and $^{208}Pb/^{204}Pb$ signals, while carbonate weathering modulated the seawater $^{206}Pb/^{204}Pb$ isotopic record. Chemical weathering of silicate and carbonate rocks can sequester atmospheric carbon over the long and short term respectively. Therefore, evidence for chemical weathering of silicates and carbonates from Antarctica supports the concept of a drawdown of atmospheric CO_2 over the EOT based on boron isotopes (Pearson et al., 2009) and presents a possible mechanism. In addition, Pb isotopes from residues illustrate a change in the intensity of weathering and the composition (provenance) of weathered material as the East Antarctic ice sheet grew. In particular, Nd and Pb isotopic data from seawater and

residues illustrate a pulse in weathering associated with each of the two steps of the EOT that have been attributed to rapid cooling and ice growth (Coxall et al. 2005; Lear et al., 2008; Katz et al., 2008). Enhanced silicate weathering at the E/O would also deliver additional silicate to the ocean needed to support the observed increase in opal accumulation in the Southern Ocean during this transition.

The carbonates weathered during the EOT are most likely old (Late Cambrian) and are believed to have formed in a shallow marine or neritic environment. Neritic carbonates commonly have high $\delta^{13}C$ compared to pelagic carbonates due to high productivity rates in this shallow, marginal environment (Stewart and Eberli, 2005). Thus weathering of these neritic carbonates might contribute to the higher seawater $\delta^{13}C$ values observed during the EOT (Figure 3-6) (Merico et al., 2008). Moreover, the associated influx of Ca^{2+} into the ocean could be a factor in the documented deepening of the CCD by ~ 1 km. (Figure 3-6), although inputs associated with global lowering of sea level and weathering of exposed shelf carbonates also probably contributed. This interpretation is consistent with a modeling study by Merico et al. (2008) that suggested carbonate weathering as a source of the carbon isotope and CCD fluctuations.

Summary

Pb isotopes from samples representing seawater and terrigenous detrital fractions from deep sea sediments document changes in the weathering regime, intensity and source rocks during the transition from the late Eocene greenhouse into the Oligocene ice house. Similar $^{206}Pb/^{204}Pb$, $^{207}Pb/^{204}Pb$ and $^{208}Pb/^{204}Pb$ values between the two fractions during the late Eocene highlight an interval of intensive chemical weathering on Antarctica during a time of warm temperatures and possible weathering of well-weathered sequences. Increased seawater $^{206}Pb/^{204}Pb$ and

decreased detrital $^{206}Pb/^{204}Pb$ during the EOT argue for incongruent weathering of freshly exposed silicate rocks that released labile, radiogenic ^{206}Pb to seawater.

Previous studies suggest this radiogenic Pb could be sourced from accessory minerals or interstitial oxides during incongruent weathering of silicates. A leaching experiment using isotopically well-defined granitic rocks suggests the radiogenic ^{206}Pb tapped a source with a relatively high U/Pb ratio, but a ratio that was within the range of the whole rock values and produced a secondary isochron. These data suggest the radiogenic Pb was contributed from metamict portions of major minerals in the silicate fraction. The overall Pb flux from this source probably represents a very small fraction of the whole rock Pb and would be insufficient to drive large changes the seawater Pb isotopic composition.

A more abundant input that could explain the different responses observed in seawater and detrital $^{206}Pb/^{204}Pb$ is weathering of Paleozoic carbonate rocks that were initially enriched in U and depleted in Th. This source also explains the observed increase in seawater $^{206}Pb/^{204}Pb$ compared to the minimal overall change in seawater $^{207}Pb/^{204}Pb$ and $^{208}Pb/^{204}Pb$ across the EOT, as well as the similarities in the values and trends of seawater and residue $^{207}Pb/^{204}Pb$ and $^{208}Pb/^{204}Pb$. Chemical weathering of old carbonates is also consistent with the observed deepening of the CCD and positive $\delta^{13}C$ shift across the EOT. Finally, increasing residue $^{207}Pb/^{204}Pb$ isotopes during the EOT, particularly in association with the second step of the E/O glaciation, also indicates intensification and expansion of silicate weathering to new regions of silicate basement rocks, which could have contributed to the drawdown of atmospheric CO_2.

Table 3-1. Average Pb isotopic values in seawater and residues in Pre-EOT, EOT, and Post-EOT intervals in Southern Ocean sites 689 and 738.

		$^{206}Pb/^{204}Pb$		$^{207}Pb/^{204}Pb$		$^{208}Pb/^{204}Pb$	
		Site 689	Site 738	Site 689	Site 738	Site 689	Site 738
Pre-EOT	Seawater	18.8	18.8	15.69	15.67	38.85	38.85
	Residue	18.8	18.8	15.69	15.68	38.85	39.0
EOT	Seawater	19.0	18.8	15.7	15.69	39.0	39.0
	Residue	18.8	18.8	15.72	15.69	39.0	39.0
Post-EOT	Seawater	19.0	19.0	15.7	15.69	39.1	39.0
	Residue	18.8	18.6	15.73	15.69	39.1	39.0

Pb isotopes for Pre-EOT, EOT, and Post-EOT are represented by range of Pb isotopic values. Numbers in the table represent approximate mean of these range of values.

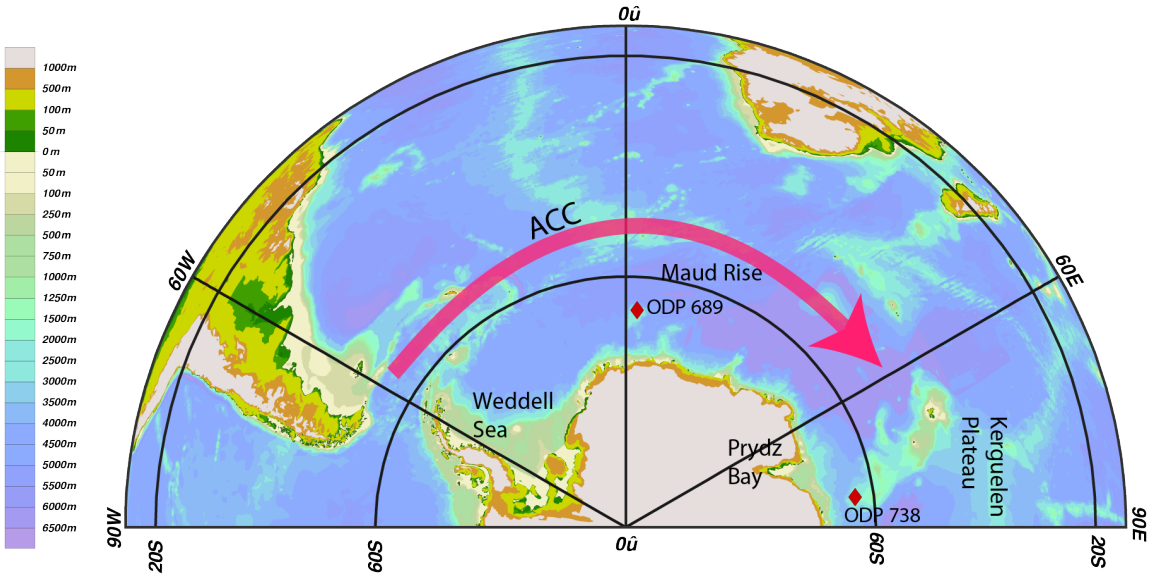

Figure 3-1. Site location showing ODP site 689 (2080 m) from the Atlantic sector and site 738 (2253 m) from the Indian sector of the Southern Ocean.

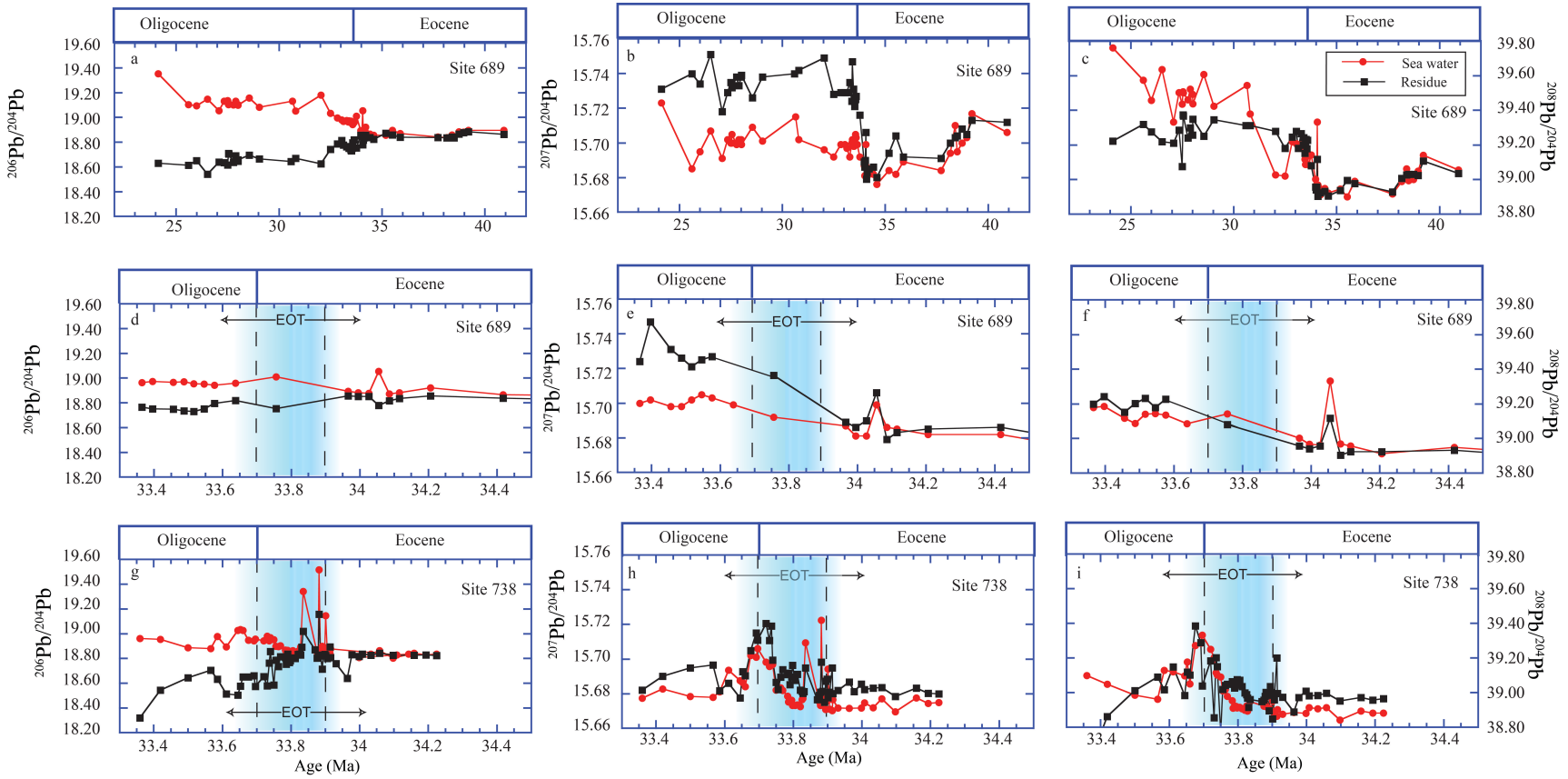

Figure 3-2. A plot of $^{206}Pb/^{204}Pb$, $^{207}Pb/^{204}Pb$, and $^{208}Pb/^{204}Pb$ ratios versus age in seawater and detrital residues from site 689 and site 738 from the late Eocene across the Eocene/Oligocene Transition (EOT). (a-c) Records of $^{206}Pb/^{204}Pb$, $^{207}Pb/^{204}Pb$, and $^{208}Pb/^{204}Pb$ ratios from 23 - 40 Ma for site 689. (d-f) Records of $^{206}Pb/^{204}Pb$, $^{207}Pb/^{204}Pb$, and $^{208}Pb/^{204}Pb$ from 33.3 – 34.5 Ma for site 689 l. (g-i) Records of $^{206}Pb/^{204}Pb$, $^{207}Pb/2^{04}Pb$, and $^{208}Pb/^{204}Pb$ ratios from 33.3- 34.5 Ma for site 738. Long term 2σ error on $^{206}Pb/^{204}Pb$, $^{207}Pb/^{204}Pb$ and $^{208}Pb/^{204}Pb$ measurements are 0.004, 0.003 and 0.008 respectively).

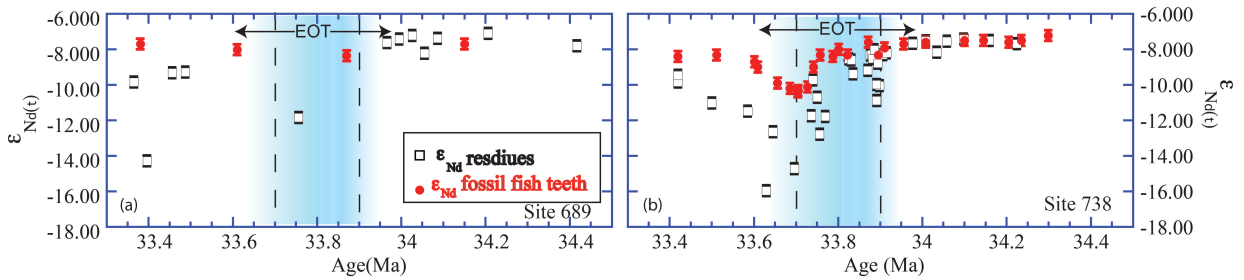

Figure 3-3. ε_{Nd} values versus age of fossil fish teeth, representing seawater, and detrital fractions for 33.3 – 34.5 Ma. (a,b) ε_{Nd} record of seawater and terrigenous material for sites 689 and 738 respectively.

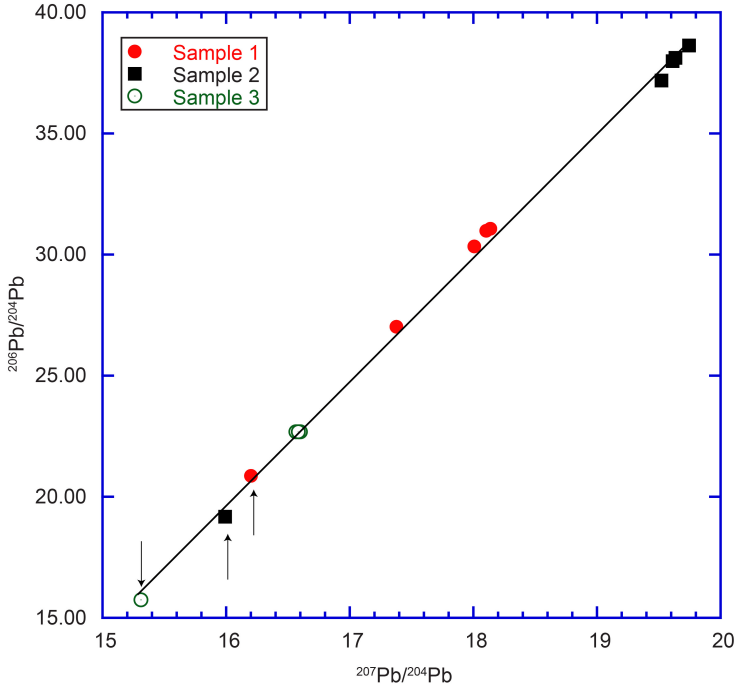

Figure 3-4. A plot of $^{206}Pb/^{204}Pb$ vs. $^{207}Pb/^{204}Pb$ from a leaching experiment. An acetic leach, a 1 day leach in 2% HNO_3, a 2 day leach in 2% HNO_3, a 3 day leach in 2% HNO_3, and the whole rock for 3 pulverized granite samples. The black arrows indicate the whole rock Pb isotopic values for each of the three granite samples.

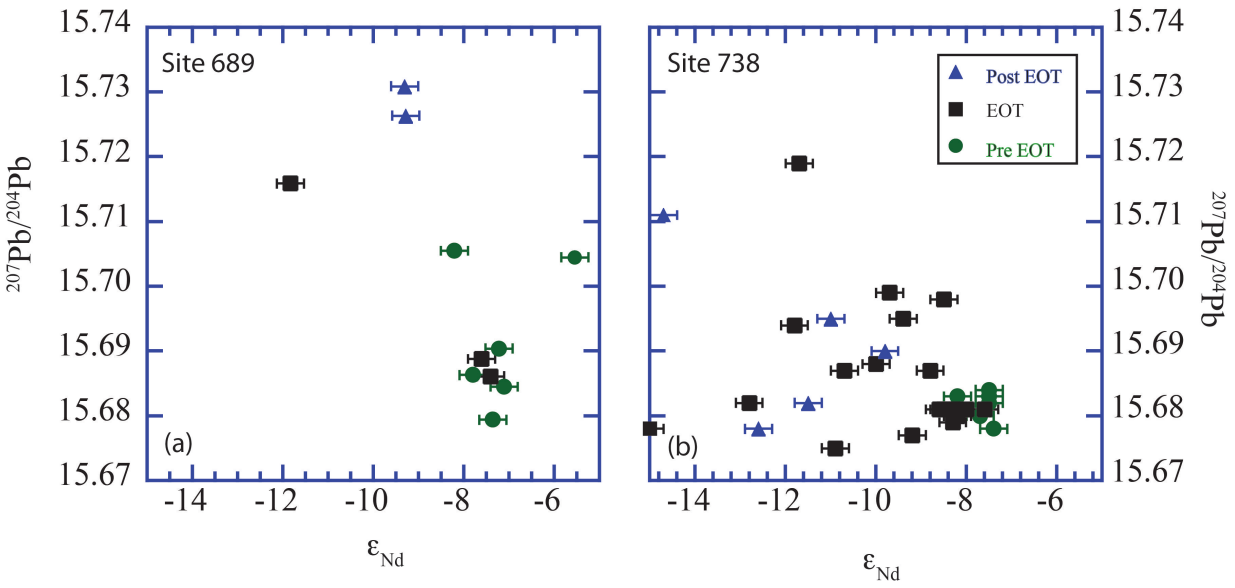

Figure 3-5. A plot of $^{207}Pb/^{204}Pb$ vs. ε_{Nd} for the detrital fractions. Green circles represent pre EOT samples, black squares represent EOT samples, and blue triangles represent post EOT samples.

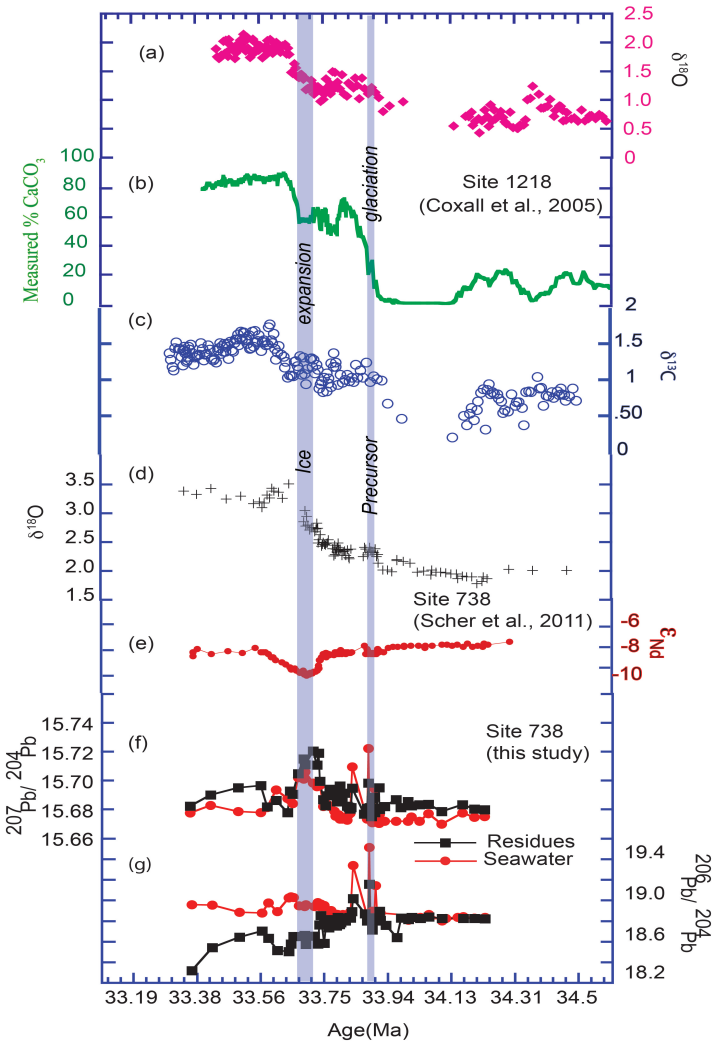

Figure 3-6. Plot showing the different proxy response to Oligocene glaciation in Antarctica ~ 34 Ma. (a-c) represent $\delta^{18}O$, $\%CaCO_3$ and $\delta^{13}C$ data from equatorial Pacific site 1218 from Coxall et al. (2005). (d-g) $\delta^{18}O$, ε_{Nd}, $^{207}Pb/^{204}Pb$, and $^{206}Pb/^{204}Pb$ from site 738. The grey bars indicate two steps of the EOT.

CHAPTER 4
SOUTHERN SOURCE OF DEGLACIAL OLD CARBON IN THE TROPICAL NORTH PACIFIC BASED ON NEODYMIUM ISOTOPES

A simultaneous drop in atmospheric $\Delta^{14}C$ (by 190‰) and rise in CO_2 during the "Mystery Interval" (17.5 to 14.5 kyr BP) are believed to have been caused by the release of ^{14}C-depleted CO_2 from the ocean to the atmosphere (Broecker and Barker, 2007). The Southern Ocean has been identified as a potential source for this old CO_2 (Marchitto et al., 2007) based on the idea that extensive sea ice cover (Stephens and Keeling, 2000) and/or upper ocean stratification (Francois et al., 1997; Sigman et al., 2000) in southern latitudes during the Last Glacial Maximum (LGM) isolated the underlying abyssal water mass from air-sea exchange, resulting in a ^{14}C-depleted reservoir. Marchitto et al. (2007) reported an ~300 per mil negative $\Delta^{14}C$ excursion in intermediate waters from the eastern North Pacific during the last deglaciation, which they attributed to injection of ^{14}C-depleted Antarctic Intermediate Water (AAIW). Although the negative $\Delta^{14}C$ findings clearly tag an old water mass, the source of the water remains controversial. Unlike $\Delta^{14}C$, which reflects the age or ventilation rate of a water mass, Nd isotopes can be used to track the source of the water mass; hence, to resolve this controversy I present Nd isotopes from fossil fish teeth/debris collected from the same core studied by Marchitto et al. (2007). My data exhibit a clear shift toward more Southern Ocean values at ~18 kyr BP. This shift is in phase with the $\Delta^{14}C$ excursion and Southern Hemisphere climatic signals, further supporting an AAIW source.

Negative radiocarbon excursions (Marchitto et al., 2007; Stott et al., 2009) observed in the eastern tropical Pacific are contemporaneous with increased upwelling in the Southern Ocean (Anderson et al., 2009) and onset of warming and rising CO_2

detected in Antarctic ice cores (Monnin et al., 2001) highlighting a possible cause and effect relationship between circulation in the Southern Hemisphere and radiocarbon in the eastern tropical Pacific. Despite these observations, there is no direct evidence that this older water was sourced from the Southern Ocean. An alternative possible source is the high latitude North Pacific. There is no clear way to distinguish between northern and southern routing on the basis of $\Delta^{14}C$, $\delta^{13}C$, or $\delta^{18}O$ because similar oceanic and atmospheric processes could theoretically act to modify the isotopic characteristics of either end-member water mass. In contrast, Nd isotopes in fossil fish teeth/debris are considered quasiconservative tracers of water mass, meaning that major water masses carry distinct Nd isotopic ratios (reported here as ε_{Nd}) that are generally only altered by mixing, although modification from local weathering inputs is possible.

Background

Nd Isotopes Systematics

Neodymium has a residence time in the ocean (~600-1200 yrs) (Jeandel, 1993; Tachikawa et al., 1997) that is shorter than the mixing time of the global conveyer (~1500 yrs) (Broecker and Peng, 1982) and it is sourced primarily from the continents (Goldstein and Jacobsen, 1987, Elderfield, 1988; Jeandel, 1993; Tachikawa et al., 1999, 2003). As a result different ocean basins have different ε_{Nd} values. For example, North Atlantic Deep Water (NADW) has a value close to -13.5 (Piepgras and Wasserburg, 1987; Lacan and Jeandel, 2005) which reflects weathering of Precambrian shield material, while Pacific Deep Water has a value between -4 to -6 (Piepgras and Jacobsen, 1988), reflecting deep sea mixing and weathering of young volcanic ash. Major water masses carry their initial Nd isotopic signal as they circulate through the ocean; however, that signal can be altered along the route by weathering inputs and

boundary exchange (Lacan and Jeandel, 2005), particularly in marginal marine settings. As a result, Nd isotopes are often referred to as “quasi-conservative” tracers of water masses. Owing to the large differences in ε_{Nd} values between the major water masses in the world oceans, minor modifications of end-member values generally do not erase the differences that distinguish water masses.

Hydrography

Under modern hydrographic conditions AAIW is a low salinity, high oxygen intermediate water mass. This intermediate water occupies depths of 500 to 1000 meters below sea level (mbsl) and over 50% of global AAIW is located in the Pacific Ocean. In general, northern flow of AAIW in the southern Pacific occurs along the eastern margin of the basin (Tomczak and Godfrey, 1994) with return flow southward along the western boundary. Near the Coral Sea some of the water from this gyre is deflected equatorward and passes through the Papua New Guinea (PNG) region before turning east near the equator and ultimately feeding into the Equatorial Intermediate water.

At its source region in the Southern Ocean modern AAIW ε_{Nd} values range between -6 to -8, representing a mixture of Atlantic and Pacific waters. Currently the intermediate water found along the equatorial Pacific is similar to AAIW with respect to its hydrological properties, while the Nd signature is strongly modified. The modified AAIW in the equatorial region has an average ε_{Nd} value of ~ - 2.8 (Lacan and Jeandel, 2001). This dramatic increase in the ε_{Nd} value of AAIW occurs through inputs from easily weathered volcanic rocks in the tropical Pacific (Lacan and Jeandel, 2001). The young volcanic rocks of PNG have an ε_{Nd} value of ~+7, which is highly distinct from seawater values and thus small inputs alter AAIW ε_{Nd} values to ~ -2.8 (Lacan and

Jenadel, 2001). My core site is located at 23°N within a shadow zone at the confluence of EqIW and NPIW. EqIW is a mixture of AAIW modified in the PNG region and upwelled PDW. There are no previously published water column or core top ε_{Nd} data for EqIW; however, limited data for PDW from the deep tropical waters indicate very little variation in ε_{Nd} since the LGM (Marchitto et al., 2005). Thus, variations in ε_{Nd} at the Baja site are expected to primarily reflect the interaction between NPIW and modified AAIW.

NPIW is a mixture of waters from the Kuroshio Current, intermediate water ventilated in the Okhotsk Sea (OSIW) and intermediate water ventilated in the western North Pacific (WNP) (You, 2003; Talley, 1999; Amakawa et al., 2004a). End-member ε_{Nd} values for these waters measured prior to ventilation and mixing are ~ -5.6 for the Kuroshio Current, -3.6 for the Okhotsk Sea, and -0.1 for the WNP (Amakawa et al., 2004b; Piepgras and Jacobsen, 1988). These three waters mix at depth to form NPIW. Varying percentages of these source waters along the flow path of NPIW account for the high spatial variability in ε_{Nd} values reported within the upper 1 km of the NW Pacific water column (-4 to 0) (Piepgras and Jacobsen, 1988; Amakawa et al., 2004a, b; Amakawa et al., 2009).

Previous studies suggest that during the LGM, NPIW (Glacial NPIW) was well ventilated (Keigwin, 1998; Matsumoto et al., 2002) with probable contributions from the Bering Sea, Okhotsk Sea and/or Gulf of Alaska (Horikawa et al., 2010) introducing additional radiogenic Nd. This is consistent with my observation that NPIW at Baja has a radiogenic value of ~-1 during the LGM. Even more pronounced intermediate and deep water production rates have been observed in the WNP during HS1 according to a drop in ventilation age of ~600 years between LGM and HS1 based on the ^{14}C age

difference between benthic and planktonic foraminifera (Okazaki et al., 2010). Increased contributions of radiogenic WNP intermediate water (ε_{Nd} ~-0.1) to NPIW would result in an NPIW ε_{Nd} value that was similar to, or more radiogenic than, LGM values. Therefore, anticipated changes in the end-member composition of NPIW during HS1 are expected to produce increasing ε_{Nd} values at the Baja site, in direct contradiction to the observed decreasing values at the onset of HS1. Moreover, modeling studies by Okazaki et al. (2010) predict this young LGM/HS1 NPIW flowed out of the Pacific Ocean as a western boundary current, leaving southern sourced waters as the primary component in the eastern Pacific.

Core Location and Method

Our core location and depth is currently situated at the boundary between Equatorial Intermediate Water (EqIW) (a mixture of AAIW and upwelled Pacific Deep Water (PDW)) (Bostock et al., 2010), and North Pacific Intermediate Water (NPIW) within the east Pacific shadow zone (Figure 4-1). Limited data for PDW from the deep tropical waters indicate very little variation in ε_{Nd} since the LGM (Marchitto et al., 2005). Thus, the ε_{Nd} value at Baja is largely controlled by the relative contributions of NPIW (higher values) and AAIW (lower values), with AAIW values being additionally modified during transit from the Southern Ocean through the Papua New Guinea region.

Fossil fish teeth/debris were handpicked from the >63 μm fraction of sieved sediments from core MV99-MC19/GC31/PC08 off Baja California. Picked fossil fish teeth/debris was dissolved in a 1:1 mixture of optima grade HNO_3 and HCl in preparation for column chemistry. A primary column with Mitsubishi resin and 1.6N HCl as an eluent was used to separate bulk REEs. Nd was then isolated by passing the

REE aliquot through Ln-spec resin with 0.25 N HNO_3 as an eluent. Procedural blanks were 14 pg Nd.

Nd isotopes were analyzed on a Nu Plasma Multi-Collector Inductively Coupled Plasma Mass Spectrometer (MC-ICPMS) at the University of Florida. Nd aliquots from column chemistry were dried and redissolved in 2% NHO_3 prior to aspiration using a DSN-100 nebulizer. Preamplifier gain calibrations were run at the beginning of each analytical session. All Nd isotope data reported in this study were analyzed using a time-resolved analysis (TRA) method (Kamenov et al., 2008). Prior to sample introduction a baseline was measured for 30 seconds. Data were acquired in a series of 0.2 seconds integrations over 1-3 minutes. All reported $^{143}Nd/^{144}Nd$ ratios were corrected for mass fractionation using $^{146}Nd/^{144}Nd$ =0.7219. International standard JNdi-1 was analyzed between every 5-6 unknown samples and the average of these standard runs were compared to a long term TIMS JNdi-1 value of 0.512103 +/- 0.000014 to determine a correction factor for each of the samples analyzed on that day. The long term 2σ external reproducibility of JNdi-1 analyses on the Nu of 0.000014 (0.3 ε_{Nd} units) has been applied to all samples unless the internal error was larger.

Results

I report a Nd isotope time series for the last 38 kyr (Table 4-1) from core MV99-MC19/GC31/PC08 near southern Baja California using the same samples and age model as Marchitto et al. (2007) in order to distinguish between potential northern and southern sources for the old, ^{14}C-depleted water detected during the last deglaciation. My record illustrates variations in ε_{Nd} values from -0.3 to -3.0. Pre-LGM (before 21 kyr BP) ε_{Nd} values range between -1 to -2.5, with values around -1 during the LGM. A prominent negative excursion to approximately -3.0 occurs at the beginning of the

deglaciation, with a subsequent increase to -1.7 during the later half of Heinrich stadial 1 (HS1). Nd isotopic values continue to increase into the Bølling-Allerød (B-A) warm interval, where they plateau at ~ -1.4. There is limited data during the cold Younger Dryas (YD) interval; however, there is a hint of a minor negative ε_{Nd} excursion during the Younger Dryas (YD) followed by a positive excursion and values ranging from -0.3 to -1.6 in the Holocene. There is some structure in the Holocene record, but the mean ε_{Nd} value is comparable to LGM values and tends to be higher than pre-LGM values.

Discussion

In general, modern AAIW ε_{Nd} values are ~ -6 to -8 ε_{Nd} units and NPIW values are ~ 0 to -4 ε_{Nd} units (Goldstein and Hemming, 2003). Thus, the overall -0.3 to -3.0 range in ε_{Nd} values observed in our data would seem to represent waters dominantly sourced from the North Pacific throughout the last 38 kyr. However, the Nd isotope signature of southern-sourced AAIW is modified during its transit through the Pacific in the region of Papua New Guinea (PNG) due to interactions with volcanic inputs that introduce much higher Nd isotopic ratios (ε_{Nd} ~ +7) (Iacan and Jeandel, 2001). As a result, the measured ε_{Nd} value of this modified AAIW is ~ -2.8 (Lacan and Jeandel, 2001), and it is this water that flows eastward along the equator to influence EqIW. In addition, our youngest ε_{Nd} value of -1.5 may be taken as a minimum value for modern NPIW in this region based on the most conservative scenario that the site is currently bathed by pure NPIW.

In the absence of any high-resolution ε_{Nd} reconstructions from the AAIW and NPIW source regions, we begin with the assumption that the end-member compositions of these two water masses have remained relatively constant since the LGM. In the context of constant end-members, ε_{Nd} excursions to more radiogenic values represent an increased flux of NPIW (or less AAIW), while excursions towards less radiogenic

values record an increased flux of AAIW (or less NPIW). Following this logic, the pre-LGM period (before 21 kyr BP) in our record indicates a mixture of NPIW and AAIW, with a relatively decreased component of AAIW during the LGM, similar to Holocene values (Figure 4-2). AAIW intensified during the deglaciation, comprising most of the water mass during the early part of the HS1 event, then decreased during the B-A warming period and might have increased slightly again during the YD. Post YD the region was once again dominated by NPIW.

The timing of major fluctuations in AAIW interpreted from Nd isotopes is broadly in agreement with the idea of depleted ^{14}C originating in the Southern Ocean (Figure 4-3B, C). The deglacial decrease in ε_{Nd} values around 18 kyr BP likely represents the first pulse of AAIW into the eastern North Pacific as the Southern Ocean recovered from surface stratification (Francois et al., 1997; Sigman and Boyle, 2000) and/or extensive sea-ice coverage (Stephens and Keeling, 2000) during the LGM. The timing of this pulse defined by Nd isotopes coincides with a negative $\delta^{13}C$ excursion of thermocline dwelling foraminifera *Neogloboquadrina dutertrei* in the EEP (Spero and Lea, 2002; Pena et al., 2008b) also interpreted to indicate an influx of older water from the Southern Ocean (Figure 4-3D). In the Southern Ocean higher productivity indicated by an increased opal flux near Antarctica also supports increased upwelling of nutrient-rich abyssal water and hence more AAIW activity (Anderson et al., 2009) at this time (Figure 4-3E). Evidence of increased deglacial AAIW has also been reported from Nd isotopic records in the Atlantic (Pahnke et al., 2008). .

Comparison of Northern (Grootes and Stuiver, 1997) and Southern Hemisphere (Monnin et al., 2001) ice core temperatures indicate that deglacial warming in the

Southern Ocean preceded deglaciation in the high latitude Northern Hemisphere (Figure 4-3A). Early warming in the Southern Hemisphere and invigorated AAIW formation are well know (Marchitto et al., 2007; Toggweiler et al., 2006; Stott et al., 2009). In contrast, the deep and shallow Northern Pacific did not start responding to deglaciation until the beginning of the B-A period (Galbraith et al., 2007) (~ 14.8 kyr BP), although localized intermediate water formation during HS1 in the Western North Pacific (WNP) has recently been reported (Okazaki et al, 2010). Therefore, temporal differences in the deglacial history between the Northern and Southern Hemispheres also imply that the Nd isotopic excursion at ~18 kyr was controlled by intermediate water mass readjustment in the Southern Hemisphere.

The deep ocean represents the most likely storage area for old carbon during the last glaciation due to the proposed mechanism of formation and the volume of the old carbon reservoir (Broecker and Barker, 2007; Broecker, 2009). Our ε_{Nd} data imply that the old carbon reported from the Baja site (Marchitto et al., 2007) was sourced from the Southern Ocean via AAIW that was modified in the equatorial Pacific. A recent study indicates (De Pol-Holz et al., 2010) no evidence for deglacial old ^{14}C in intermediate waters off Chile, close to one of the main regions of AAIW formation today. Part of that AAIW takes a complicated route in the South Pacific before reaching the Baja site. Another portion of this AAIW passes from the Southeastern Pacific, through the Drake Passage (Talley, 1999) and circumnavigates Antarctica where it could have picked up old carbon from the deep southern abyss before circulating back into the Indian and Pacific Oceans. The Chilean site (De Pol-Holz et al., 2010) may be too close to the region of active AAIW formation to have been influenced by AAIW that acquired older

carbon during its journey around Antarctica. Recent evidence of radiocarbon depleted AAIW reported from tropical South Atlantic off Brazil during the HS1 and YD intervals (Mangini et al., 2010) and from the deep Southern Ocean (Skinner et al., 2010) during the last glacial period are consistent with acquisition of old abyssal carbon east of the Drake Passage.

Half way through the HS1 event ε_{Nd} values in the Baja record become more positive in a pattern that does not match the Baja $\Delta^{14}C$ record. The $\Delta^{14}C$ record depicts a strong influence of aged water until the beginning of B-A period (Figure 4-3C), whereas the ε_{Nd} record illustrates increasing values during the later half of HS1, which could be interpreted as decreasing AAIW. However, no other lines of evidence support diminished AAIW at this time (Anderson et al., 2009; Monnin et al., 2001; Spero and Lea, 2002) (Figure 4-3). Alternatively, an increased NPIW flux could potentially explain the observed discrepancy during the mid HS1. Although the WNP is known to be a region of active intermediate-deep water formation during HS1, these waters were relatively enriched in ^{14}C and do not appear to have reached the eastern Pacific (Okazaki et al., 2010). In the absence of any compelling evidence in favor of diminished AAIW or increased NPIW, we must appeal to modified end-member ε_{Nd} values of AAIW or NPIW to explain the decoupling between $\Delta^{14}C$ and ε_{Nd}. Given that ε_{Nd} values suggest the water at the Baja site is dominated by AAIW by mid HS1, we focus on this end-member. Changes in weathering in the PNG region, possibly due to a southward shift of the Intertropical Convergence Zone (Krebs and Timmerman, 2007) and increased rainfall around PNG during deglaciation, could have introduced more positive PNG-type ε_{Nd} values to AAIW.

Changes in ε_{Nd} during the B-A and YD are more subtle but appear to be consistent with anticipated variations in NPIW and AAIW. During B-A opal flux data from the Southern Ocean indicates reduced nutrient upwelling and AAIW formation (Andersen et al., 2009). A relative increase in the proportion of NPIW versus AAIW during the B-A period is consistent with the small increase observed in ε_{Nd} at the Baja site. A minor negative ε_{Nd} excursion (albeit a one-point low) during the YD is consistent with rejuvenation of AAIW in accordance with $\Delta^{14}C$ and other indicators of increased AAIW from the Southern Ocean (figs. 4-3b, 4-3c). Post YD values are comparable to LGM values, reflecting increased influence of NPIW during the Holocene. This scenario is consistent with rearrangements in Holocene deep and intermediate circulation patterns leading to a modern system that is dominated by NPIW at this site.

Summary

Evidence of old carbon at intermediate depths in the eastern North Pacific has been one of the most intriguing paleoceanographic findings establishing the mechanism of atmospheric CO_2 leakage at the end of the last glaciation. Direct and indirect evidence in favor of an old carbon reservoir and increased AAIW have been reported from the Southern Ocean (Spero and Lea, 2002; Anderson et al., 2009; Skinner et al., 2010), but there is no direct proof that these Southern waters reached the tropical North Pacific during deglaciation. This coupled study of ε_{Nd} and $\Delta^{14}C$ reports variations in the relative dominance of more radiogenic NPIW and less radiogenic AAIW over the past 38 ky and supports the concept of an increased contribution of AAIW at the beginning of the deglaciation, suggesting that the old carbon was transported from the deep southern abyss to the shallow tropics via AAIW.

Table 4-1. Nd isotopes from fossil fish teeth/derbis of core MV99-MC19/GC31/PC08

Sample	Composite depth (m)	Calendar Age (kyr BP)	ε_{Nd}	error (+/-)
MC19, 10-11cm	0.100	0.32	-1.4	0.4
MC19, 25-26cm	0.250	0.81	-0.7	0.2
MC19, 40-41cm	0.400	1.29	-0.9	0.2
GC31-3, 22-23cm	0.475	1.54	-0.9	0.2
GC-31-3, 50-51cm	0.755	2.44	-0.3	0.2
GC31-3, 70-71 cm	0.950	3.08	-0.4	0.3
GC31-3, 100-101 cm	1.255	4.07	-1.6	0.2
GC-31-3, 123-124 cm	1.480	4.79	-0.8	0.2
GC31-2, 0-1cm	1.755	5.69	-1.1	0.2
GC31-2, 50-51cm	2.255	7.31	-1.0	0.1
GC31-2, 100-101cm	2.755	9.01	-1.3	0.2
GC31-1, 8-9 cm	3.255	10.79	-0.8	0.2
PC08-9, 60cm	3.410	11.32	-0.3	0.5
PC08-9, 85cm	3.660	12.12	-1.7	0.2
PC08-9, 110cm	3.910	12.88	-1.4	0.2
PC08-9, 130cm	4.110	13.57	-1.3	0.2
PC08-9, 140-142cm	4.220	13.94	-1.5	0.3
PC08-9, 140-142cm	4.220	13.94	-1.7	0.3
PC08-9, 150 cm	4.310	14.2	-2.0	0.3
PC08-8, 16-17cm	4.475	14.65	-1.8	0.2
PC08-8, 25-26 cm	4.565	14.96	-1.7	0.2
PC08-8, 35 cm	4.660	15.3	-1.7	0.1
PC08-8, 45-46cm	4.765	15.67	-2.0	0.2
PC08-8, 65-66 cm	4.965	16.37	-3.0	0.3
PC08-8,105-106	5.365	17.78	-1.9	0.1
PC08-8,115-117cm	5.470	18.12	-1.3	0.1
PC08-8,125cm	5.560	18.41	-0.9	0.2
PC08-7,60-61cm	6.415	21.14	-1.0	0.1
PC08-7,80-81cm	6.615	21.77	-1.9	0.2
PC08-7,132-133cm	7.135	23.43	-1.5	0.2
PC08-6,20-21	7.585	25.15	-1.8	0.2
PC08-5,25cm	9.010	30.7	-2.2	0.2
PC08-5,130cm	10.060	34.55	-2.3	0.2
PC08-4,15cm	10.410	35.89	-1.8	0.2
PC08-4,65cm	10.910	37.92	-0.9	0.2

$\varepsilon_{Nd}=((^{143}Nd/^{144}Nd)_{measured}/(^{143}Nd/^{144}Nd)_{CHUR})-1) * 10^4$. All reported $^{143}Nd/^{144}Nd$ ratios were corrected for mass fractionation using $^{146}Nd/^{144}Nd$ =0.7219. International standard JNdi-1 was analyzed between every 5-6 unknown samples and the average of these standard runs were compared to a long term TIMS JNdi-1 value of 0.512103 +/- 0.000014 to determine a correction factor for each of the samples analyzed on that day. Long term external reproducibility of JNdi-1 analyses on the Nu is 0.000014 (0.3 ε_{Nd} units). Error bars for all figures in the text represent external reproducibility unless the internal error is larger.

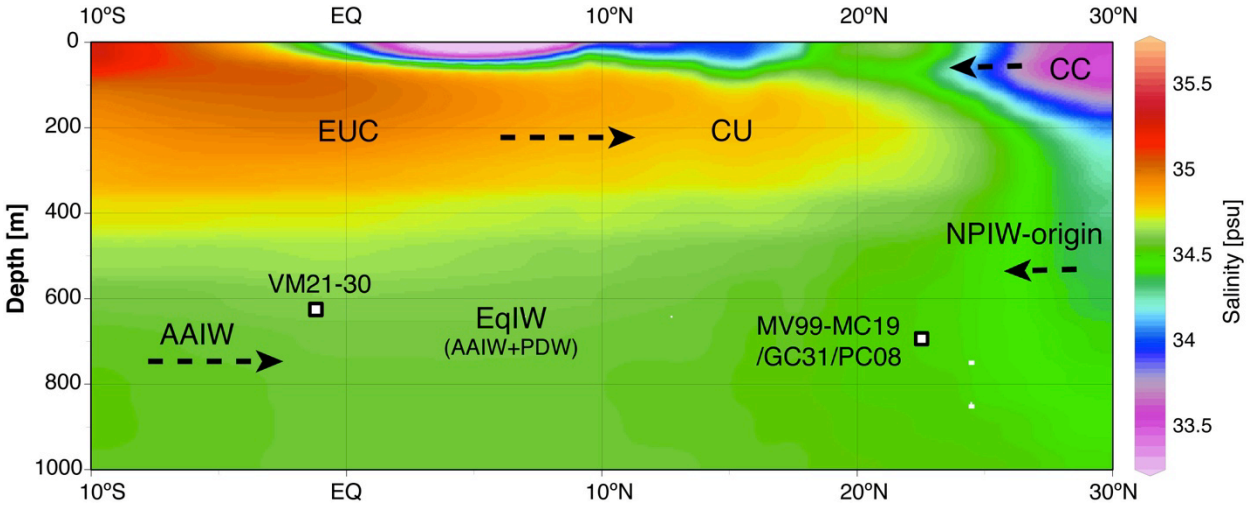

Figure 4-1. Modern hydrography. Depth profile of annual mean salinity along the continental margin of the eastern North Pacific. Cores MV99-MC19/GC31/PC08 (23.5°N, 111.6°W) and VM21-30 (1°S, Eastern Equatorial Pacific (EEP)) are bathed by EqIW, which is largely a combination of NPIW, AAIW, and PDW. AAIW: Antarctic Intermediate Water; CC: California Current; CU: California Undercurrent; EqIW: Equatorial Intermediate Water; EUC: Equatorial Undercurrent; NPIW: North Pacific Intermediate Water; PDW: Pacific Deep Water.

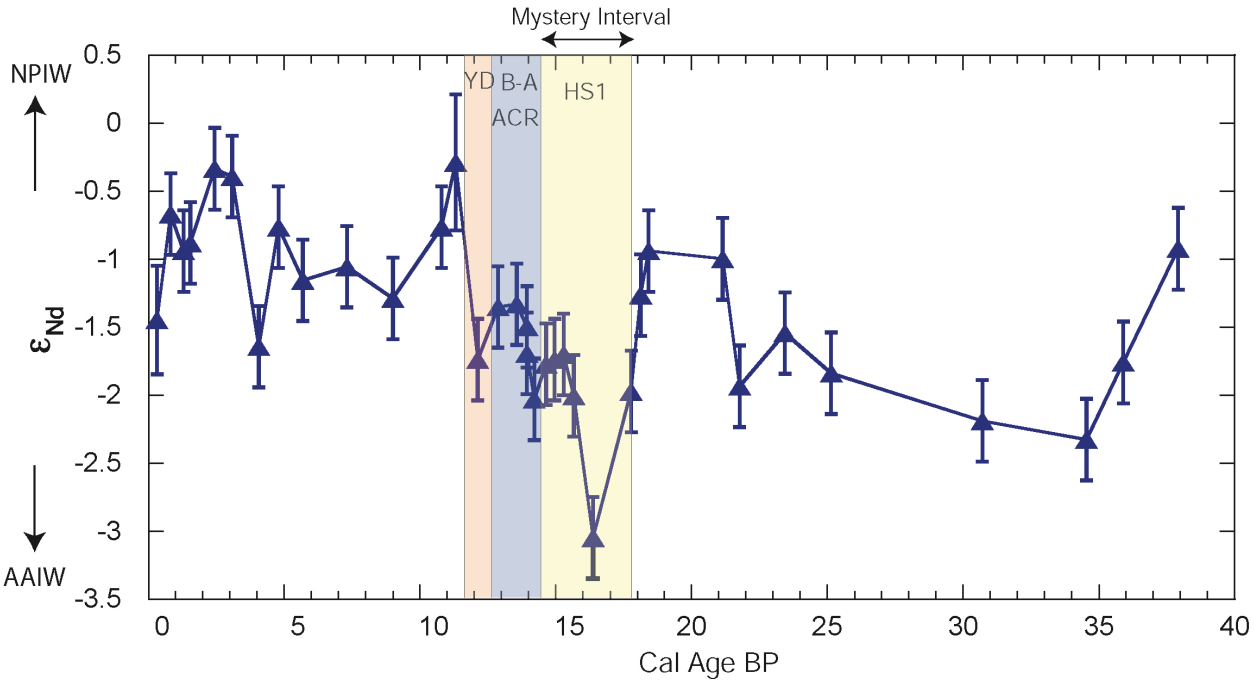

Figure 4-2. ε_{Nd} record from Baja California for the last 38kyr BP. ε_{Nd} of fossil fish teeth/debris plotted against calendar age. [$\varepsilon_{Nd}=(((^{143}Nd/^{144}Nd)_{measured}/(^{143}Nd/^{144}Nd)_{CHUR})-1) * 10^4$]. Vertical error bars represent long term external reproducibility of the JNdi-1 standard (0.3 ε_{Nd} units) except for samples with a higher internal error. The yellow, blue, and pink shaded areas indicate Heinrich Stadial (HS1), Bølling-Allerød (B-A), and Younger Dryas (YD) climate episodes. The period between 14.5 and 17.5 kyr BP has been referred to as the "Mystery Interval".

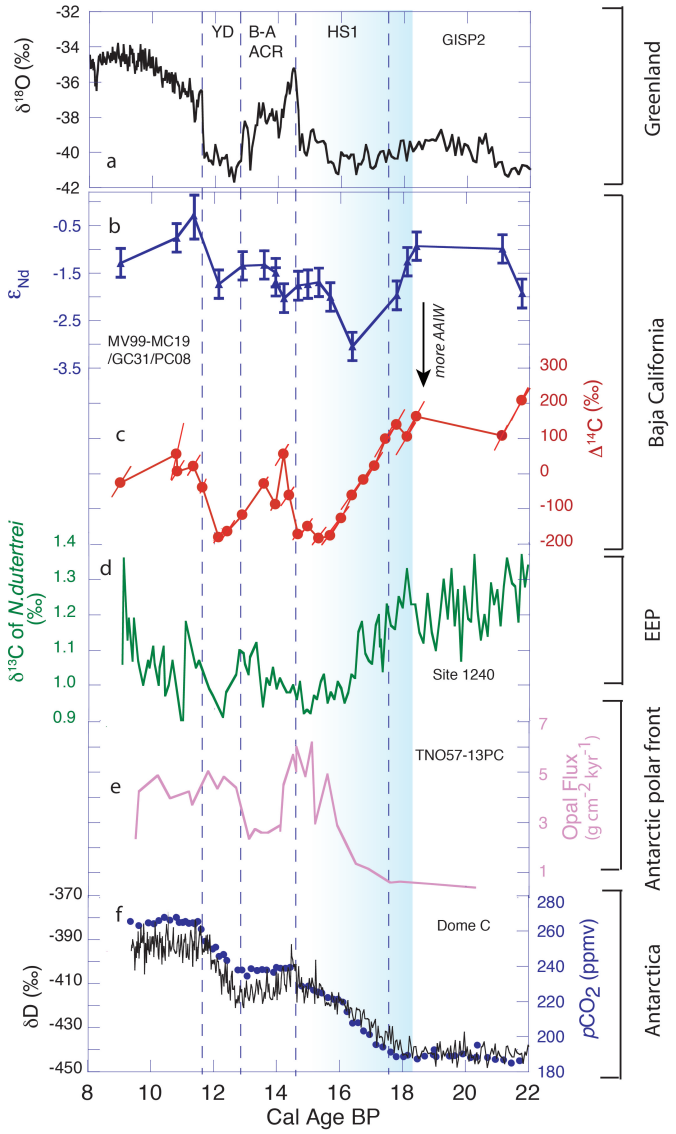

Figure 4-3. Meridional multi-proxy responses to the last deglaciation (8 to 22kyr BP). (a) Greenland ice cores temperatures, (b) ε_{Nd} from MV99-MC19/GC31/PC08, (c) $\Delta^{14}C$ from MV99-MC19/GC31/PC08 (ref.2), (d) $\delta^{13}C$ of thermocline dwelling foraminifera *Neogloboquadrina dutertrei* in the Eastern Equatorial Pacific (EEP), (e) opal flux data from the Antarctic Polar Front, (f) atmospheric CO_2 (blue circles) and ice core deuterium (δD) temperature proxy (black) from Antarctic Dome C placed on the GISP 2 time scale. The blue shaded area highlights the initial deglaciation.

CHAPTER 5
CONCLUSIONS

The over arching goals of this dissertation have been to better understand the climatic response to changing weathering regimes and reorganization of ocean circulations during two climatically important threshold events; namely the onset of large Cenozoic ice sheets at the Eocene-Oligocene boundary (~34 Ma) and the end of the last major Northern Hemisphere glaciation during the last deglacial (~18 kry) ago. In order to achieve these goals the research design included developing a geochemical proxy for weathering, application of the newly established proxy to develop time series records, and application of an existing water mass tracer proxy to understand water mass reorganization during a threshold climatic event.

The first step uses Pb isotopes from seawater and deep sea residues to demonstrate that reliable seawater Pb isotopes could be extracted from deep sea sediments. Bulk sediment from ten samples ranging in age from mid Eocene to early Miocene from ODP site 1090 on the Agulhus Ridge was subjected to a sequential leaching protocol that involved exposure to acetic acid, followed by a first and second HH extraction. Agreement of Pb isotopes between the three fractions indicates a common deep water source. During the course of this study, excellent inter and intra-lab reproducibility of Pb isotopes in the HH extracts were observed, which emphasize the reliability of the developed extraction protocol. Several lines of evidence provide additional support for the idea that measured Pb isotopes represent seawater. These include an Al mass balance approach to evaluate the impact of detrital contaminants, comparison of Sr isotopes from the HH extraction and the seawater Sr isotope curve, and comparison of Nd isotopes from the HH extraction and co-existing fossil fish teeth.

Fe-Mn oxide nodule standards NOD-A1 and NOD-P1 are recognized to record ambient bottom water isotopic signatures and close agreement between total digestion and HH extracted Pb isotopes from these nodules also indicates that the HH extracted Pb isotopes represent bottom water values. Thus, all tests suggest that the measured Pb isotopes in HH extractions not only represent seawater, but presumably record bottom water values. During the course of this study, the fossil fish teeth were tested as another potential archive for bottom water Pb isotopic signals. Unconstrained combinations of initial Pb incorporated in the biophosphate, Pb incorporated during diagenietic enrichment, and radiogenic Pb produced from in situ decay of U and Th renders this archive unsuitable for Pb isotopic studies. Major element data from the leaching experiment indicates the presence of manganon carbonate, a refractory carbonate phase, in addition to Fe-Mn oxides. Cross plots between HREE/LREE vs. MREE/MREE* indicate that such plots can be an effective tool to identify cross contamination during the leaching experiment.

Once the Pb isotopes in Fe-Mn oxides and similar authigenic phases extracted from bulk sediments were established as archives for bottom water Pb isotopes, this proxy was used to understand the weathering history of Antarctica during the Eocene-Oligocene (E/O) transition. The E/O transition marks the beginning of large-scale glaciation on continental Antarctica. Distinct radiogenic changes in residue $^{206}Pb/^{204}Pb$, $^{207}Pb/^{204}Pb$ and $^{208}Pb/^{204}Pb$ during the E/O boundary indicate weathering intensification of fresh, continental silicate rocks, while decoupling of seawater and residue $^{206}Pb/^{204}Pb$ indicate that one of the major contributors to Antarctic weathering fluxes during the EOT glaciation was old carbonate.

Seawater Nd isotopes preserved in fossil fish teeth are a well-recognized water mass tracer that is frequently used in paleoceanography reconstruction of water mass sources and flowpaths. It is believed that the glacial Southern Ocean played a critical role in the storage of a high density, saline, CO_2-rich, ^{14}C-depleted water mass during the last glacial period. Recent study of $\Delta^{14}C$ from foraminifera revealed evidence of ^{14}C-depleted old water from intermediate ocean depths (~700 m) in the tropical North Pacific. Studies of $\Delta^{14}C$ from foraminifera provide the age of the water mass involved, but they provide no information about source. In this study I used Nd isotopes in fossil fish teeth/debris to demonstrate that Antarctic Intermediate Water most likely carried this old carbon-rich water from the deep Southern abyss during the last deglaciation.

LIST OF REFERENCES

Abouchami, W., Goldstein, S.L., 1995. A lead isotopic study of Circum-Antarctic manganese nodules. Geochimica et Cosmochimica Acta, 59(9), 1809-1820.

Abouchami, W.G., S L; Galer, S J G; Eisenhauer, A., Mangini, A., 1997. Secular changes of lead and neodymium in Central Pacific seawater recorded by a Fe-Mn crust. Geochimica et Cosmochimica Acta, 61(18), 3957-3974.

Albarede, F., Goldstein, S.L., 1992. A world map of Nd isotopes in seafloor ferromanganese deposits. Geology, 20, 761-763.

Albarede, F., Goldstein, S.L., Dautel, D., 1997. $^{143}Nd/^{144}Nd$ of Mn nodules from the Southern and Indian oceans, the global oceanic Nd budget, and their bearing on the deep ocean circulation during the Quarternary. Geochimica et Cosmochimica Acta, 61, 1277-1291.

Alleman L. Y., Veron A. J., Church T. M., Flegal A. R. and Hamelin B., 1999. Invasion of the abyssal North Atlantic by modern anthropogenic lead. Geophysical Research Letters, 26, 1477–1480.

Arsouze, T., Dutay, J.-C., Lacan, F., Jeandel, C., 2009. Reconstructing the Nd oceanic cycle using a coupled dynamical – biogeochemical model. Biogeosciences, 6, 2829-2846.

Amakawa H., Nozaki Y., Alibo D. S., Zhang J., Fukugawa K., Nagai H., 2004a. Neodymium isotopic variations in Northwest Pacific water. Geochim. Cosmochim. Acta . 68, 715–727.

Amakawa H., Alibo D. S., Nozaki Y., 2004b. Nd abundance and isotopic composition distributions of surface seawaters of the Northwest Pacific Ocean and its adjacent seas. Geochem. J., 38, 493–504.

Amakawa, H., Sasaki, K., Ebihara, M., 2009. Nd isotopic composition in the central North Pacific. Geochimica et Cosmochimica Acta, 73(16), 4705-4719

Anderson, R.F., Ali, S., Bradtmiller, L.I., Nielsen, S.H.H., Fleisher, M.Q., Anderson, B.E., Burckle, L.H., 2009. Wind-Driven Upwelling in the Southern Ocean and the Deglacial Rise in Atmospheric CO_2. Science, 323(5920), 1443-1448.

Axelsson, M.D., Rodushkin, I., Ingri, J., Ohlander, B., 2002. Multielemental analysis of Mn–Fe nodules by ICP-MS: optimisation of analytical method. Analyst, 127, 76–82.

Baker, J., Peate, D., Waight, T., Meyzen, C., 2004. Pb isotopic analysis of standards and samples using a 207Pb-204Pb double spike and thallium to correct for mass bias with a double-focusing MC-ICP-MS. Chemical Geology, 211(3-4), 275-303.

Barker, P.R., Kennett, J.P., et al., 1988. Proc. ODP Sci. Results. Ocean Drilling Program, College Station, TX. 113, pp. 785.

Basak, C., Martin, E.E., Horikawa, K., Marchitto, T.M., 2010. Southern Ocean source of ^{14}C-depleted carbon in the North Pacific Ocean during the last deglaciation. Nature Geoscience, 3(11), 770-773.

Basak, C., Martin, E.E., Kamenov, G.D., 2011. Seawater Pb isotopes extracted from Cenozoic marine sediments Chemcial Geology, *in press*.

Bayon, G., German, C.R., Boella, R.M., Milton, J.A., Taylor, R.N., Nesbitt, R.W., 2002. An improved method for extracting marine sediment fractions and its application to Sr and Nd isotopic analysis. Chemical Geology, 187(3-4), 179-199.

Berner, R.A., 1999. A new look at the long-term carbon cycle. GSA Today, 9(11).

Blum, J.D., Erel, Y., 2003. Radiogenic Isotopes in Weathering and Hydrology. In: Holland, H.D., Turekian, K.K. (Eds.), Surface and Ground Water, Weathering, and Soils. Treatise of Geochemistry. Elsevier-Pergamon, Oxford, pp. 365-392.

Bohaty, S.M., 2006. Middle Eocene to early Oligocene paleoceanography of the Southern Ocean: critical events in the green house to icehouse transition, Ph.D. Thesis, University of California, Santa Cruz, Santa Cruz, CA, 305 pp.

Bostock, H.C., 2004. Geochemcially tracing the intermediate and surface waters in the Tasman Sea, southwest Pacific, Ph.D. Thesis, Australian National University, 207 pp.

Bostock, H.C., Opdyke, B.N., Williams, M.J.M., 2010. Characterising the intermediate depth waters of the Pacific Ocean using [delta]13C and other geochemical tracers. Deep Sea Research Part I: Oceanographic Research Papers, 57, 847-859.

Boyle, E.A., 1983. Manganese carbonate overgrowths on foraminifera tests. Geochimica et Cosmochimica Acta, 47(10), 1815-1819.

Boyle, E.A., Keigwin, L.D., 1985. A Comparison of Paleochemical Records from the North Atlantic and North Pacific Ocean: Changes in Deep Ocean Circulation and Chemical Inventories. Earth and Planetary Science Letters, 76, 135-150.

Boyle, E.A., Chapnick, S.D., Shen, G.T., 1986. Temporal variability of lead in the western North Atlantic. Journal of Geophysical Research, 91, 8573-8593.

Broecker, W., 2009. The Mysterious ^{14}C Decline. Radiocarbon, 51(1), 109-119.

Broecker, W.S., Peng, T.H., 1982. Tracers in the sea. Report, Lamont-Doherty Geol. Obs. Lamont-Doherty Geol. Obs., Palisades, N.Y.

Broecker, W., Barker, S., 2007. A 190 ‰ drop in atmosphere's $\Delta^{14}C$ during the "Mystery Interval" (17.5 to 14.5 kyr). Earth and Planetary Science Letters, 256(1-2), 90-99.

Brown, H., Silver, L.T., 1955. The possibility of obtaining long-term supplies of uranium, thorium, and other substances of uranium from igneous rocks. , Proceedings of Conference on Peaceful Use of Atomic Energy, Geneva, pp. 91–95.

Browning, J.V., Miller, K.G., Pak, D.K., 1996. Global implications of lower to middle Eocene sequence boundaries on the New Jersey coastal plain: The icehouse cometh. Geology, 24(7), 639-642.

Burton, K.W., Ling, H.-F., O'Nions, R.K., 1997. Closure of the Central American Isthmus and its effect on deep-water formation in the north Atlantic. Nature, 386, 382-385.

Byrne, R.H., Liu, X., Schijf, J., 1996. The influence of phosphate co-precipitation on rare earth element distributions in natural waters. Geochimica et Cosmochimica Acta, 60, 3341-3346.

Cande, S.C., Kent, D.V., 1995. Revised calibration of the geomagnetic polarity timescale for the Late Cretaceous and Cenozoic. Journal of Geophysical Research, 100(B4), 6093-6095.

Channell, J.E.T., Galeotti, S., Martin, E.E., Billups, K., Scher, H.D., Stoner, J.S., 2003. Eocene to Miocene magnetostratigraphy, biostratigraphy. and chemostratigraphy at ODP Site 1090 (sub-Antarctic South Atlantic). Geological Society of America Bulletin, 115, 607-623.

Charette, M.A., Sholkovitz, E.R., Hansel, C.M., 2005. Trace element cycling in a subterranean estuary: Part 1. Geochemistry of the permeable sediments. Geochimica et Cosmochimica Acta, 69(8), 2095-2109.

Chen, J.H., Lawrence Edwards, R., Wasserburg, G.J., 1986. ^{238}U,^{234}U and^{232}Th in seawater. Earth and Planetary Science Letters, 80(3-4), 241-251.

Chester, R., Hughes, M.J., 1967. A chemical technique for the separation of ferromanganese minerals, carbonate minerals and adsorbed trace elements from pelagic sediments. Chemical Geology, 2, 249–262.

Coffin, M.F., 1992. Subsidence of the Kerguelen Plateau: the Atlantis Concept, Proceedings of the Ocean Drilling Program, Scientific Results, Ocean Drilling Program, College Station, TX, Vol. 120, pp. 945-950.

Coxall, H.K., Wilson, P.A., Palike, H., Lear, C.H., Backman, J., 2005. Rapid stepwise onset of Antarctic glaciation and deeper calcite compensation in the Pacific Ocean. Nature, 433(7021), 53-57.

Craig H., Krishnaswami S., Somayajulu B. L. K., 1973. ^{210}Pb-^{226}Ra, Radioactive disequilibrium in the deep sea. Earth and Planetary Science Letters, 17, 295-305.

DeConto, R.M., Pollard, D., 2003. Rapid Cenozoic glaciation of Antarctica induced by declining atmospheric CO_2. Nature, 421(6920), 245-249.

De Pol-Holz, R., Keigwin, L., Southon, J., Hebbeln, D., Mohtadi, M., 2010. No signature of abyssal carbon in intermediate waters off Chile during deglaciation. Nature Geoscience, 3(3), 192-195.

Elderfield H., 1988. The oceanic chemistry of the rare-earth elements. Phil. Trans. Roy. Soc. London Ser. A: Math. Phys. Eng. Sci., 3256(1583), 105–12.

Elderfield H. , Greaves, M.J., 1982. The rare earth elements in seawater. Nature, 296, 214–219.

Elliot, D.H., 1975. Tectonics of Antarctica: A review. American Journal of Science, 275(A), 45-106.

EPICA community members, 2004. Eight glacial cycles from an Antarctic ice core. Nature, 429(6992), 623-628.

Erel Y., Harlavan Y., Blum J. D., 1994. Lead isotope systematics of granitiod weathering. Geochimica et Cosmochimica Acta, 58, 5299–5306.

Exon, N., 2000. Climate change; history documented in Tasmanian waters. Australian Geoscience News, 56, 10–11.

Fairbanks, R.G., Mortlock, R.A., Chiu, T.-C., Cao, L., Kaplan, A., Guilderson, T.P., Fairbanks, T.W., Bloom, A.L., Grootes, P.M., Nadeau, M.-J., 2005. Radiocarbon calibration curve spanning 0 to 50,000 years BP based on paired $^{230}Th/^{234}U/^{238}U$ and ^{14}C dates on pristine corals. Quaternary Science Reviews, 24(16-17), 1781-1796.

Foster, G.L., Vance, D., 2006. Negligible glacial-interglacial variation in continental chemical weathering rates. Nature, 444(7121), 918-921.

Francois, R., Altabet, M.A., Yu, E.-F., Sigman, D.M., Bacon, M.P., Frank, M., Bohrmann, G., Bareille, G., Labeyrie, L.D., 1997. Contribution of Southern Ocean surface-water stratification to low atmospheric CO_2 concentrations during the last glacial period. Nature, 389(6654), 929-935.

Frank, M., 2002. Radiogenic Isotopes: Tracers of past Ocean circulation and erosional input. Reviews of Geophysics, 40(1).

Galbraith, E.D., Jaccard, S.L., Pedersen, T.F., Sigman, D.M., Haug, G.H., Cook, M., Southon, J.R., Francois, R., 2007. Carbon dioxide release from the North Pacific abyss during the last deglaciation. Nature, 449(7164), 890-893.

Gersonde, R., Hodell, D.A., Blum, P., et. al., 1999. Site 1090. Proceedings of the Ocean Drilling Program, Initial Reports, 177, 1-101.

Goldstein, S.L., Jacobsen, S.B., 1987. The Nd and Sr isotopic systematics of river-water dissolved material: Implications for the sources of Nd and Sr in the seawater. Chemical Geology, 66, 245-272.

Goldstein, S.L., Hemming, S.H., 2003. Long lived isotopic tracers in oceanography, paleoceanography, and ice sheet dynamics. In: Elderfield, H. (Ed.), Treatise on Geochemistry. Elsevier, New York, pp. 453–489.

Goodge, J.W., Myrow, P., Williams, I.S., Bowring, S.A., 2002. Age and Provenance of the Beardmore Group, Antarctica: Constraints on Rodinia Supercontinent Breakup. The Journal of Geology, 110, 393–406.

Gourlan, A.T., Meynadier, L., Allègre, C.J., 2008. Tectonically driven changes in the Indian Ocean circulation over the last 25 Ma: Neodymium isotope evidence. Earth and Planetary Science Letters, 267(1-2), 353-364.

Grootes, P., Stuiver, M., 1997. Oxygen 18/16 variability in Greenland snow and ice with 10^{-3} to 10^{5} year time resolution. Journal of Geophysical Research, 102(C12), 26455-26470.

Grün, R., Aubert, M., Hellstrom, J., Duval, M., 2010. The challenge of direct dating old human fossils. Quaternary International, 223-224, 87-93.

Gutjahr, M., Frank, M., Stirling, C.H., Klemm, V., van de Flierdt, T., Halliday, A.N., 2007. Reliable extraction of a deepwater trace metal isotope signal from Fe-Mn oxyhydroxide coatings of marine sediments. Chemical Geology, 242, 351-370.

Gutjahr, M., Frank, M., Stirling, C.H., Keigwin, L.D., Halliday, A.N., 2008. Tracing the Nd isotope evolution of North Atlantic deep and intermediate waters in the western North Atlantic since the Last Glacial Maximum from Blake Ridge sediments. Earth and Planetary Science Letters, 266, 61-77.

Gutjahr, M., Frank, M., Halliday, A.N., Keigwin, L.D., 2009. Retreat of the Laurentide ice sheet tracked by the isotopic composition of Pb in western North Atlantic seawater during termination 1. Earth and Planetary Science Letters, 286(3-4), 546-555.

Haley, B.A., Klinkhammer, G.P., McManus, J., 2004. Rare earth elements in pore waters of marine sediments. Geochimica et Cosmochimica Acta, 68(6), 1265-1279.

Haley, B.A., M. Frank, R. F. Spielhagen, and J. Fietzke, 2008. Radiogenic isotope record of Arctic Ocean circulation and weathering inputs of the past 15 million years. Paleoceanography, 23, PA1S13.

Hamelin, B., Grousset, F.E., Biscaye, P.E., Zindler, A., 1989 Lead isotopes in Trade Wind aerosols at Barbados: the influence of European emissions over the North Atlantic. Journal of Geophysical Research, 94, 16243-16250.

Harlavan, Y., Erel, Y., Blum, J.D., 1998. Systematic Changes in Lead Isotopic Composition with Soil Age in Glacial Granitic Terrains. Geochimica et Cosmochimica Acta, 62(1), 33-46.

Henderson, G.M., Maier-Reimer, E., 2002. Advection and removal of ^{210}Pb and stable Pb isotopes in the oceans: a general circulation model study. Geochimica et Cosmochimica Acta, 66(2), 257-272.

Herguera, J.C., Herbert, T., Kashgarian, M., Charles, C., 2010. Intermediate and deep water mass distribution in the Pacific during the Last Glacial Maximum inferred from oxygen and carbon stable isotopes. Quaternary Science Reviews, 29(9-10), 1228-1245.

Hodell, D.A., Woodruff, F., 1994. Variations in the strontium isotopic ratio of seawater during the Miocene: Stratigraphic and geochemical implications. Paleoceanography, 9, 405-426.

Horikawa, K., Asahara, Y., Yamamoto, K., Okazaki, Y., 2010 Intermediate water formation in the Bering Sea during glacial periods: Evidence from neodymium isotope ratios. Geology, 38 (5), 435-438

Huber, B.T., 1991. Paleogene and early Neogene planktonic foraminifera biostratigraphy of sites 738 and 744, kerguelen Plateau (southern Indian Ocean) Proc. ODP, Sci. Results, Ocean Drilling Program, College Station, TX, 110, pp. 427-449.

Huber, B.T., Quillevere, F., 2005. Revised paleogene planktonic foraminiferal biozonation for the austral realm. Journal of Foraminiferal Research, 35(4), 299-314.

Hughen, K., Lehman, S., Southon, J., Overpeck, J., Marchal, O., Herring, C., Turnbull, J., 2004. ^{14}C Activity and Global Carbon Cycle Changes over the Past 50,000 Years. Science, 303(5655), 202-207.

Jaccard, S.L., Haug, G.H., Sigman, D.M., Pedersen, T.F., Thierstein, H.R., Rohl, U., 2005. Glacial/Interglacial Changes in Subarctic North Pacific Stratification. Science, 308(5724), 1003-1006.

Jahn, B.-M., Cuvellier, H., 1994. Pb-Pb and U-Pb geochronology of carbonate rocks: an assessment. Chemical Geology, 115(1-2), 125-151.

Jeandel, C., 1993. Concentration and isotopic composition of Nd in the South Atlantic Ocean. Earth and Planetary Science Letters, 117(3-4), 581-591.

Jones, K.M., Khatiwala, S.P., Goldstein, S.L., Hemming, S.R., van de Flierdt, T., 2008. Modeling the distribution of Nd isotopes in the oceans using an ocean general circulation model. Earth and Planetary Science Letters, 272(3-4), 610-619.

Jouzel, J., Masson-Delmotte, V., Cattani, O., Dreyfus, G., Falourd, S., Hoffmann, G., Minster, B., Nouet, J., Barnola, J.M., Chappellaz, J., Fischer, H., Gallet, J.C., Johnsen, S., Leuenberger, M., Loulergue, L., Luethi, D., Oerter, H., Parrenin, F., Raisbeck, G., Raynaud, D., Schilt, A., Schwander, J., Selmo, E., Souchez, R., Spahni, R., Stauffer, B., Steffensen, J.P., Stenni, B., Stocker, T.F., Tison, J.L., Werner, M., Wolff, E.W., 2007. Orbital and Millennial Antarctic Climate Variability over the Past 800,000 Years. Science 317, 793-796.

Katz, M.E., Miller, K.G., Wright, J.D., Wade, B.S., Browning, J.V., Cramer, B.S., Rosenthal, Y., 2008. Stepwise transition from the Eocene greenhouse to the Oligocene icehouse. Nature Geoscience1(5), 329-334.

Kamenov, G.D., Mueller, P., Perfit, M., 2004. Optimization of mixed Pb-Tl solutions for high precision isotope analyses by MC-ICP-MS. Journal of Analytical Atomic Spectrometry, 19, 1262–1267.

Kamenov, G.D., Perfit, M., Mueller, P.A., Jonasson, I.R., 2008. Controls on magmatism in an island arc environment: study of lavas and sub-arc xenoliths from the Tabar–Lihir–Tanga–Feni island chain, Papua New Guinea. Contributions to Mineralogy and Petrology, 155, 635–656.

Kamenov. G.D., Dekov, V.M., Willingham, A.L., Savelli, C., Belluci, L.G., 2009. Anthropogenic Pb in recent hydrothermal sediments from the Tyrrhenian Sea: implications for seawater Pb control on low-temperature hydrothermal systems. Geology, 37(111-114).

Keeling, R.F., 2007. Deglaciation Mysteries. Science 316, 1440-1441.

Keigwin, L.D., 1998. Glacial-age hydrography of the far northwest Pacific Ocean. Paleoceanography, 13, 323-339.

Kennett, J.P., 1977. Cenozoic evolution of Antarctic glaciation, the Circum-Antarctic Ocean, and their impact on global paleoceanography. Journal of Geophysical Research, 82, 3843–3860.

Kennett, J.P., Barker, P.F., 1990. Latest Cretaceous to Cenozoic climate and oceanographic developments in the Weddell Sea, Antarctica: an ocean drilling perspective. Proc. ODP Sci. Results. Ocean Drilling Program, College Station, TX pp. 937-960.

Klemm, V., Reynolds, B., Frank, M., Pettke, T., Halliday, A.N., 2007. Cenozoic changes in atmospheric lead recorded in central Pacific ferromanganese crusts. Earth and Planetary Science Letters, 253(1-2), 57-66.

Kocsis, L., Trueman, C.N., Palmer, M.R., 2010. Protracted diagenetic alteration of REE contents in fossil bioapatites: Direct evidence from Lu-Hf isotope systematics. Geochimica et Cosmochimica Acta, 74(21), 6077-6092.

Krebs, U., Timmermann, A., 2007. Tropical Air-Sea Interactions Accelerate the Recovery of the Atlantic Meridional Overturning Circulation after a Major Shutdown. Journal of Climate 20 (19), 4940-4956.

Kump, L.R., Arthur, M.A., 1997. Tectonic Uplift and Climate Change In: Ruddiman, W.F. (Ed.), Plenum, New York, pp. 399–426.

Kurzweil, F., Gutjahr, M., Vance, D., Keigwin, L., 2010. Authigenic Pb isotopes from the Laurentian Fan: Changes in chemical weathering and patterns of North American freshwater runoff during the last deglaciation. Earth and Planetary Science Letters, 299(3-4), 458-465.

Lacan, F., Jeandel, C., 2001. Tracing Papua New Guinea imprint on the central Equatorial Pacific Ocean using neodymium isotopic compositions and Rare Earth Element patterns. Earth and Planetary Science Letters, 186(3-4), 497-512.

Lacan, F., Jeandel, C., 2005. Neodymium isotopes as a new tool for quantifying exchange fluxes at the continent-ocean interface. Earth and Planetary Science Letters, 232(3-4), 245-257.

Lear, C.H., Bailey, T.R., Pearson, P.N., Coxall, H.K., Rosenthal, Y., 2008. Cooling and ice growth across the Eocene-Oligocene transition. Geology, 36(3), 251-254.

Ling, H.-F., Jiang, S.-Y., Frank, M., Zhou, H.-Y., Zhou, F., Lu, Z.-L., Chen, X.-M., Jiang, Y.-H., Ge, C.-D., 2005. Differing controls over the Cenozoic Pb and Nd isotope evolution of deepwater in the central North Pacific Ocean. Earth and Planetary Science Letters, 232(3-4), 345-361.

Lynch-Stieglitz, J., Adkins, J.F., Curry, W.B., Dokken, T., Hall, I.R., Herguera, J.C., Hirschi, J.I.J.-M., Ivanova, E.V., Kissel, C., Marchal, O., Marchitto, T.M., McCave, I.N., McManus, J.F., Mulitza, S., Ninnemann, U., Peeters, F., Yu, E.-F., Zahn, R., 2007. Atlantic Meridional Overturning Circulation During the Last Glacial Maximum. Science 316, 66-69.

Mangini, A., Godoy, J.M., Godoy, M.L., Kowsmann, R., Santos, G.M., Ruckelshausen, M., Schroeder-Ritzrau, A., Wacker, L., 2010. Deep sea corals off Brazil verify a poorly ventilated Southern Pacific Ocean during H2, H1 and the Younger Dryas. Earth and Planetary Science Letters, 293(3-4), 269-276.

Manhes, G., 1978. Comparative uranium-thorium-lead and rubidium-strontium study of teh Saint Severin amphoterite; consequences for early solar system chronology. Earth and Planetary Science Letters, 39, 14-24.

Marchitto, T.M., Lynch-Stieglitz, J., Hemming, S.R., 2005. Deep Pacific $CaCO_3$ compensation and glacial-interglacial atmospheric CO_2. Earth and Planetary Science Letters, 231(3-4), 317-336.

Marchitto, T.M., Lynch-Stieglitz, J., Hemming, S.R., 2005. Deep Pacific $CaCO_3$ compensation and glacial-interglacial atmospheric CO_2. Earth and Planetary Science Letters, 231(3-4), 317-336.

Martin, E.E., Blair, S.W., Kamenov, G.D., Scher, H.D., Bourbon, E., Basak, C., Newkirk, D.N., 2010. Extraction of Nd isotopes from bulk deep sea sediments for paleoceanographic studies on Cenozoic time scales. Chemical Geology, 269(3-4), 414-431.

Martin, E.E., Haley, B.A., 2000. Fossil fish teeth as proxies for seawater Sr and Nd isotopes. Geochimica et Cosmochimica Acta, 64(5), 835-847.

Martin, E.E., Scher, H.D., 2004. Preservation of seawater Sr and Nd isotopes in fossil fish teeth: bad news and good news. Earth and Planetary Science Letters, 220(1-2), 25-39.

Martin, J.H., Knauer, G.E., 1983. VERTEX:Manganese transport with $CaCO_3$. Deep Sea Research, 30, 411-425.

Matsumoto, K., Oba, T., Lynch-Stieglitz, J., Yamamoto, H., 2002. Interior hydrography and circulation of the glacial Pacifi c Ocean. Quaternary Science Reviews 21, 1693–1704.

McManus, J.F., Francois, R., Gherardi, J.M., Keigwin, L.D., Brown-Leger, S., 2004. Collapse and rapid resumption of Atlantic meridional circulation linked to deglacial climate changes. Nature, 428(6985), 834-837.

Mead, G.A., Hodell, D.A., 1995. Controls on the $^{87}Sr/^{86}Sr$ composition of seawater from the Middle Eocene to Oligocene: Hole 689B, Maud Rise, Antarctica. Paleoceanography 10, 327-346.

Merico, A., Tyrrell, T., Wilson, P.A., 2008. Eocene/Oligocene ocean de-acidification linked to Antarctic glaciation by sea-level fall. Nature, 452(7190), 979-982.

Miller, K.G., Wright, J.D., Farnham, C.A., 1991. Unlocking the ice house: Oligocene-Miocene oxygen isotopes, estuary and marine erosion. Journal of Geophysical Research, 96, 6829-6848.

Monnin, E., Indermuhle, A., Dallenbach, A., Fluckiger, J., Stauffer, B., Stocker, T.F., Raynaud, D., Barnola, J.-M., 2001. Atmospheric CO2 Concentrations over the Last Glacial Termination. Science, 291(5501), 112-114.

Mucci, A., 1991. The solubility and free energy of formation of natural Kutnahorite. Canadian Mineralogist 29, 113-121.

Mucci, A., 2004. The Behavior of Mixed Ca-Mn Carbonates in Water and Seawater: Controls of Manganese Concentrations in Marine Porewaters. Aquatic Geochemistry 10(1), 139-169.

Newkirk, D.R., Martin, E.E., 2009. Circulation through the Central American Seaway during the Miocene carbonate crash. Geology, 37(1), 87–90.

O'Nions, R.K., Frank, M., von Blanckenburg, F., Ling, H.F., 1998. Secular variation of Nd and Pb isotopes in ferromanganese crusts from the Atlantic, Indian and Pacific Oceans. Earth and Planetary Science Letters, 155(1-2), 15-28.

Okazaki, Y., Timmermann, A., Menviel, L., Harada, N., Abe-Ouchi, A., Chikamoto, M.O., Mouchet, A., Asahi, H., 2010. Deepwater Formation in the North Pacific During the Last Glacial Termination. Science, 329(5988), 200-204.

Opdyke, B.N., Wilkinson, B.H., 1988. Surface area control of shallow cratonic to deep marine carbonate accumulation. Paleoceanography (3), 685–703.

Pagani, M., Zachos, J.C., Freeman, K.H., Tipple, B., Bohaty, S., 2005. Marked Decline in Atmospheric Carbon Dioxide Concentrations During the Paleogene Science, 309(5734), 600-603.

Pahnke, K., Goldstein, S.L., Hemming, S.R., 2008. Abrupt changes in Antarctic Intermediate Water circulation over the past 25,000 years. Nature Geoscience 1(12): 870-874.

Palike, H., Norris, R.D., Herrle, J.O., Wilson, P.A., Coxall, H.K., Lear, C.H., Shackleton, N.J., Tripati, A.K., Wade, B.S., 2006. The Heartbeat of the Oligocene Climate System Science, 314(5807), 1894-1898.

Palmer, M.R., Elderfield, H., 1985. Variations in the Nd isotopic composition of foraminifera from Atlantic Ocean sediments. Earth and Planetary Science Letters, 73, 299–305.

Pearson, P.N., Foster, G.L., Wade, B.S., 2009. Atmospheric carbon dioxide through the Eocene-Oligocene climate transition. Nature, 461(7267), 1110-1113.

Pekar, S.F., DeConto, R.M., 2006. High-resolution ice-volume estimates for the early Miocene: evidence for a dynamic ice sheet in Antarctica. Palaeogeography, Palaeoclimatology, Palaeoecology, 231, 101–109.

Pekar, S.F., Christie-Blick, N., Kominz, M.A., Miller, K.G., 2002. Calibration between eustatic estimates from backstripping and oxygen isotopic records for the Oligocene. Geology, 30, 903-906.

Pekar, S.F., DeConto, R.M., Harwood, D.M., 2006. Resolving a late Oligocene conundrum: deep-sea warming versusAntarctic glaciation. Palaeogeography, Palaeoclimatology, Palaeoecology, 231, 29–40.

Pekar, S.F., Christie-Blick, N., 2008. Resolving apparent conflicts between oceanographic and Antarctic climate records and evidence for a decrease in pCO_2 during the Oligocene through early Miocene (34-16 Ma). Palaeogeography, Palaeoclimatology, Palaeoecology, 260(1-2), 41-49.

Peltier, W.R., Fairbanks, R.G., 2006. Global glacial ice volume and Last Glacial Maximum duration from an extended Barbados sea level record. Quaternary Science Reviews, 25(23-24), 3322-3337.

Pena, L.D., Calvo, E., Cacho, I., Eggins, S., Pelejero, C., 2005. Identification and removal of Mn-Mg-rich contaminant phases on foraminiferal tests: Implications for Mg/Ca past temperature reconstructions. Geochem. Geophys. Geosyst., 6.

Pena, L.D., Cacho, I., Calvo, E., Pelejero, C., Eggins, S., Sadekov, A., 2008a. Characterization of contaminant phases in foraminifera carbonates by electron microprobe mapping. Geochem. Geophys. Geosyst., 9.

Pena, L.D., Cacho, I., Ferretti, P., M. A. Hall, M.A., 2008b. El Nin˜o–Southern Oscillation–like variability during glacial terminations and interlatitudinal teleconnections. Paleoceanography, 23.

Petit, J.R., Jouzel, J., Raynaud, D., Barkov, N.I., Barnola, J.M., Basile, I., Bender, M., Chappellaz, J., Davis, M., Delaygue, G., Delmotte, M., Kotlyakov, V.M., Legrand, M., Lipenkov, V.Y., Lorius, C., Pepin, L., Ritz, C., Saltzman, E., Stievenard, M., 1999. Climate and atmospheric history of the past 420,000 years from the Vostok ice core, Antarctica. Nature, 399(6735), 429-436.

Piepgras, D.J., Wasserburg, G.J., 1987. Rare earth element transport in the western North Atlantic inferred from Nd isotopic observations. Geochimica et Cosmochimica Acta, 51(5), 1257-1271.

Piepgras, D.J., Jacobsen, S.B., 1988. The isotopic composition of neodymium in the North Pacific. Geochimica et Cosmochimica Acta, 52(6), 1373-1381.

Pike, A.W.G., Hedges, R.E.M., Van calsteren, P., 2002. U-series dating of bone using the diffusion-adsorption model. Geochimica et Cosmochimica Acta, 66(24), 4273-4286.

Pin, C., Bassin, C., 1992. Evaluation of a Sr-specific extraction chromatographic method for isotopic analysis in geologic materials. Analytica Chimica Acta, 269, 49–255.

Piotrowski, A.M., Goldstein, S.L., Hemming, S.R., Fairbanks, R.G., 2004. Intensification and variability of ocean thermohaline circulation through the last deglaciation. Earth and Planetary Science Letters, vol.225(1-2), 205-220.

Piotrowski, A.M., Goldstein, S.L., Hemming, S.R., Fairbanks, R.G., 2005. Temporal relationships of carbon cycling and ocean circulation at glacial boundaries. Science, vol.307(no.5717), pp.1933-1938.

Planavsky, N.J., Rouxel, O.J., Bekker, A., Lalonde, S.V., Konhauser, K.O., Reinhard, C.T., Lyons, T.W., 2010. The evolution of the marine phosphate reservoir. Nature, 467(7319), 1088-1090.

Ravizza, G., Peucker-Ehrenbrink, B., 2003. The marine $^{187}Os/^{188}Os$ record of the Eocene-Oligocene transition: the interplay of weathering and glaciation. Earth and Planetary Science Letters, 210(1-2), 151-165.

Reid, J.L., 1986. On the total geostrophic circulation of the South Pacific Ocean: flow patterns, tracers and transport Progresss in Oceanography, 16, 1-16.

Reynard, B., Lecuyer, C., Grandjean, P., 1999. Crystal-chemical controls on rare-earth element concentrations in fossil biogenic apatites and implications for paleoenvironmental reconstructions. Chemical Geology, 155(3-4), 233-241.

Reynolds, B.C., Frank, M., O'Nions, R.K., 1999. Nd- and Pb-isotope time series from Atlantic ferromanganese crusts: implications for changes in provenance and paleocirculation over the last 8 Myr. Earth and Planetary Science Letters, 173(4), 381-396.

Robert, C., Kennett, J.P., 1997. Antarctic continental weathering changes during Eocene-Oligocene cryosphere expansion: Clay mineral and oxygen isotope evidence. Geology 25 (7), 587-590.

Robert, C., Diester-Haass, L., Chamley, H., 2002. Late Eocene-Oligocene oceanographic development at southern high latitudes, from terrigenous and biogenic particles: a comparison of Kerguelen and Mause Rise, ODP sites 744 and 689. Marine Geology, 191, 37-54.

Roberts, N.L., Piotrowski, A.M., McManus, J.F., Keigwin, L.D., 2010. Synchronous Deglacial Overturning and Water Mass Source Changes. Science, 327(5961), 75-78.

Rollinson, H.R., 1993. Using Geochemical Data: Evaluation, Presentation, Interpretation. Prentice Hall.

Rosenthal, Y., Boyle, E.A., Labeyrie, L., 1997. Last glacial maximum paleochemistry and deepwater circulation in the Southern Ocean: Evidence from foraminiferal cadmium. Paleoceanography, 12(6), 787-796.

Rowell, A.J., Rees, M.N., 1987. Setting and significance of the Shackleton Limestone, central Transantarctic Mountains. In: Thomson, M.R.A., Crame, J.A., Thomson, J.W. (Eds.), Geological Evolution of Antarcitca. Cambridge University Press, Cambridge.

Rutberg, R.L., Hemming, S.R., Goldstein, S.L., 2000. Reduced North Atlantic Deep Water flux to the glacial Southern Ocean inferred from neodymium isotope ratios. Nature 405(6789), 935-938.

Salamy, K.A., Zachos, J.C., 1999. Latest Eocene-Early Oligocene climate change and Southern Ocean fertility: inferences from sediment accumulation and stable isotope data. Palaeogeography, Palaeoclimatology, Palaeoecology, 145, 61-77.

Schaule, B.K., Patterson, C.C., 1981. Lead concentration in the northeast Pacific: evidence for global anthropogenic perturbations. Earth and Planetary Science Letters, 54, 97-116.

Scher, H.D., Martin, E.E., 2004. Circulation in the Southern Ocean during the Paleogene inferred from neodymium isotopes. Earth and Planetary Science Letters, 228(3-4), 391-405.

Scher, H.D., Martin, E.E., 2006. Timing and Climatic Consequences of the Opening of Drake Passage. Science, 312(5772), 428-430.

Scher H.D., Bohaty S.M., Zachos J.C., M.L., D., 2007. A weathering pulse during the Eocene Oligocene climate transition, 9th International Conference on Paleoceanography, Shanghai, China, pp. P-4-58.

Scher, H.D., and E. E. Martin, 2008. Oligocene deep water export from the North Atlantic and the development of the Antarctic Circumpolar Current examined with neodymium isotopes. Paleoceanography, 23, PA1205.

Scher, H.D., Bohaty, S.M., Zachos, J.C., Delaney, M.L., 2011. Two-stepping into the icehouse: East Antarctic weathering during progressive ice-sheet expansion at the Eocene-Oligocene transition. Geology, 39(4), 383-386.

Sexton, P.F., Norris, R.D., Wilson, P.A., Palike, H., Westerhold, T., Rohl, U., Bolton, C.T., Gibbs, S., 2011. Eocene global warming events driven by ventilation of oceanic dissolved organic carbon. Nature, 471(7338), 349-352.

Sholkovitz, E.R., 1989. Artifacts associated with the chemical leaching of sediments for rare-earth elements. Chemical Geology, 77(1), 47-51.

Siddall, M., Khatiwala, S., van de Flierdt, T., Jones, K., Goldstein, S.L., Hemming, S., Anderson, R.F., 2008. Towards explaining the Nd paradox using reversible scavenging in an ocean general circulation model. Earth and Planetary Science Letters, 274(3-4), 448-461.

Sigman, D.M., Hain, M.P., Haug, G.H., 2010. The polar ocean and glacial cycles in atmospheric CO2 concentration. Nature, 466(7302), 47-55.

Spero, H.J., Lea, D.W., 2002. The Cause of Carbon Isotope Minimum Events on Glacial Terminations. Science, 296(5567), 522-525.

Swart, P.K., Eberli, G., 2005. The nature of $\delta^{13}C$ of periplatform sediments:Implications for stratigraphy and the global carbon cycle. Sedimentary Geology, 175, 115–129

Tachikawa K., Jeandel C., Roy-Barman M., 1999. A new approach to the Nd residence time in the ocean: the role of atmospheric inputs. Earth Planetary Science Letters, 170(4), 433–446.

Tachikawa, K., Athias, V., Jeandel, C., 2003. Neodymium budget in the modern ocean and paleo-oceanographic implications. Journal of Geophysical Research,108(C8), 3254.

Talley L.D., 1999. Some aspects of ocean heat transport by the shallow,intermediate and deep overturning circulations. In: Clark, P.U., Webb, R.S., Keigwin, L.D. (Eds.), Mechanisms of Global Climate Change at Millennial Time Scales. Geophysical Monograph, 1–22.

Thomas, D.J., Via, R.K., 2007. Neogene Evolution of Atlantic Thermohaline Circulation: Perspective from Walvis Ridge, southeastern Atlantic Ocean. Paleoceanography, 22(PA2212).

Tovar-Sanchez, A., Sanudo-Wilhemy, S.A., Garcia-Vargas, M., Weaver, R.S., Popels, L.C., Hutchins, D.A., 2003. A trace metal clean reagent to remove surface-bound ironfrom marine phytoplankton. Marine Chemistry, 82, 91–99.

Tomczak, M., Godfrey, J.S., 1994. Regional oceanography: an introduction. Pergamon Press.

Tripati, A., Backman, J., Elderfield, H., Ferretti, P., 2005. Eocene bipolar glaciation associated with global carbon cycle changes. Nature, 436, 341–346

Trueman, N.C., Tuross, N., 2002. Trace Elements in Recent and Fossil Bone Apatite. In: Kohn, J.M., Rakovan, J., Hughes, M.J. (Eds.), Reviews in Mineralogy & Geochemistry, pp. 489-521.

van de Flierdt, T., Frank, M., Halliday, A.N., Hein, J.R., Hattendorf, B., Gunther, D., Kubik, P.W., 2003. Lead isotopes in North Pacific deep water - implications for past changes in input sources and circulation patterns. Earth and Planetary Science Letters, 209(1-2), 149-164.

van de Flierdt, T., Frank, M., Halliday, A. N., Hein, J. R., Hattendorf, B., Gunther D., Kubik, P. W., 2004. Deep and bottom water export from the Southern Ocean to thePacific over the past 38 million years. Paleoceanography, 19, PA1020.

van de Flierdt, T., Hemming, S.R., Goldstein, S.L., Abouchami, W., 2006. Radiogenic isotope fingerprint of Wilkes Land–Adelie Coast Bottom Water in the circum-Antarctic Ocean. Geophysical Research Letters, 33(L12606).

Via, R.K., Thomas, D.J., 2006. Evolution of Atlantic thermocline circulation: Early Oligocene onset of deep-water production in the North Atlantic. Geology, 34, 441-444.

von Blanckenburg, F., Nagler, T.F., 2001. Weathering versus circulation-controlled changes in radiogenic isotope tracer composition of the Labrador Sea and North Atlantic deep water. Paleoceanography, 16(4), 424-434.

Wei, W., Thierstein, H.R., 1991. Upper Cretaceous and Cenozoic calcareous nannosfossils of the Kerguelen Plateau (southern Indian Ocean) and Prydz bay (East Antarctica). Proc. ODP Sci. Results. Ocean Drilling Program, College Station, TX, pp. 979-999.

Wu J., A., Boyle, E. A., 1997 Lead in the western North Atlantic Ocean: complete response to leaded gasoline phaseout Geochimica et Cosmochimica Acta, 61, 3279–3283.

You, Y., 2003. The pathway and circulation of North Pacific intermediate water. Geophysical Research Letters, 30(24).

Zachos, J.C., Breza, J.R., Wise, S.W., 1992. Early Oligocene ice-sheet expansion on Antarctica: Stable isotope and sedimentological evidence from Kerguelen Plateau, southern Indian Ocean. Geology 20, 569-573.

Zachos, J.C., Quinn, T.M., Salamy, K.A., 1996. High resolution (10^4 yr) deep-sea foraminiferal stable isotope records of the Eocene-Oligocene climate transition. Paleoceanography 11, 251-266.

Zachos, J.C., Opdyke, B.N., Quinn, T.M., Jones, C.E., Halliday, A.N., 1999. Early cenozoic glaciation, antarctic weathering, and seawater 87Sr/86Sr: is there a link? Chemical Geology, 161(1-3), 165-180.

Zachos, J., Pagani, M., Sloan, L., Thomas, E., Billups, K., 2001. Trends, Rhythms, and Aberrations in Global Climate 65 Ma to Present. Science, 292(5517), 686-693.

Zachos, J.C., Kump, L.R., 2005. Carbon cycle feedbacks and the initiation of Antarctic glaciation in the earliest Oligocene. Global and Planetary Change, 47(1), 51-66.

BIOGRAPHICAL SKETCH

Chandranath Basak was born in Calcutta, India. He went to Presidency College, Calcutta, India for his bachelor's degree and became interested in geology during his first geochemistry course. Following graduation from college, he pursued a master's degree at Jadavpur University, Calcutta, India where he studied an inverted Barrovian sequence in the eastern Himalayas and was exposed to a range of problems related to metamorphic petrology. Following successful completion of the master's program, Chandranath joined Indiana State University (ISU), Terre Haute, Indiana to pursue a second Master of Science degree. For this research he was involved in a modern proxy calibration study using stable isotopes in live benthic foraminifera from Alaska and the Australian margin under the guidance of Dr. Anthony E. Rathburn. Towards the end of his second master's he decided he wanted to continue in academics and pursue a PhD using the calibrated proxy to understand past climate. At that point he joined the Ph.D. program at the University of Florida, Gainesville working on research in paleoclimatology under the guidance of Dr. Ellen E. Martin. Chandranth's research at UF focused on establishing new paleoceanographic proxies as well as using those proxies to reconstruct paleoclimatic histories across dramatic climatic events on a range of time scales. After his Ph.D. he plans on continuing research in the field of paleoceanography/paleoclimatology and intends to remain dedicated to the world of academia.